STUDY OF HYGROTHERMAL EFFECTS AND CURE KINETICS ON THE STRUCTURE-PROPERTY RELATIONS OF EPOXY-AMINE THERMOSETS: FUNDAMENTAL ANALYSIS AND APPLICATION

By

SUNGWON CHOI

A DISSERTATION PRESENTED TO THE GRADUATE SCHOOL
OF THE UNIVERSITY OF FLORIDA IN PARTIAL FULFILLMENT
OF THE REQUIREMENTS FOR THE DEGREE OF
DOCTOR OF PHILOSOPHY

UNIVERSITY OF FLORIDA

2011

To my wife, Kyongah

ACKNOWLEDGMENTS

First of all, I deeply appreciate my advisor, Dr. Douglas for his intellectual guidance and encouragement which enable all this work to be possible. Without his support, none of this work would be successful. I would also like appreciate the valuable advice and encouragement from my committee members for developing on my research: Dr. Hamilton, Dr. Mecholsky, Dr. Sigmund, and Dr. Craciun.

I would also like to express my gratitude to all the members of the Dr. Douglas group: Sangjun Lee, Changhua Liu, Andrew Stewart, Laura Diers, Justin Dennison, Andrew Janisse, Sasha Perkins, and Andrea Phantu. They really gave me a lot of kind support and collaboration necessary to make out all these things.

The research work carried out in this dissertation was funded by National Science Foundation and the Alumni Graduate Award from the University of Florida.

TABLE OF CONTENTS

page

LIST OF TABLES

LIST OF FIGURES

Abstract of Dissertation Presented to the Graduate School
of the University of Florida in Partial Fulfillment of the
Requirements for the Degree of Doctor of Philosophy

STUDY OF HYGROTHERMAL EFFECTS AND CURE KINETICS ON THE STRUCTURE-PROPERTY RELATIONS OF EPOXY-AMINE THERMOSETS: FUNDAMENTAL ANALYSIS AND APPLICATION

By

Sungwon Choi

May 2011

Chair: Elliot P. Douglas
Major: Materials Science and Engineering

For decades, epoxy systems have shown outstanding physical properties for various applications with numerous advantages over other thermoset resins such as lower cure shrinkage, lower residual stress, chemical resistance, and insulating properties. However, property degradation due to hygrothermal exposure is a critical issue in applications, in which their nature to absorb moisture results in a significant loss in glass transition temperature (T_g), modulus, tensile strength, and adhesive strength. These detrimental effects often include some complex behavior in that both increase and decrease in T_g and/or modulus is observed during the course of exposure.

In this study, to specifically describe the mechanism for this complex hygrothermal behavior, direct experimental measurement has been conducted employing thermodynamic analysis and spectroscopic measurements. Fourier transform near-infrared (FT-NIR) spectroscopic measurements showed that an increase in conversion was responsible for the increase in T_g, while plasticization occurred simultaneously, rendering the hygrothermal behavior to be complex. To evaluate those factors affecting this complex hygrothermal behavior separately, a relationship between T_g and

conversion was constructed for the unexposed system and compared to the corresponding T_g values for the exposed system at the same point of each conversion value.

For another part of this dissertation, the effect of water on cure kinetics was investigated with the hypothesis that water significantly accelerates the cure kinetics of epoxy-amine systems. The near FT-IR demonstrated that a small amount of water addition significantly accelerated the cure reaction in terms of epoxide conversion. A modified mechanistic model was successfully used to directly compare the effect of hydroxyl from water addition and that from auto-acceleration by the reaction.

In the final section, in an effort to enhance the durability of bonding properties of an epoxy adhesive for structural strengthening application, silane coupling agents were applied to the surface of concrete before the adhesive was applied. Slant shear testing results show that the durability of the interfacial bonding was significantly enhanced with the use of an epoxy-functional silane coupling agent. The results indicate that the chemical nature of bonding plays a large role at the interface bonding of epoxy resin for structural strengthening applications.

CHAPTER 1
INTRODUCTION

Over past decades, epoxy resins have shown outstanding performances in various applications such as surface coatings, structural adhesives, packaging, and engineering composites, providing high performances of strength, stiffness, and resistance to creep.[1, 2]

Epoxy resins have numerous advantages over other thermoset resins such as lower cure shrinkage and residual stress, chemical resistance, insulating properties and availability of the resin ranging from low viscous liquid to tack-free solids, but the most distinctive attraction of the epoxy resins can be described as "*a convenient use of a wide range of temperatures by judicious selection of curing agents enabling good control over the degree of cross-linking"*.[3]

In these uses of epoxy materials, additional variables are often included into a given system such as solvent, concentrations, viscosity, and mixing rates, providing another method to control degree of cross-linking or the speed of reaction.[4-9] Also, an additional incorporation of catalysts such as imidazole have extensively been utilized as a convenient way to regulate the condition of manufacturing processes.[10-13] This has been preferred in many industrial areas such as outdoor or electronic applications where high temperature cannot be used easily as a means of accelerating the curing reaction in order to take advantages of easy installation. Addition of hydroxyl containing coupounds such as water or various types of alcohols and phenols has also known to increase the rate of cure reaction. Catalysis effects of hydroxyl groups in those types of added compounds contribute the ring opening of epoxides, although the exact impact of added water has not been suggested quantitatively.[4, 14, 15]

Although the epoxy resins have shown the excellent performances in various engineering fields, it is a major limitation of cross-linked epoxy resins that their tendency to absorb considerable amounts of moisture up to 7~8 wt% because the absorbed moisture induces detrimental effects on their physical properties. A number of investigations have reported that hygrothermal exposure of epoxy systems results in significant loss of properties such as glass transition temperatures (T_gs)[16-26], modulus[27-31], tensile[28, 29, 31], and adhesive strength[32]. Plasticization by absorbed water is considered to be a primary reason to induce property loss, whereas other mechanisms such as hydrolysis and hygrothermal stresses causing swelling, formation of microcracks and crazes, and polymer chain scission may also be factors depending on the material and exposure condition.[25, 26, 28, 29, 31]

Regarding the interface bonding degradation of epoxy adhesives with hygrothermal exposure, the property loss can be explained by general features of bond degradation, in which water penetrates through a permeable adherend or adhesives and causes deterioration of the bond by altering mechanical properties of adhesives.[33] On the other hand, there can be another viewpoint describing that disruption of hydrogen bonds at the interface between the adhesive and given adherent plays an important role. In this description, displacement of epoxy with water under water/moisture exposure induces broken hydrogen bonds between epoxy and given adherent, resulting in reduced interface bond strength.[34, 35]

Although some studies on epoxy-metal adhesion have supported the theory that broken hydrogen bonds at the interface results in significant loss of adhesive bond strength[34, 35], the chemical nature of epoxy adhesive for structural strengthening

applications at the interface with ceramic materials still remains unanswered and almost nothing known about how that bond is affected by moisture.

In addition, hygrothermal exposure often introduces complex behaviors of epoxy resin itself, which lead the overall understanding of the system under environmental exposure to be complicated. In such complex behaviors under the exposure, not only the property decrease by plasticization is shown, but an increase in physical properties is also observed, i.e., an increase in T_gs and/or modulus with hygrothermal exposure.[29, 36-40] Particularly, in order to obtain the advantages of easy installation in electronic or structural applications, many adhesives or coatings have been often cured at low temperature where complete curing reactions of thermosets have not been reached. In such cases, with changes in environments from initial condition such as elevated temperature or with passage of time, additional cure can occur which has resulted in an increase of the glass transition with property decrease by plasticization at the same time, hence rendering the hygrothermal behavior to be complex.

Various mechanisms have been suggested to describe such complex hygrothermal behaviors such as reactivation of the post-curing reaction[29, 36-40], different types of hydrogen-bonded water[41-43], and micro-structural effect[41], but none of these explanations is there any direct experimental evidence supporting them, and a clear explanation of the mechanism for this anomalous behavior remains unanswered.

In this study, hygrothermal behaviors of both epoxy resin itself and the interface between epoxy and cementitious material have been investigated. The epoxy-amine systems being examined in this study are the generic system including DGEBA and

polyoxypropylene diamine with different commercial epoxy products which used as a seal coat, impregnating resins and adhesives for structural applications.

For the first part of this work, hygrothermal effects on physical properties of epoxy-amine thermosets were investigated to evaluate each possible factor which affects the hygrothermal behaviors of the systems. In this investigation, direct experimental evaluations with a thermodynamic analysis and spectroscopic measurements have been proposed to specifically describe the mechanism for the complex hygrothermal behavior. The study has also focused on trying to quantify different factors separately (Chapters 3 and 4).

Afterwards, in order to evaluate effect of hydroxyl from water on cure kinetics with the hypothesis that water can significantly accelerates the cure kinetics of epoxy-amine systems, small amount of water was added to initial mixture of an epoxy-amine system. This study has focused on the direct evaluation of the hydroxyl effect from water addition quantitatively using a modified mechanistic modeling with a spectroscopic analysis (Chapter 5).

At the final section of this work, in an effort to enhance the durability of bonding properties of an epoxy adhesive for structural strengthening application, silane coupling agents were utilized to concrete surfaces before the adhesive applied. In this work, the hypothesis was examined that the coupling agents form covalent bonding at the interface and improve durability by preventing the water from displacing the epoxy at the interface (Chapter 6).

The specific aims of this work are summarized and shown as follows. (1) Examine and modify the mechanisms for the description of the complex hygrothermal behavior,

i.e. anti-plasticization in terms of increase in glass transition temperatures with hygrothermal exposure (Chapters 3 and 4); (2) How each factor affecting complex hygrothermal behavior can be separately evaluated (Chapters 3 and 4); (3) Investigate the effect of moisture/water addition on cure kinetics (Chapter 5); (4) Test the hypothesis that hydrogen bonding plays a large role for the adhesive bonding (Chapter 6); (5) Utilize silane coupling agents between the epoxy resins and concrete to improve the durability of the bond between epoxy and concrete under water/moisture exposure (Chapter 6)

We hope that this study lead us to advance our fundamental understanding of structure-property relationships in epoxy systems under hygrothermal exposure, allowing us to improve the performance of epoxy systems in various applications under humid environments.

CHAPTER 2
REVIEW OF LITERATURE

Effect of Water on Physical Properties of Epoxy-Amine Thermosets

Plasticization with Hygrothermal Exposure in Epoxy Systems

In epoxy resins, property degradation due to hygrothermal exposure is a critical issue, in which their nature to absorb moisture up to 7-8 wt% results in a significant loss in T_g[16-26], modulus[27-31], tensile[28, 29, 31], and adhesive strength[32]. For these detrimental effects with hygrothermal exposure in epoxy systems, the property loss is mostly attributed to the plasticization effect, whereas other mechanisms such as hydrolysis, polymer chain scission, formation of microcracks may also be factors depending on the materials and exposure condition.[25, 26, 28, 29, 31]

Plasticization is generally referred to the phenomenological behavior associated with the depression of glass transition temperature or the decrease of mechanical properties, which were caused by moisture sorption, in which water molecules act as a plasticizer or crazing agents, significantly affecting the properties of the system under the changes in temperature and humidity.[27] In this detrimental effect, combined with the external factors of exposure conditions such as degree of humidity, exposed temperatures and time, the chemical structure of the polymer matrix as well as processing also plays larger roles in that different degree of cure, network formation and hydrogen bonding sites induce different amount of water absorption.

For the studies on the effect of water sorption on physical properties of epoxies, the role of absorbed water associated with plasticization has been often described from two different viewpoints: (1) absorbed water as “molecules forming an ordinary polymer-

diluent solution" and (2) absorbed water bonded to specific polar groups in polymer network with interaction.[20]

For the first viewpoint, the structure of the epoxy is considered to be the primary factor to degrade the physical properties with water sorption, generally describing that the absorbed water in a polymer matrix as "molecules forming an ordinary polymer-diluent solution". The absorbed water molecules is described to simply reside in the free volume of the network without any interaction between the polymer and water, which enhances the chain mobility, resulting in a structural relaxation transition at lower temperatures.[44-46]

With this point of view, in order to predict the decrease in T_g which is often suggested as a parameter indicating the degree of plasticization quantitatively, the composition dependence of T_g in polymer-diluent systems have been employed via the free volume approach.[47] The compositional model was derived by Kelley and Bueche, and then firstly developed by McKague et al. to describe the decrease in T_g of epoxy systems.[21, 47, 48] In this description, the degree of plasticization of the polymer network structure was expected by the diluent volume fraction and the thermal expansion coefficients at the glass transition through the following expression

$$T_{g,wet} = \frac{T_{g,p}\alpha_p V_p + T_{g,d}\alpha_d V_d}{\alpha_p V_p + \alpha_d V_d} \quad (2\text{-}1)$$

where subscripts p and d indicates diluent or water and polymer, α and V is thermal expansion at glass transition and free volume, respectively.

Ellis and Karasz reported the T_g depression for a series of epoxies, in which overall, they observe T_g depressions of 8-15º C/wt% water for stoichiometric compositions, but only 4-5º C/wt% water for non-stoichiometric compositions.[18] They

also suggested the depression in stoichiometric compositions could be modeled with a compositional model for the T_g depression. Browning and Wright also used the compositional model with the free volume theory to relate their experimental observation of the T_g depression in epoxy resins.[49, 50]

From another point of view, the absorbed water in polymer network bonds to specific polar groups, such as hydroxyl groups, disrupts interchain hydrogen bonds, also resulting in a loss in properties.[19, 51, 52] In this description, it assumes a second mechanism of plasticization, “strong mutual interaction between water and polar nature of the networks”.[53] This approach often employs the configurational entropy model rather than free volume as the temperature-dependent function to propose an important role of the absorbed water, which localized at strongly polar molecular groups, suggesting the formation of hydrogen bonding.[54] Moy et al. successfully applied this type of model to predict their T_g depressions in a high-T_g epoxy system where other supplemental experiment also supported their assumption that strong interaction between the dispersed water and some specific segments or groups in the polymer.[22] Feng also found significant decreases in T_g due to absorbed moisture, in which he found that the compositional approach could not predict the T_gs of the plasticized materials.[55] An entropy model was used, and this was explained as being caused by the decrease in entropy caused when water molecules become hydrogen-bonded to the epoxy.

Adamson also identified three distinct stages of water sorption, and postulated that those stages correspond to water first entering the free volume, then water becoming bound to hydrogen-bonding sites, and finally water entering the more densely

crosslinked phase.[56] In a series of papers, Soles et al. carefully examined the role of free volume or “nanopores”, concluding that transport is primarily governed by the hydrogen bonding of water to the epoxy.[57-59]

In some cases, both effects of ordinary polymer-diluent solution and disruption of interchain hydrogen bonds are considered to describe property loss under hygrothermal exposure in the same system.[22, 29, 56, 60]

Thus, the same amount of absorbed water could result in different degree of plasticization due to the multiplicity of the polymer-water interactions in which absorbed moisture could be present in the network in different forms. However, in any case, the absorbed water seems to undoubtedly act as a critical stimulus to degrade the properties of epoxy resins. In addition to the presence of absorbed water, the elevated temperature also contributes to the property loss in that the increased rate of water diffusion results in a larger amount of water absorption, whereas chain mobility is also enhanced at higher temperatures.

Anti-Plasticization with Hygrothermal Exposure in Epoxy Systems

Although the numerous reports have suggested that water absorption induces property loss in physical properties of epoxy systems as previously stated, some studies have revealed anomalous behavior, i.e., an increase in physical properties of epoxy systems after hygrothermal exposure, such as an increase in T_g or tensile modulus.

There have been many studies which report about some abnormal anti-plasticization for various polymer systems such as polycarbonate-dibutyl phthalate, polystyrene, poly (vinyl chloride), tricesyl phosphate, starch, and nylon-water. Anti-plasticization of a polymer has been conventionally designated as a polymer mixed with a low molar mass additive (plasticizers), which found to be harder and more brittle than

the pure polymer.[61] Generally in this observation of the behavior for various polymers, the T_g of the system and its free volume decreases, but the mechanical properties altered, causing the polymer become stiff and brittle.[62]

To describe such unusual behavior of anti-plasticization which is opposite to that expected of plasticized materials, various mechanisms and explanations have been suggested: suppression of the secondary relaxation transitions, polymer-diluent interactions decreasing segmental mobility of the polymer chain, a chain end effect by a decrease of fractional free volume at the chain ends, re-orientation of polymer chain which decrease free volume under high stress, reduced mobility of the diluents-possible solid diluents with higher glass transition temperatures.[62-68]

In epoxy systems, there have been also some reports associated with anti-plasticization behavior during hygrothermal exposure. Nogueira et al. reported that in an epoxy system, the tensile modulus was slightly increased at certain amounts of water sorption, although it immediately decreased as water content increased.[29] They attribute these results to the reactivation of the post-curing reaction. Wu and coworkers also observed anomalous hygrothermal behavior for a nonstoichiometric epoxy system cured at room temperature, in which after 500 days of water immersion at 45°C, the T_g values and moduli of the specimens with a lower ratio of hardener increased.[40] For an epoxy-based primer, Devasahayam also found increases in T_g up to 10°C for exposure to 95% RH at 55 and 68°C, whereas almost no change in T_g was found for samples exposed at lower temperatures.[36] Other authors have found similar results, in which an increase of cross-link density by the reactivation of the post-curing reaction is generally attributed as the mechanism for this anomalous behavior.[37-39]

There have also been other descriptive hypotheses for the anomalous increase in physical properties with hygrothermal exposure. Zhou and Lucas found initial stages of sharp T_g depression followed by significant increases of T_g in three different epoxy resins during hygrothermal exposure.[43] Combined with their previous work investigating two types of bound water in epoxy resins through absorption/desorption profiles,[42] a theory of different types of hydrogen bonded water was suggested to explain the anomalous behavior. In this theory, single-hydrogen-bonded water acts as a plasticizer, increasing chain mobility and contributing to property loss (Type 1), whereas water molecules interconnected with multiple sites of the resin network through hydrogen bonds create secondary cross-linking, resulting in an increase in physical properties (Type 2). Papanicolaou et al. also employed this model to describe anomalous hygrothermal behavior in an epoxy resin. From dynamic mechanical thermal analysis (DMTA), they found increases in T_g values with decreases in tan δ values during hygrothermal exposure, whereas storage modulus values showed almost no change.[41] They explained this phenomena with the theory of different types of hydrogen bonded water in that Type 1 bound water contributed to the decrease of tan δ by disrupting initial hydrogen bonds, whereas Type 2 water was responsible for the increase in T_g.

It has also been suggested that the biphasic structure in epoxy systems contributes to this anomalous behavior.[41] According to this hypothesis, distribution of compression and expansion forces due to differences in water diffusion between hard and soft phases causes an anomalous increase in mechanical properties.

The three suggested mechanisms above for the description of the anomalous behavior of “property gain” under hygrothermal exposure are summarized as follows: (1)

post-curing reactions caused by the elevated temperature of the water used for exposure; (2) different states of hydrogen bonded water molecules, one of which creates secondary cross-linking; and (3) effect of biphasic structure. It is important to note, however, that for none of these explanations is there any direct experimental evidence supporting them, and a clear explanation of the mechanism for this anomalous behavior remains unanswered.

Effect of Crosslink Density on Glass Transition in Epoxy-Amine Thermosets

Cross-link density is known to be one of the important factors to determine the T_g in network polymers. An increase in the cross-link density reduces the chain mobility resulting in an increase in T_g, whereas an increase in molecular weight as well as a decrease in low-molecular-weight components during the curing reaction also increases the T_g.[69] The relationship between T_g of a network polymer and conversion is well-described elsewhere.[70-72]

For derivation of the relationship, a thermodynamic theory is used in which the reduction in configurational entropy describes the relationship as cross-linking increased as shown in following equation,

$$\frac{T_g(X) - T_g(0)}{T_g(0)} = \frac{KX}{1 - KX} \tag{2-2}$$

where $T_g(X)$ is the T_g of a polymer with a degree of cross-linking X, $T_g(0)$ is the T_g of un-cross-linked linear polymer, and K is a dimensionless constant that is independent of the material.

For another approach, Couchman and Karasz suggested the use of a thermodynamic theory in which changes in heat capacity of each component and its T_g

are correlated to describe the glass transition in copolymer systems as shown in following equation,[70]

$$\sum x_i \int_{Tgi}^{Tg} \frac{\Delta C_{pi}}{T} dT = 0 \qquad (2\text{-}3)$$

where ΔC_{pi} is the change in heat capacity of the component i at the glass transition temperature T_{gi}, and x_i is the amount of the component i in solution. The features of the Equation 2-3 include the description of a partially cured polymer being a solution of the polymer in the monomer and the composition being related to the degree of conversion.

The theory was then developed into the following semi-empirical equation to describe T_g in cross-linked systems with the variation in conversion, assuming ΔC_p is inversely proportional to temperature where α is conversion, T_{g0} and $T_{g\infty}$ are the T_g values of the monomer and the fully cured network, and ΔC_{p0} and $\Delta C_{p\infty}$ are the heat capacity changes at T_{g0} and $T_{g\infty}$, respectively.

$$T_g = \frac{(1-\alpha)T_{g0} + \alpha(\Delta C_{p\infty} / \Delta C_{p0})T_{g\infty}}{(1-\alpha) + (\Delta C_{p\infty} / \Delta C_{p0})\alpha} \qquad (2\text{-}4)$$

Using a similar approach assuming ΔC_p is constant, another semi-empirical equation can be derived as shown below.

$$\ln(T_g) = \frac{(1-\alpha)\ln(T_{g0}) + (\Delta C_{p\infty} / \Delta C_{p0})T_{g\infty}\alpha \ln(T_{g\infty})}{(1-\alpha) + (\Delta C_{p\infty} / \Delta C_{p0})\alpha} \qquad (2\text{-}5)$$

Cure Kinetics of Epoxy-Amine Thermosets

Mechanism of Epoxy Cure Reaction

For the epoxy-amine reaction, it is well-know that the main features include (1) reaction of primary amine with an epoxide to form a secondary amine and (2) further reaction of the secondary amine with another epoxide to form a tertiary amine.[73, 74]

Although other possibilities can be also employed such as homo-polymerization by epoxide-epoxide and etherification by epoxide-hydroxyl reactions, those only occur under certain conditions, such as in the presence of acid/base catalysts or at higher cure temperatures.[75-80]

When homo-polymerization and etherification reactions are neglected, the main cure mechanism can be generally described by two reaction paths: (1) reactions catalyzed by compounds containing nitrogen-hydrogen bonds (designated as “non-catalytic” by previous workers) and (2) those by oxygen-hydrogen bonds (designated as “catalytic”).[74, 81-85]

For the mechanism in this cure reactions, it has been generally proposed that the reactions occur through a concerted termolecular intermediate consisting of epoxides, amines, and/or hydroxyls, although some reports suggested other possibilities of more complexes can affect the reactions.[86, 87] In this mechanism, the ring opening of epoxide groups is catalyzed by hydrogen bond between the oxygen of the epoxide and the hydrogen of the donor. This protonation is followed by nucleophilic attack of the amine, in which epoxide ring is now easily opened via a termolecular transition step. Subsequently, the reaction completed with a rapid displacement of the proton.[14] The reactions with the assumption of the formation of termolecular intermediates can be displayed as shown in Figure 2-1.

Since the epoxy-amine reaction can be greatly affected by the catalyzed effect of the compounds which generate hydrogen bonds as the mechanism suggested, many studies also found that the addition of such compounds could significantly accelerate

the reaction between epoxide and amines or other nucleophilic reagents, such as water, alcohols, phenols and imidazole.[10-13, 86, 88]

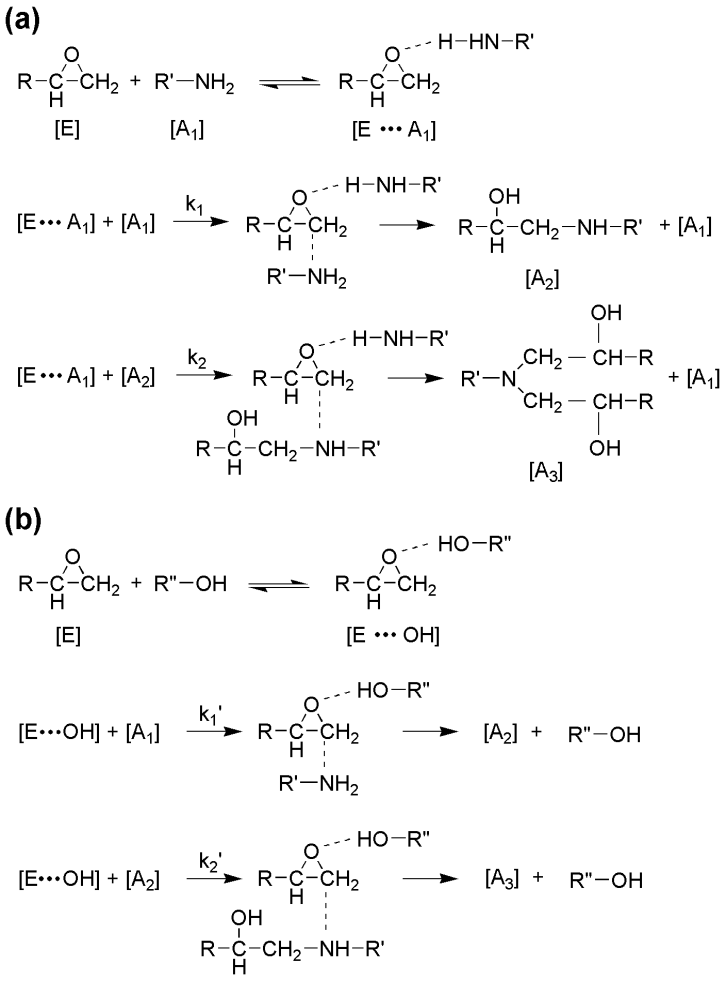

Figure 2-1. Suggested cure mechanism for epoxide-amine reaction involving the formation of termolecular intermediates: (a) non-catalytic reaction, (b) catalytic reaction[74]

One of the unique features in epoxy-amine reaction is the in-situ-formed hydroxyl groups during the reaction, resulting in typical autocatalytic behavior. Since the ring opening of epoxide groups was protonated by hydroxyl containing compound as suggested, the generated hydroxyl group by the reaction accelerates the entire reaction.[14]

Another critical feature of epoxy-amine reaction is the changes of the reaction from chemically controlled in early stages to diffusion-controlled in later stage of curing as the cure progresses and a rigid three-dimensional network is formed. Thus, for the kinetic studies of epoxy-amine reaction, only the early stage of reactions should be considered to obtain pure kinetic parameters while many other studies also suggested modified kinetic models to evaluate the diffusional effect of the later stage of curing reactions.

Cure Kinetic Models for Epoxy-Amine Cure Reactions

The epoxy-amine systems are one of the oldest cross-linked glassy polymers, but the kinetic study of epoxy-amine reaction still remains an attractive field of investigation due to the increasing range of applications of epoxy based products.[89, 90]

To represent a possible kinetic scheme of the cure reaction in epoxy resins, the various kinetic models have been developed, in which the studies have generally followed two approaches: (1) phenomenological; and (2) mechanistic modeling. [91, 92]

In phenomenological or empirical modeling, it employs empirical or semi-empirical kinetic relationships which tend to ignore the chemical detail of the reactions. In this method, the simple n^{th}-order kinetic expression has been utilized combined with another expression describing auto-catalytic behavior for the epoxy-amine reaction.

The well-known Kamal's model combined two kinetic expressions as shown below, and many studies have showed successful applications, in which they have used either original[93-96] or modified expressions[97, 98].

$$\frac{d\alpha}{dt} = \left(K_0 + K_1\alpha^m\right)(1-\alpha)^n \qquad (2\text{-}6)$$

Although the studies employing empirical relationships for the reaction also provide valuable information for process design, the application should be confined to those

conditions in that the approach has not been based upon the fundamental reaction mechanisms.[74] Also, the both expressions of n^{th}-order and autocatalytic behavior assume the existence of a single rate constant throughout the cure, which limited accuracy of the models.[91]

On the other hand, the approach from mechanistic modeling provides a more accurate method, which is analyzed from the balance of chemical species involved in the entire chemical reaction to form mathematical relations connecting the reaction rate path to cure time and temperature.[91] The mechanistic modeling provides advantageous method to understand the given kinetic reaction in terms that they can also be applied into the same systems, but employing different formulations or different temperature histories. For the construction of a kinetic model using this approach, the reaction scheme which represents the cure mechanism should be established in accordance with theoretical and experimental evidences, which need to apply multiple parameters estimation for a non-analytical expression of kinetics.[91]

A number of kinetic models with this mechanistic modeling method have been established to describe the cure reaction of either the pure epoxy-amine systems or the systems in the presence of other compounds such as hydroxyl-containing accelerators. Xu et al. derived a kinetic model with three parameters to describe the cure mechanisms of pure epoxide-amine reactions assuming the non-catalyzed reaction of secondary amines are much slow, thus ignored.[74] Mijovic et al. suggested a modified kinetic model with four parameters based upon their investigation that different types of hydrogen-bonded transition complexes could influence the entire reaction in various epoxy-amine systems.[87, 99, 100] Paz-Aubin used a four parameter model, which consider

the effect of free volume of polymer network on cure kinetics.[101] Raman and Palmese suggested a two parameter model to describe the effect of added solvent on epoxy-amine cure kinetics.[6]

Although various kinetic models have been established through the mechanistic modeling method to show the kinetic relations in their own system, the generalized feature can be expressed as descirbing the two principal paths of non-catalytic reaction and catalytic reaction based on the existence of different transition complexes Thus, when the general feature of the two reaction is considered into the basic epoxy-amine systems, the kinetic equations can be derived as follows, which take account of the catalyzed effect of compounds containing nitrogen-hydrogen bonds (non-catalytic) and those by oxygen-hydrogen bonds (catalytic).

$$-\frac{d[A_1]}{dt} = -k_1[E][A_1]^2 + k_1'[E][A_1][OH] \quad (2\text{-}7)$$

$$\frac{d[A_3]}{dt} = -k_2[E][A_1][A_2] + k_2'[E][A_2][OH] \quad (2\text{-}8)$$

where k_1' and k_1 indicates that the non-catalytic and catalytic kinetic parameters for epoxy-primary amine addition while k_2' and k_2 are the those for epoxy-secondary amine addition, respectively.

In this work, the general kinetic expression shown above has been modified to directly compare the effect of hydroxyl from water addition and that from auto-acceleration by the reaction. The detailed description is discussed in Chapter 4.

Functional Group Analysis using FT-IR Spectrometry

In order to monitor the cure kinetics of the epoxy-amine systems, various techniques have been utilized such as epoxide titration, size exclusion chromatography,

differential scanning calorimetry, nuclear magnetic resonance (NMR), and Fourier Transform infrared (FT-IR) spectroscopy. FT-IR spectroscopy has been mostly used for this purpose, providing a convenient way to observe a quantitative amount of functional groups involved in the reaction with sufficient quality to allow differential analysis of the data.[6, 79]

In order to investigate of cure kinetics of epoxy-amine thermoset, concentrations of various functional groups involved in this reaction should be revealed. To monitor the changes in the concentrations of primary amines and epoxides, near IR spectra directly provide quantitative profiles of concentrations. From typical NIR spectra for DGEBA-Jeffamine system, the area of the peak around 4530 cm^{-1} provides the information about the concentration of epoxide while the area of the peak around 4930cm^{-1} presents the concentration about the primary amine. In addition, the phenyl peak around 4622 cm^{-1} gives the convenient method to normalize the each area of epoxide and primary amine, which used as an internal standard.[6, 74, 102, 103]

On the other hand, for the concentration profiles of secondary and tertiary amines, mass balance equation shown below has been utilized.[6, 79]

$$[A_1] + [A_2] + [A_3] = [A_1]_0 \quad (2\text{-}9)$$

$$[E]_0 - [E] = [A_2] + 2[A_3] = [OH]_{auto} \quad (2\text{-}10)$$

where [E], $[A_1]$, $[A_2]$, $[A_3]$, and [OH] are the concentrations of epoxide, primary amine, secondary amine, tertiary amine and hydroxyl groups present in the system, respectively. $[OH]_{auto}$ refers to the hydroxyl groups generated during the chemical reaction.

Epoxy Resins for Structural Strengthening Application

Durability of Interfacial Bonding between Epoxy and Cementitious Materials with Hygrothermal Exposure

Epoxy resin as a seal coat and impregnating resin has been widely used for structural strengthening application such as a rehabilitation of concrete structures using externally bonded carbon fiber-reinforced polymer (CFRP) composites, providing high performances of strength, stiffness, and resistance to creep.[15, 104] Although epoxy resins provide the high qualities of tensile and adhesive properties for the structural strengthening, the strengthened systems with epoxies has shown critical degradation of its performance with environmental exposure conditions such as moisture, temperature, and various solutions like chloride, alkali, and salt water.[105-112]

Many studies have revealed that degradation of interfacial bonding between epoxy resin and cemetitious materials with environmental exposure is the main reason for the loss of strength in this structural application.[106, 108, 112] These authors showed that environmental exposure induced adhesive failure, which occurred between epoxy resin and concrete, while the unexposed system displayed cohesive failure, i.e. the failure occurred from a crack, which is initiated from the concrete specimen, which supports the concept that interfacial bond degradation is most responsible for the loss of performance in this system.

The studies of environmental effects on the durability of bond strength between cementitious materials and epoxy resins can be generally categorized into three groups, based upon the exposure environment into which a given system has been introduced: (1) Continuous exposure to pure water (immersion or high humidity); (2) Continuous exposure to various synthetic chemical solutions other than pure water such as alkali,

chloride, salt water, and sea water; and (3) Cyclic exposure (wet/dry or freeze/thaw). Tables 2-1, 2-2, and 2-3 summarize results from the literature regarding the durability of bond strength of either CFRP bonded concrete/mortar using epoxy adhesives or epoxy bonded concrete/mortar without the presence of carbon fibers. As shown in the results, it is observed that either significant losses in bond strength or change in failure mode from cohesive to adhesive occurs with exposure.

Although there are many studies reporting a decrease in bond strength between epoxy and cemetitious materials under various environmental exposure, few studies investigate methods to effectively maintain or enhance the durability of the bond strength under the exposure.

Table 2-1. Effects of continuous water exposure on the durability of epoxy/concrete or FRP bond strengths

Materials	Exposure conditions	Testing	Results
Pre-cured CFRP laminate bonded with epoxy	100% RH, 23˚C, 50˚C / 0-56 days	Shear / peel tests	Dry specimens failed cohesively. Wet specimens failed adhesively. 50-60% loss in fracture toughness.[106]
Concrete bonded with epoxy	Immersion / 135 days	Bond strength (ASTM C882)	20-50% loss in bond strength[113]
Concrete bonded with epoxy	Immersion at 23˚C / 48 hrs + 48 hrs drying	Bond strength (ASTM C882)	17-35% loss in bond strength[105]
CFRP wet layup on mortar	Immersion at ambient temp. / 60 days	4 point flexure	24-33% loss in strength[109]
CFRP wet layup on mortar	Immersion at ambient temp. / 60 days	Peel test	10-20% decrease in G_{IIc}. Fracture mode changes from primarily cohesive to adhesive. Almost no change in G_{Ic}.[110]
CFRP wet layup on concrete	Immersion / 3-8 weeks	Modified double cantilever beam	Dry specimens failed cohesively. Wet specimens failed adhesively. 35-75% loss in interfacial fracture toughness.[112]

Table 2-2. Effect of continuous exposure to synthetic solutions and sea water on the durability of epoxy/concrete or FRP bond strengths

Materials / Fluid	Exposure conditions	Testing	Results
Concrete bonded with epoxy / Seawater	RT / 6, 12, 18 months	Split tensile, slant shear	25% decrease in bond strength after 18 months. Failure mode changes from cohesive to adhesive with aging time.[108]
Concrete bonded with epoxy / Seawater	Ambient, 60˚C, 80˚C / Up to 18 months	Split tensile, slant shear, flexure, compression	No apparent difference in strengths[114]
CFRP wet layup on mortar / Synthetic seawater	Ambient temp. / 60 days	4 point flexure	13-26% loss in strength[109]
CFRP wet layup on mortar / Synthetic seawater	Ambient temp. / 60 days	Peel test	25-30% decrease in G_{IIc}. Almost no changes in G_{Ic}[110]

Table 2-3. Effects of cyclic exposure on the durability of epoxy/concrete or FRP bond strengths

Materials /Fluid	Exposure conditions	Testing	Results
CFRP or GFRP wet layup / Simulated seawater	4hrs immersion / 2hrs at 35˚C, 90%RH (75 days)	4 point flexure	7-33% loss in flexural strength[111]
CFRP wet layup, one steel bar in concrete / Calcium chloride solution	16 hrs at -17˚C / 8 hrs at RT; or 16 hrs immersion / 8 hrs dry (50 / 100 days)	4 point flexure	18-21% loss in strength for freeze-thaw, 10-19% loss in strength for immersion[107]
Concrete bonded with epoxy / Seawater	Immersed during high tide only (6, 12, 18 months)	Split tensile, slant shear	25% decrease in bond strength after 18 months. Specimens become protected by build-up of shells. Failure mode changes from cohesive to adhesive with aging time.[108]
CFRP wet layup / Salt water, outdoor exposure	17 months salt water at 10~60˚C / 6 months outdoor ; 23 months outdoor	Torsion, tension (metal disk / CFRP)	0-55% loss in bond strength for salt water exposure; 0-45% loss in bond strength for outdoor exposure[115]
CFRP wet layup on mortar / Freeze-thaw	-15.5ºC for 24 hrs / 20ºC for 24 hrs (60 days)	4 point Flexure	0-15% loss in strength[109]
CFRP or GFRP wet layup on mortar / Freeze-thaw	-15.5ºC for 24 hrs / 20ºC for 24 hrs (60 days)	Peel test	0-30% increase in both G_{Ic} and G_{IIc}[110]

Adhesion Mechanism of Epoxy Bonding with Cementitious Materials

For the general description of the adhesion between various types of materials, several categories of mechanisms have been proposed: mechanical interlocking, chemical bonding, electrostatic adhesion, inter-diffusion, and adsorption.[116-120] In the case of the structural strengthening application which employs an adhesive bonding between organic adhesives and cemetitious materials, the theories of mechanical interlocking and chemical bonding can be generally accepted as operative mechanisms.[121]

The mechanical interlocking theory suggests that good adhesion between two materials occurs when an adhesive penetrates into the pores, holes and crevices and other irregularities of the adhered surface of a substrate, and locks mechanically to the substrate.[110, 116-118, 120] Lin et al. have shown that, in their strengthening application of epoxy resins, more rough and deep surface topography of concrete surface before bonding, attained by water-jet or blast sanding, enhanced the bond strength of the system.[122] Momayez et al. also suggested that rough surface preparation of concrete lead to higher bond strength through their pull-off and slant shear testing method.[123] Although the mechanical interlocking seems to promote the bonding strength between two materials, when considering that good adhesion is also accompanied with smooth adherened as well, there should be another type of mechanism which strongly affects the bonding.

For another type of the adhesion mechanism to describe the bonding between epoxy adhesives and cementitious materials, the mechanism of chemical bonding is taken into account. Based upon the chemical nature of both materials in which the concrete surface contains silanol groups and epoxy adhesives contains hydroxyl

groups, it is highly probable that hydrogen bonding plays a larger role for the bonding. A few studies that examine the chemical nature of the interface also suggest that hydrogen bonds are formed between epoxy and concrete, and that water tends to cluster at the interface and form hydrogen bonds.[124-126] When considering similar mechanism proposed for the description used for the degradation in epoxy-metal adhesion under humid environments, in which a decrease in bond strength have been ascribed to displacement of epoxy with water, which preferentially forms hydrogen bonds with the adherend, the hydrogen bonding at the epoxy-concrete interface could also be considered as a factor to affect the durability in the bonding of epoxy-cememtitous materials.[34, 35]

Silane Coupling Agents to Enhance the Durability of Adhesive Strength during Hygrothermal Exposure

To enhance the durability of bond strength between various organic and inorganic materials, silane coupling agents has been extensively attempted, in which the coupling agents connect two materials through covalent bonds which are more durable against water attack than hydrogen bonds.

Adhesion enhancement is also attributed to the blocking of lateral diffusion of water by barriers due to the presence of the hydrophobic silane.[127] In addition, capture of the excess moisture coming from the surrounding environment occurs by the hydrolysis reactions of active alkoxy groups in modified resins, by which the free-state water absorbed can be consumed.[128]

Silane coupling agents are silicon-based chemicals that contain two types of reactants – inorganic and organic – in the same molecule. A typical general structure is $(RO)_3Si(CH)_nX$, where RO is a hydrolyzable group such as methoxy, ethoxy, and X is

an organofunctional group such as amino, epoxy. A silane coupling agent acts at an interface between an inorganic substrate such as glasses, metals or minerals and organic materials to bond two incompatible materials.[129]

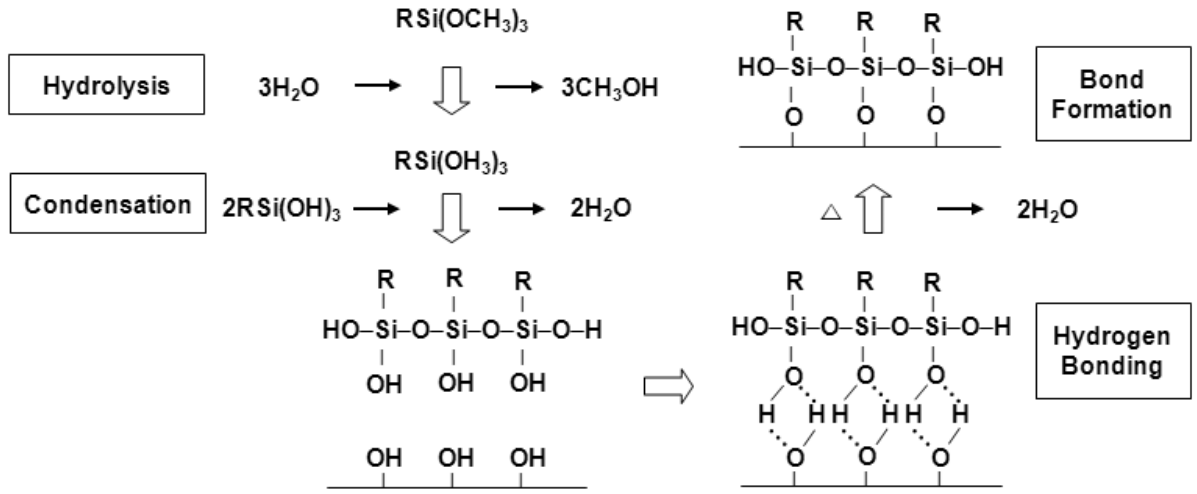

Figure 2-2. Reaction process of Alkoxy Silane, R is organofunctional group in this figure.[129]

There are four steps for the silane coupling reactions (Figure 2-2). First, the alkoxy (RO) groups are hydrolyzed. Second, after the hydrolysis of the first and second alkoxy groups, condensation to oligomers occurs. Third, the hydroxyl group is hydrogen-bonded with hydroxyl sites on the substrate after orientation of third methoxy group on hydrolysis. Finally, a covalent bond is formed with the substrate during drying or curing with water liberated. At the interface, there is usually only one bond from each silicon of the organosilane to the substrate surface. A moderate cure cycle will leave silanol groups remaining in free form and, along with any silane organofunctionality, may bond with the subsequent topcoat, forming an interpenetrating polymer network and providing improved adhesion.[129]

Silane coupling agents as a primer are widely used for improving adhesion between organic materials and inorganic materials. Many papers have reported enhanced durability of bond strength between metals/ceramics and epoxy resins under humid environments.[130-132] Lin Ye et al reported the use of a silane coupling agent to improve the adhesion bonding between CFRP and concrete using epoxy adhesive.[122] 3-Glycidoxypropyltrimethoxysilane, one of the epoxy-functional silane coupling agents was employed to the system, and its use was not very helpful for the mechanical properties of the system. The fracture energy of crack growth was slightly increased by the silane coupling agent. However, the system was not under environmental exposure such as water and temperature before the fracture testing. If the system had been under water/moisture exposure, it is expected that the system would have demonstrated improved durability of mechanical properties by the effects of the silane coupling agent which prevents the water from displacing the epoxy at the interface.

CHAPTER 3
COMPLEX HYGROTHERMAL EFFECTS ON GLASS TRANSITION OF EPOXY-AMINE THERMOSETS: A STUDY OF A MODEL EPOXY-AMINE

Background

The glass-transition temperature (T_g) of a polymer is the temperature at which dramatic changes in properties occur, particularly reduction in strength, stiffness, and resistance to creep. Thus, there is a desire among structural engineers and designers to use the T_g as a materials specification in codes and standards. However, for thermosetting materials used as adhesives and as a component of FRP, such as epoxies and vinyl esters, the glass transition is not a single value. In these materials, the glass transition can vary with factors such as degree of cure and extent of water absorption. These factors are exacerbated by the fact that in civil engineering applications, the material is cured under ambient conditions, and thus is typically not fully cured. Thus, an understanding of how these factors affect the glass transition is of particular importance for defining upper temperature use limits in these applications.

Water absorption into various types of polymer systems has been extensively studied including amorphous[133-136], semi-crystalline[137-139], cross-linked polymers[18, 21], and copolymers[140, 141], because of the general tendency of water absorption to induce a loss in physical properties such as a decrease in T_g. Plasticization by absorbed water has been generally regarded as the major factor resulting in this property loss.

As previously discussed in Chapter 2, although property degradation due to hygrothermal exposure is also a critical issue in epoxy resins, many studies have reported anomalous behavior, i.e., an increase in physical properties of epoxy systems after hygrothermal exposure, such as an increase in T_g or tensile modulus. There has been mechanisms suggested to describe this abnormal behavior, such as post-curing

reactions caused by the elevated temperature of the water used for exposure; different states of hydrogen bonded water molecules, one of which creates secondary cross-linking; and effect of biphasic structure.

It is important to note, however, that for none of these explanations is there any direct experimental evidence supporting them, and a clear explanation of the mechanism for this anomalous behavior remains unanswered. In this study, we have also observed similar anomalous increases in T_g with hygrothermal exposure. We focus on direct experimental measurements that allow us to specifically describe the mechanism for this behavior

Experimental Section

Materials

The material used in this work is a two-part epoxy, diglycidyl ether of bisphenol A (DGEBA) and poly(oxypropylene) diamine (POPDA, Jeffamine D-230), purchased from Huntsman. Figure 3-1 illustrates the chemical structures of DGEBA and POPDA. The mass ratio of DGEBA to POPDA was 100 to 32.9, corresponding to stoichiometric equivalence between functional groups. The two liquid components were mixed vigorously for 10 min to ensure even mixing. The mixed material was then degassed for 30 mins under vacuum to remove air bubbles. Specimens were cured at room temperature (RT, 22-23°C) for 4 weeks before the exposure was started, ensuring enough time for the curing reaction at RT. Exposure environments consisted of immersion into clean tap water at temperatures of 30, 40, 50, and 60°C. Details of the cure and exposure conditions for hygrothermal exposure are shown in Table 3-1.

To construct a master plot of T_g versus cross-link density for the unexposed epoxy, we employed various cure conditions to obtain specimens with a wide range of

conversion values. The specific information for cure conditions for these specimens is shown in Table 3-2.

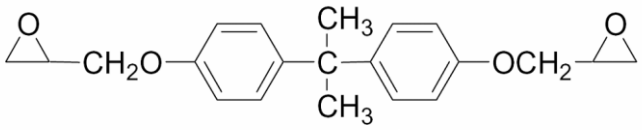

DGEBA

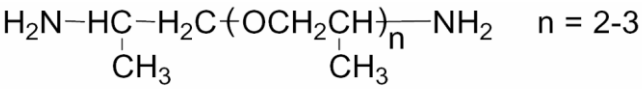

POPDA

Figure 3-1. Chemical structures of diglycidyl ether of bisphenol A (DGEBA) and poly(oxypropylene)diamine (POPDA).

Table 3-1. Cure and exposure conditions for hygrothermal exposure.

Type of Experiment	Cure condition	Exposure Condition
Monitoring of changes in T_g using DSC Monitoring of changes in crosslink density using FT-IR	RT/28days	Water immersion at 30°, 40°, 50°, and 60°C / 1, 2, 4, 7, 14 and 28 days

Table 3-2. Cure conditions for the master plot of T_g vs. crosslink density for unexposed epoxy.

Cure condition	T_g (°C)	Epoxide conversion
RT/0~28days	-56.2~46.8	0.00~0.86
80°C/110min	54.4	0.90
90°C/80min	61.1	0.93
90°C/110min	69.0	0.97
50°C/60min + 80°C/120min + 125°C/180min	76.7	1.00

Techniques

Differential scanning calorimetry (DSC; DSC 220, Seiko instruments) was utilized to identify changes in T_g with hygrothermal exposure. Samples were prepared by depositing a small amount of the epoxy formulation directly into the bottom of a DSC aluminum pan before the system was cured in order to maximize the thermal contact between the sample and the pan and avoid the artifacts often observed during first DSC scans when there is poor thermal contact. After the sample was cured in the bottom of the pan either the pan with the sample in it was immersed in water for hygrothermal exposure, or the pan was immediately used for T_g measurement. Following hygrothermal exposure, the surface of the sample was wiped carefully with a paper tissue to remove any excess surface water. The pan was immediately sealed and placed directly into the DSC chamber for the measurement. To reduce the potential for any cure occurring during the measurement, we determined the T_g from the first run of each specimen. After placing the sample in the DSC, the heat flow signal was allowed to fully equilibrate before beginning the temperature scan. The temperature range for the measurement was -30 to 130°C at a heating rate of 10°C/min, and three replicas were fabricated for each exposure condition to obtain the average value. The T_g was chosen from the midpoint of the tangent between the extrapolated baselines before and after the transition.

To measure cross-link density and the amount of absorbed water, we used Fourier transform infrared spectrometry (FTIR; Nicolet Magna 760, Thermo Electron Cooperation) with a CaF beamsplitter and an MCT detector. Near-infrared spectra were recorded over the range of 3800-7400 cm^{-1} using 32 scans at a resolution of 4 cm^{-1}. Thin films with 0.5 mm thickness were cast between glass plates using Teflon® spacers.

After the selected cure condition as shown in Tables 3-1 and 3-2, the films were either immersed in water for hygrothermal exposure or directly used for the FTIR measurement.

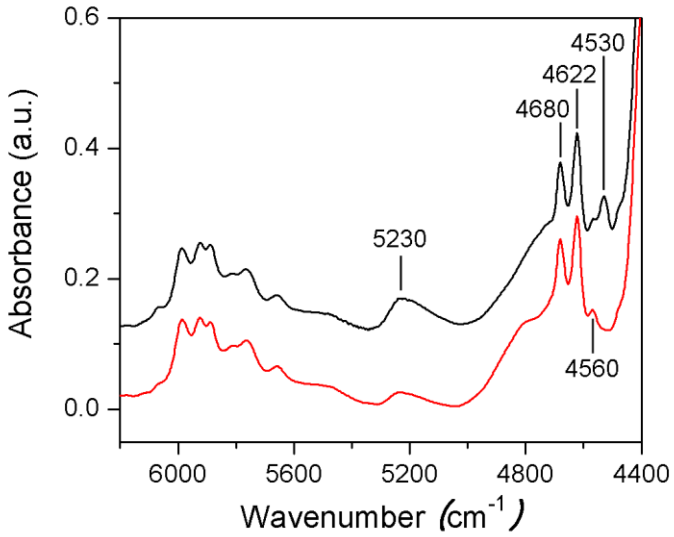

Figure 3-2. Typical NIR spectra for unexposed systems with different cure conditions: Cured at RT for 28 days (top) and cured at 50°C for 1 h followed by 80°C for 2 h and 125°C for 3 h (bottom).

Typical NIR spectra for stoichiometric systems without exposure are shown in Figure 3-2. The reduction in the epoxide absorbance at 4530 cm^{-1} for the higher temperature cure is evident in this figure. For the quantitative analysis of cross-link density changes, the area of the epoxide peak around 4530 cm^{-1} normalized to the phenyl peak around 4622 cm^{-1} was calculated for each exposure condition. The epoxy conversion was then calculated by $\alpha = 1 - A(t)/A(0)$, where $A(t)/A(0)$ is the ratio of normalized peak area with respect to the uncured and unexposed system. For quantitative analysis in accordance with the Beer-Lambert law, the absorbance was less than 1.0. The baselines for area calculation of those peaks were chosen as suggested

by Dannernberg without any baseline correction.[103] In Figure 3-2, there is a small unknown peak at around 4560 cm^{-1} that overlaps the epoxide peak. The area of this peak as measured on a stoichiometric, fully cured sample was subtracted from the total area of the peaks in that region in order to determine the absorbance due only to epoxide groups.

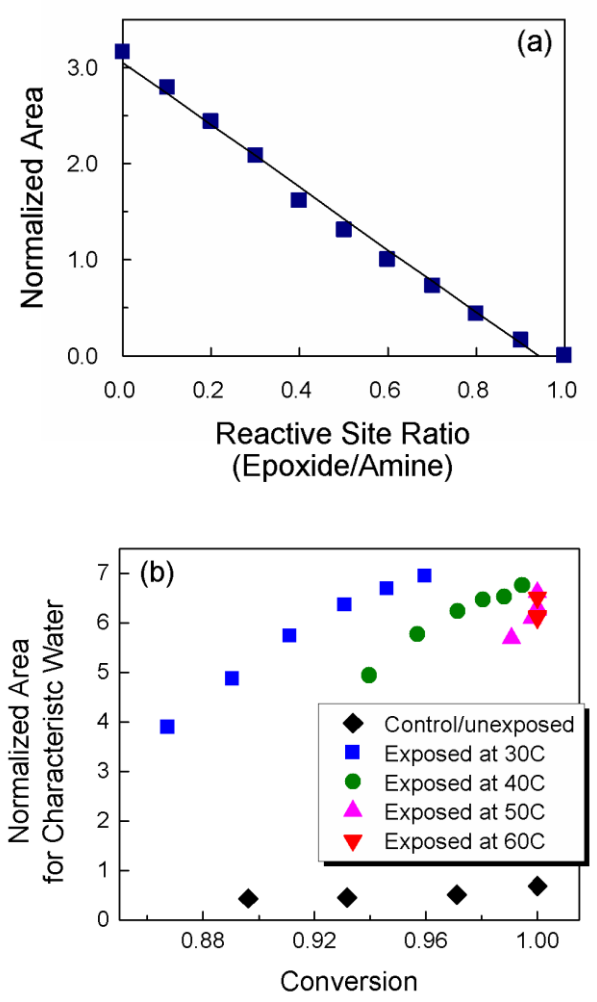

Figure 3-3. Experimental confirmation of reliability of quantitative analyses from FTIR: (a) Plot of normalized area assigned to epoxide at 4530 cm^{-1} with variation in epoxide/amine ratio. The correlation coefficient value, R^2 is 0.99. (b) Normalized area for characteristic water peak around 5230 cm^{-1} for various unexposed and exposed systems.

Although the reliability of this quantitative analysis of the epoxy cure reaction was confirmed by previous workers[102, 103], we reconfirmed it for our system. To demonstrate the reliability, normalized peak areas in the spectra were measured with respect to the epoxide concentration. In this experiment, specimens with different epoxide concentrations were cured at high temperature for enough time to ensure complete reaction between epoxide and amine functional groups. The cure condition was 50°C for 1 hour followed by 80°C for 2 hours and 125°C for 3 hours. Formulations were smeared onto KBr IR disposable cards for the samples with pure DGEBA and those with a lower amine ratio because they did not solidify after the cure. The other samples were prepared by casting thin films with a 0.5 mm thickness using glass plates and Teflon® spacers. As shown in Figure 3-3 (a), the normalized absorbances decrease linearly as epoxide concentration decreases, which indicates that our analysis is reliable and obeys the Beer-Lambert law.

To estimate the amount of absorbed water for each exposure condition, the normalized area of the characteristic water peak around 5230 cm^{-1} was obtained, which has been assigned to a combination of asymmetric stretching (υas) and in-plane deformation (δ) of water.[142-144] The normalized area of the characteristic water peak is known to be a way to measure the amount of absorbed water in various polymer-water systems, where the normalized area is proportional to the real amount of absorbed water.[142-145] In this work, the region from 4972 to 5342 cm^{-1} was taken to measure the area and normalized by the phenyl absorbance at 4622 cm^{-1}. Because these are normalized values we can not use them to determine absolute concentrations of water present; however, because the normalized areas are proportional to the amount of

water they can be used for relative comparisons. It is also important to note that this peak includes hydroxyl groups generated in the epoxy network due to the cure reaction. To check the contribution of these hydroxyl groups to the total absorbance, we made measurements for both exposed and unexposed samples over a range of conversions. As shown in Figure 3-3 (b), for the range of epoxide conversion between 0.86 and 1.00, the absorbance due to the hydroxyl groups is approximately constant, indicating that the change in absorbance of this peak is due to the change in amount of absorbed water.

Results

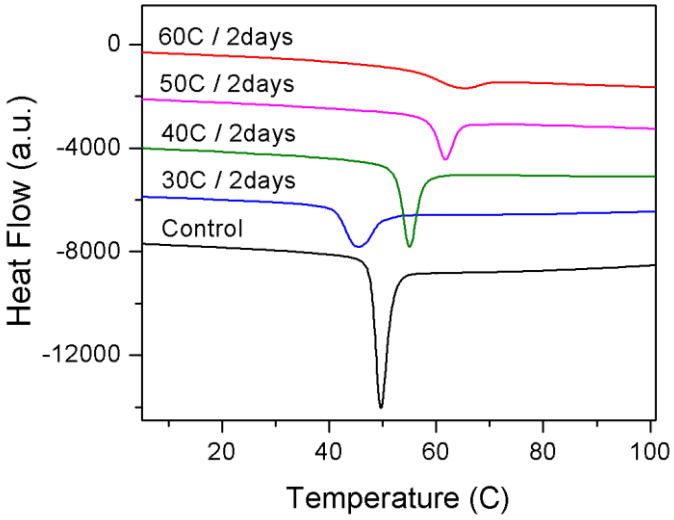

Figure 3-4. Typical DSC curves after water immersion for 2 days at different temperatures compared with no exposure.

Our results, shown in Figure 3-4, clearly indicate that “anomalous” behavior, defined as an increase in glass transition after exposure to water, occurs. As shown in Figure 3-4, exposure to 40, 50, and 60°C water for 2 days results in significant increases in T_g as compared to the control specimen that was measured before the exposure was started. On the contrary, when the specimens were exposed to 30°C water for 2 days, they showed a lower T_g than the control.

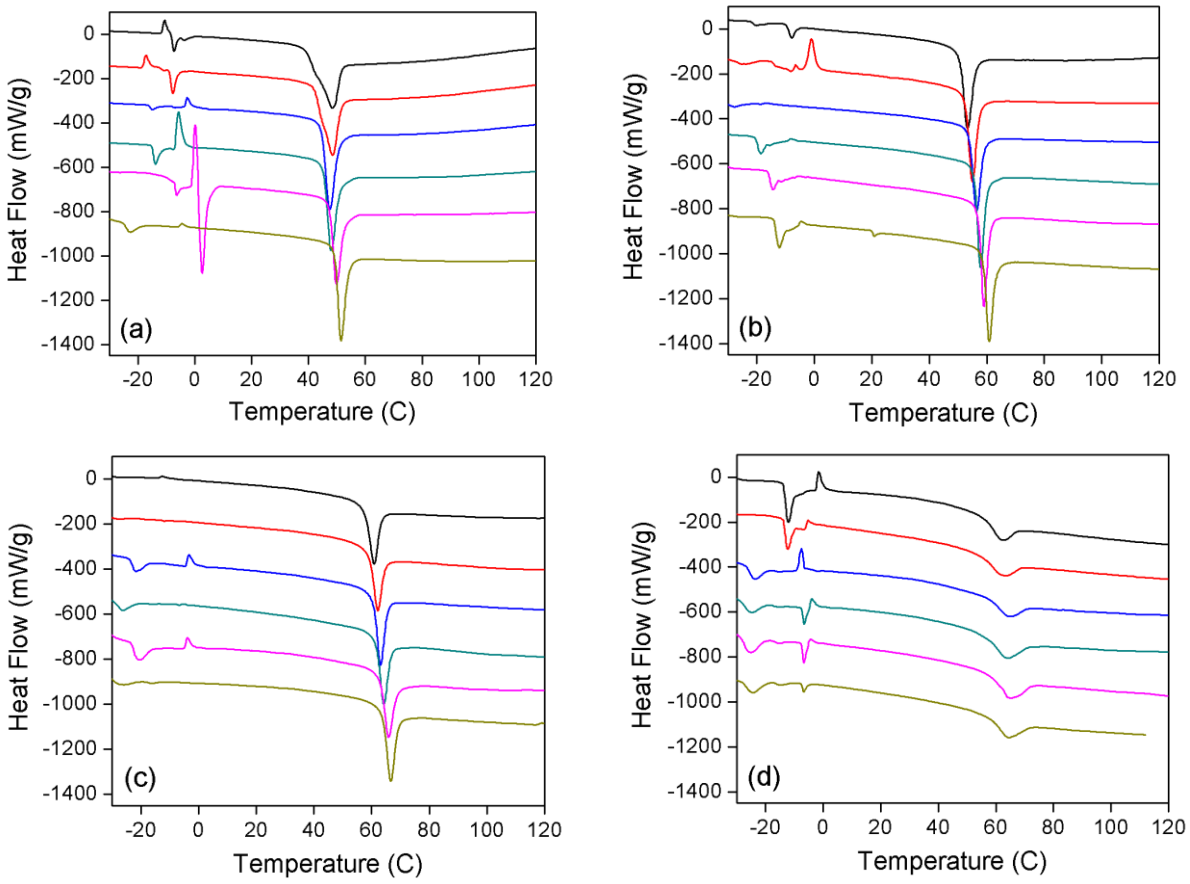

Figure 3-5. Changes in DSC curves as a function of immersion time for each exposure condition. From top of each set of DSC scans: Exposed for 1, 2, 4, 7, 14, and 28 days. Exposed in (a) 30, (b) 40, (c) 50, and (d) 60°C water.

From Figure 3-5 showing the entire DSC scans for each exposed system, it is shown that endothermic aging peaks are superimposed around the glass-transition region. Amorphous polymers, which are cooled down to below T_g or isothermally cured at a temperature below T_g, typically show enthalpy relaxation upon reheating, which is observed as an endothermic peak in the DSC scan. This behavior is well-known as a structural enthalpy relaxation or physical aging, and is a result of the recovery of enthalpy trapped in the glassy state of the material during aging.[146-151] Figure 3-5 shows that the intensity of the endothermic peaks rapidly decreased upon exposure at 60°C,

which is attributed to the fact that the exposure temperature is above T_g of the system, leading the system closer to thermodynamic equilibrium as exposure continues.[147, 149]

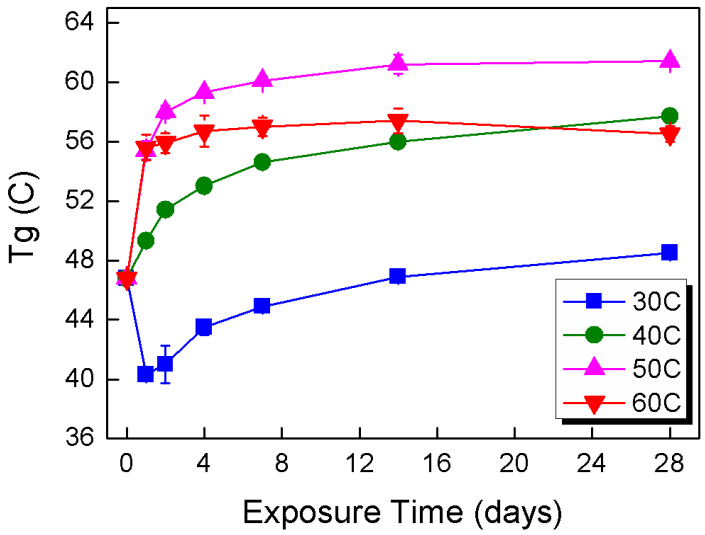

Figure 3-6. Changes in T_g after water immersion at different temperatures. Samples were cured for 4 weeks at room temperature in air before exposure was started. In this picture, the size of the error bars displaying the standard deviation is too small to be shown at some points.

To follow the changes in T_g for each exposure condition, we measured T_g as a function of time for each exposure condition. As shown in Figure 3-6, samples exposed at 40 and 50°C show continuous increases in T_g with exposure until the rates of increase slow down and approach saturation points. Exposures at 30 and 60°C show some interesting results that are contrary to each other. For samples exposed at 30°C, an initial decrease in T_g was followed by an increase, whereas samples exposed at 60°C showed an increase in T_g at the beginning stage, but a slight decrease in T_g at the later stage of exposure.

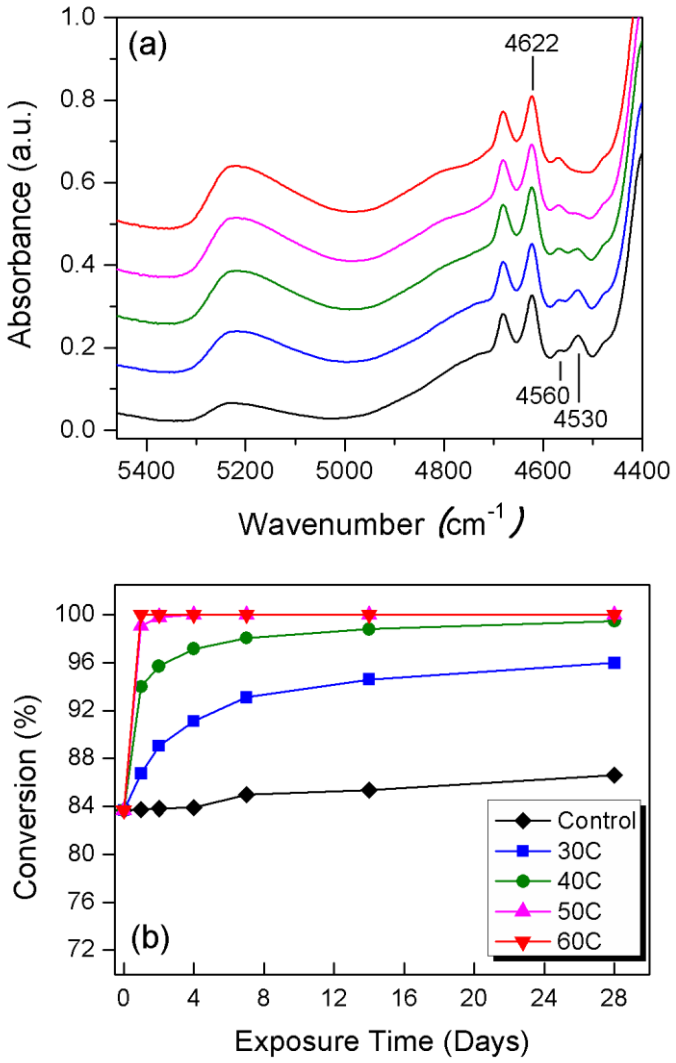

Figure 3-7. Typical Near-Infrared spectra and changes in conversion for samples with different exposure conditions: (a) Near-infrared spectra for samples immersed in water for 1 day at different temperatures compared with an unexposed control sample. Cure condition was 4 weeks at room temperature in air before the exposure was started. (b) Changes in conversion at different exposure conditions after curing 4 weeks at room temperature in air.

To examine the mechanisms of this anomalous “property gain”, changes in conversion were investigated using NIR spectroscopy. Typical NIR spectra are displayed in Figure 3-7 (a), in which samples exposed to water immersion for 1 day at different temperatures are compared with control samples which had been exposed to

air for 1 day. The cure condition was the same as used for measuring changes in T_g, namely, 4 weeks at room temperature in air before the exposure was started. As shown in Figure 3-7 (a), the area of the epoxide peak around 4530 cm^{-1} decreased after hygrothermal exposure compared with the control, indicating a post-curing reaction occurred during the exposure that resulted in an increase in conversion.

To follow the changes in conversion for each exposure condition, we measured conversion as a function of time for each exposure condition. Figure 3-7 (b) shows that the epoxide conversion increased for all the exposure conditions, resulting in significant increases in cross-link density compared with the unexposed sample. This result shows that the elevated temperature of the water caused additional cure, even at a low temperature such as 30°C.

When this figure is compared to the changes in T_g with hygrothermal exposure in Figure 3-6, it is obvious that the increase in cross-link density leads to the “anomalous” increase in T_g with hygrothermal exposure. Careful comparison of Figures 3-6 and 3-7 (b) also shows that the hygrothermal behavior is complex. For example, the samples exposed at 30°C showed an initial decrease in T_g, and samples exposed at 60°C showed a decrease in T_g at the latter stages of exposure, even though the conversion is continuously increasing with exposure. Thus, we can conclude that plasticization also plays a significant role in determining the properties of this system.

Discussion

For the epoxy system being examined in this study, hygrothermal exposure induces complex behavior in which an increase in glass transition due to increasing cure simultaneously occurs with a decrease in glass transition due to plasticization. From the comparison of the two figures showing changes in T_g and conversion with

hygrothermal exposure (Figures 3-6 and 3-7 (b)), we can see that the increase in T_g due to additional cure and the decrease in T_g due to plasticization are in competition with each other during exposure.

When observing the initial stage of the sample exposure between 0 and 1 day at 30°C, plasticization has the predominant effect on T_g, compared with additional cure, causing a decrease in T_g despite an increase in cross-link density. However, as exposure continues, the additional cure becomes the dominating factor, resulting in an increase in T_g. On the contrary, for exposure at 60°C, a continuous increase in T_g at the initial stage of the exposure indicates that additional cure dominates the change in T_g. The effect of plasticization becomes more important at the later stage of exposure, resulting in a slight decrease in T_g. With regards to exposure at 40 and 50°C, it is observed that the increase in cross-link density is dominant throughout the exposure, resulting in a monotonic increase in T_g. When comparing samples at 50 and 60°C, the T_g for 50°C samples is larger than T_g for 60°C samples after 8 days exposure even though both had already reached 100% conversion, which indicates that at 60°C there is more absorbed water, resulting in greater plasticization.

As described previously, two other factors that have been hypothesized to cause this “anomalous” behavior are creation of a hydrogen-bonded network of water and the influence of the epoxy microstructure. To determine the relative importance of these effects, T_g for the unexposed system was plotted as a function of conversion. This “master plot” can then be used to exclude the influence of crosslink density by plotting the results from Figures 3-6 and 3-7 (b) onto this “master plot”, which makes it possible

to compare the T_g values directly between exposed and unexposed systems at the same conversion value.

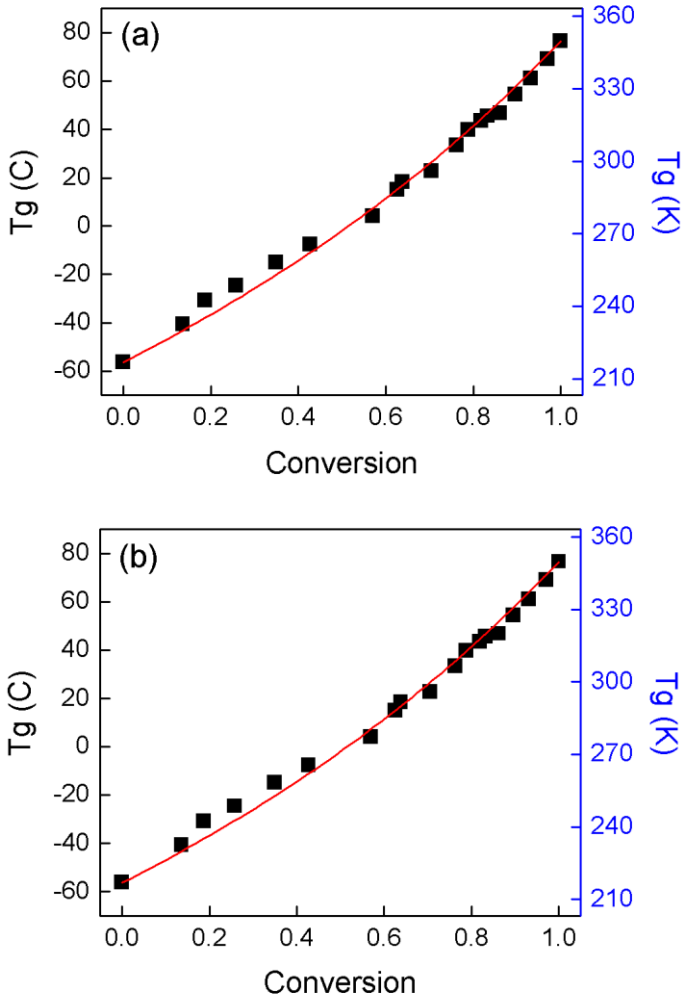

Figure 3-8. T_g versus conversion "master plot" for unexposed epoxy. Points were experimentally obtained and solid lines are fits to theoretical: (a) Equation 3-1 and (b) Equation 3-2.

Cross-link density is known to be one of the important factors to determine the T_g in network polymers. An increase in the cross-link density reduces the chain mobility resulting in an increase in T_g, whereas an increase in molecular weight as well as a decrease in low-molecular-weight components during the curing reaction also increases

the T_g.[69] The relationship between T_g of a network polymer and conversion is well-described elsewhere.[70-72] For derivation of the relationship, a thermodynamic theory is used in which changes in heat capacity of each component and its T_g are correlated to describe the glass transition in copolymer systems. The theory was then developed into the following semi-empirical equation to describe T_g in cross-linked systems with the variation in conversion, assuming ΔC_p is inversely proportional to temperature.

$$T_g = \frac{(1-\alpha)T_{g0} + \alpha(\Delta C_{p\infty} / \Delta C_{p0})T_{g\infty}}{(1-\alpha) + (\Delta C_{p\infty} / \Delta C_{p0})\alpha} \quad (3\text{-}1)$$

where α is conversion, T_{g0} and $T_{g\infty}$ are the T_g values of the monomer and the fully cured network, and ΔC_{p0} and $\Delta C_{p\infty}$ are the heat capacity changes at T_{g0} and $T_{g\infty}$, respectively. Using a similar approach assuming ΔC_p is constant, another semi-empirical equation can be derived as shown below.

$$\ln(T_g) = \frac{(1-\alpha)\ln(T_{g0}) + (\Delta C_{p\infty} / \Delta C_{p0})T_{g\infty}\alpha\ln(T_{g\infty})}{(1-\alpha) + (\Delta C_{p\infty} / \Delta C_{p0})\alpha} \quad (3\text{-}2)$$

To construct the master plot of Tg as a function of conversion, Tg and conversion values under identical cure conditions were experimentally obtained for the unexposed system. Equations 3-1 and 3-2 were used for fitting the experimentally obtained data as shown in Figure 3-8. Both equations have good agreement to the experimental data, with coefficients of determination of 0.99 for both cases. The values of $\Delta C_{p\infty}/\Delta C_{p0}$ as a fitting parameter were 0.69 and 0.88 for Equations 3-1 and 3-2, respectively.

Finally, the values of T_g and conversion for exposed systems, shown in Figures 3-6 and 3-7 (b), were applied to the master plots using Equation 3-2 for the fitting. As shown in Figure 3-9, all the T_g points for the exposed systems are below the line, showing the effect of plasticization independent of crosslink density. This result also

suggests that the contribution of other factors suggested to cause “property gain”, such as different types of hydrogen bonded water and the influence of microstructure are small compared to plasticization.

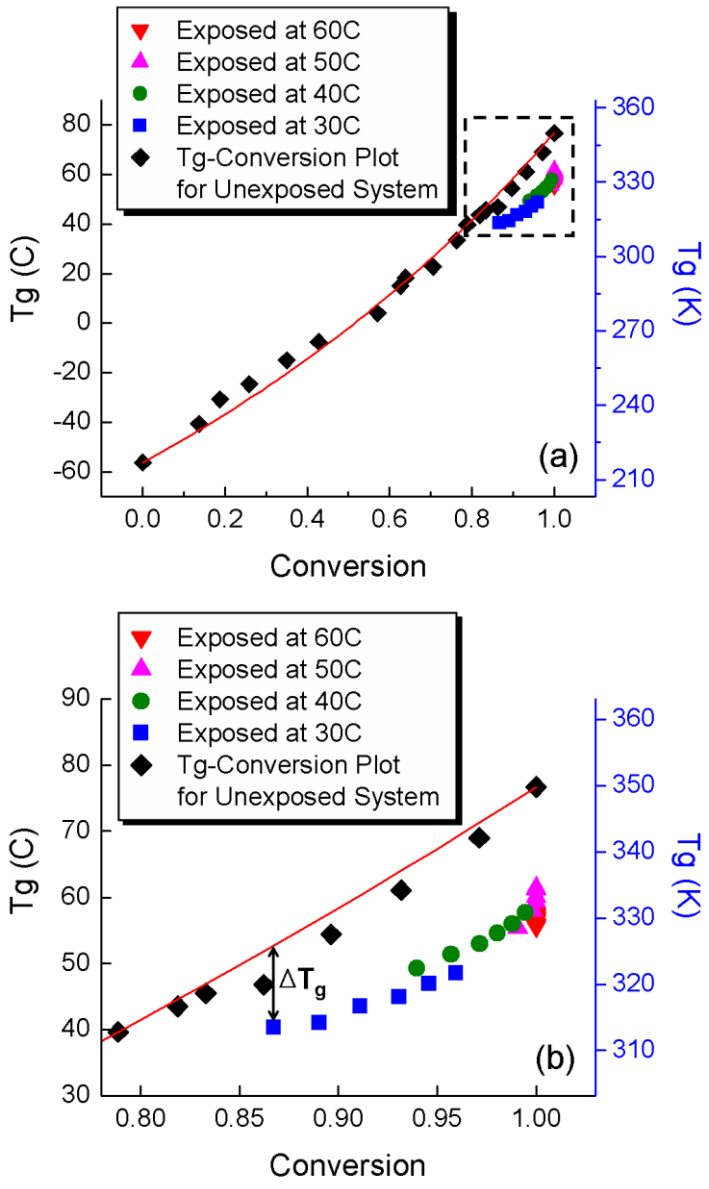

Figure 3-9. Direct comparison of T_g between unexposed and exposed systems using the master plot of T_g versus conversion. The section marked with dotted lines in (a) is magnified in (b).

To further evaluate the plasticization effect quantitatively, we determined ΔT_g, the difference in T_g between unexposed and exposed samples at the same conversion value. Glass transition temperatures for the exposed system were determined directly from DSC measurements, whereas T_g values at the corresponding conversion for the unexposed system were obtained from the values on the fitted curve as indicated in Figure 3-9 (b). Finally, to correlate ΔT_g with the absorbed water amount at each exposure condition, the relative amount of water uptake was determined from the characteristic water peak around 5230 cm^{-1}, which was well-resolved in the NIR spectra of this system.

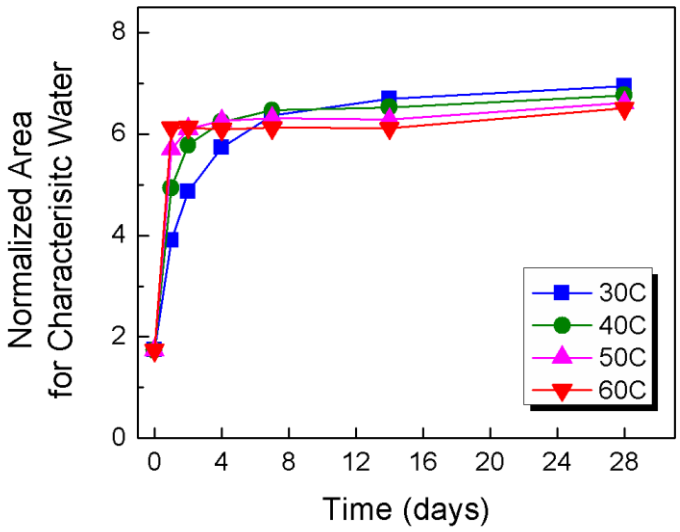

Figure 3-10. Relative amount of water absorption with exposure time estimated by normalized area of the characteristic water peak from NIR.

When the relative amount of absorbed water is evaluated by this method, it shows the typical features of water uptake with exposure time in which water amount increases as exposure continues, ultimately approaching some saturation point, as shown in

Figure 3-10. The rate of increase in absorbed water at the initial stage of the exposure is enhanced as exposure temperature increases, which is also a typical feature in that water absorption of the epoxy system is accelerated with an increase in diffusion rate as temperature increases.

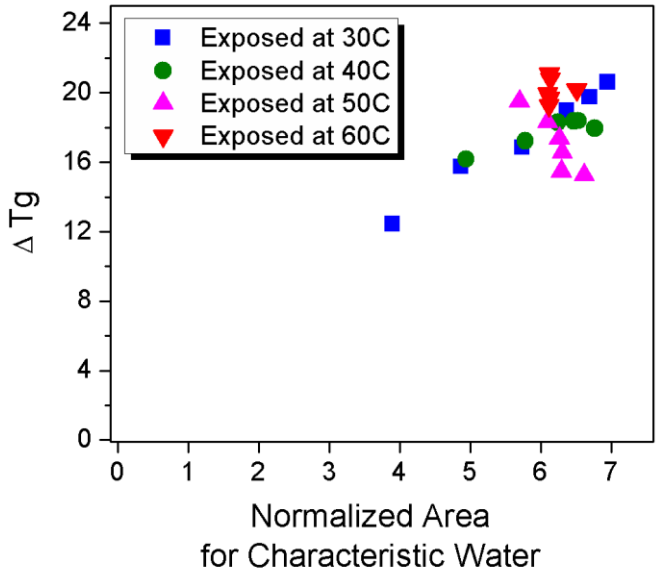

Figure 3-11. T_g differences between unexposed and exposed systems as a function of estimated amount of absorbed water.

Finally, ΔT_g was plotted as a function of the relative absorbed water amount for each exposure condition (Figure 3-11). For samples exposed at 30 and 40°C, ΔT_g increases with water amount, showing the expected behavior of increase in plasticization as the amount of absorbed water increases. However, for the 50 and 60° C samples, some anomalous behavior is observed in which ΔT_g changes independently of water content. This anomalous behavior possibly indicates that there are other factors affecting “property gain” such as secondary types of hydrogen-bonded water and microstructure, although these effects are very small compared with plasticization.

Summary

For the anomalous hygrothermal behavior of an epoxyamine thermoset, in which T_g increased with exposure to water immersion at different temperatures, FT-NIR spectroscopic studies demonstrated that increases in cross-link density due to additional cure during the elevated temperature exposure led to an increase in properties. However, from the feature that the T_g decreased at certain stages of the exposure, it is evident that plasticization by water occurred simultaneously, rendering the hygrothermal behavior to be more complex than originally hypothesized. In this complex hygrothermal behavior, “property gain” by an increase in cross-link density and “property loss” by plasticization occurred simultaneously.

Constructing the plot of T_g versus conversion for the unexposed system provided an excellent method to consider contributions of other factors and exclude the factor of crosslink density. By applying the results for the exposed system onto this “master plot”, it is possible to directly compare the T_g values between exposed and unexposed samples while ruling out the factor of cross-link density. The result indicates that the effect of other factors, such as different types of hydrogen-bonded water and influence of the microstructure, are very small compared to the plasticization effect.

To evaluate the plasticization effect quantitatively, we measured ΔT_g, the difference of T_g between unexposed and exposed samples at the same conversion value, as a function of absorbed water amount. It is observed that ΔT_g increases with absorbed water amount at lower exposure temperatures, whereas ΔT_g changes independently of water amount at higher exposure temperatures. Thus, factors other than additional cure and plasticization may affect T_g at these higher exposure temperatures. Examination of these other factors such as changes in the relative

amounts of the hard and soft phases and different states of hydrogen-bonded water molecules are currently ongoing in order to provide an in-depth understanding of the anomalous behavior in this system.

CHAPTER 4
COMPLEX HYGROTHERMAL EFFECTS ON GLASS TRANSITION OF EPOXY-AMINE THERMOSETS: A STUDY OF COMMERCIAL PRODUCTS

Background

In order to take advantage of easy installation in outdoor or electronic applications, many epoxy-amine adhesives and coatings are cured under ambient conditions, and thus are typically not fully cured. For these systems, changes in the environments such as an increase in temperatures or exposure to water can cause additional cure resulting in an increase in physical property while properties can decrease simultaneously due to plasticization, rendering this hygrothermal behavior to be complex. For such systems with complex hygrothermal behaviors, it is complicated to evaluate their own effect of degradation by environments in that the materials properties are simultaneously influenced by two combinational effects.

From the previous study (Chapter 3), a tool was successfully proposed to evaluate those two factors separately with a model epoxy-amine system.[152] When the glass transition temperatures (T_gs) are measured to describe the current states of materials specifications for the given system, constructing the plot of T_g versus conversion for the unexposed system provided an excellent method to exclude the factor of cross-link density. By applying the results for the exposed system onto this “master plot”, it is possible to directly compare the T_g values between exposed and unexposed samples while ruling out the factor of cross-link density.

In this study, we have also found complex hygrothermal behaviors of two commercial epoxy products, both used as a seal coat and impregnating resin for structural strengthening applications, where T_g has been changed in a complicated manner due to competing effects of both additional cure and plasticization. The study

has focused on how to quantify those two effects separately with the suggested method, using a thermodynamic analysis and spectroscopic measurements.

Experimental Section

Materials

Both of the epoxy adhesive systems used in this work were for the structural strengthening application as a seal coat and impregnating resin, purchased from Sika Corporation and BASF, respectively. Each system consists of two liquid components, where part A and part B refers to epoxy resin component and hardener component, respectively. In system I, part A consists of diglycidyl ether of bisphenol A (DGEBA) and Part B consists of blend of amines. In system II, part A consists of epoxy resin, alkyl glycidyl ether, aliphatic diglycidyl ether, and ethyl benzene, while part B consists of polyoxypropylene diamine, Isophorone diamine, eposy resin, benzyl alcohol, hexanediamine, and Imidazole, as found on the manufacturers' information. As suggested by the manufacturers, the mix ratio between part A and part B was 1 to 0.345 and 1 to 0.3 by weight for the systems I and II, respectively.

For the sample preparation, the two liquid components were mixed vigorously for 5 mins to ensure even mixing. The mixed material was then degassed for 30~60 mins under vacuum to remove air bubbles. Specimens were cured at room temperature (RT, 22-23°C) for 4 weeks prior to exposure, ensuring enough time for the curing reaction at RT.

Table 4-1 shows the basic thermal properties of systems I and II without any exposure to water immersion. The corresponding values of T_gs and conversion were measured by differential scanning calorimetry and Fourier transform infrared spectrometry (techniques of measurements are described in the following section). As

shown in Table 4-1, T_g values between two systems are very close for various cure condition, which indicates the similarity in thermal properties between both of the unexposed systems.

Exposure environments consisted of immersion into de-ionized water at temperatures of 30, 40, 50, and 60°C. Details of the cure and exposure conditions for hygrothermal exposure are shown in Table 4-2.

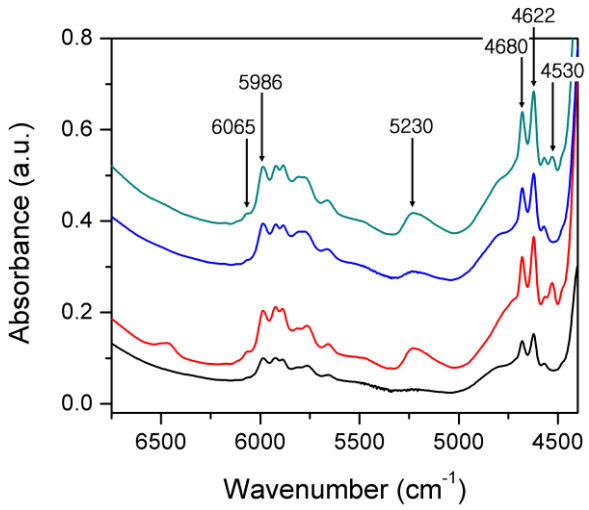

Figure 4-1. Comparison of typical NIR spectra for each system with different cure conditions: System I cured at 50°C for 1 h followed by 80°C for 2 h and 125°C for 3 h, System I cured at RT for 28 days, System II cured at 50°C for 1 h followed by 80°C for 2 h and 125°C for 3 h, System II cured at RT for 28 days (from bottom to top).

Table 4-1. Comparison of observed T_gs and epoxide conversion for unexposed systems between systems I and II

Cure Condition	System I		System II	
	T_g (°C)	Conversion	T_g (°C)	Conversion
Right after mixing	−45.9	0.00	−48.6[a]	0.00
28days at RT	52.5	0.80	53.0	0.88
Fully Cured	82.1	1.00	74.2	1.00

[a] Estimated from a T_g-conversion construction
[b] Cured at 50°C for 60mins followed by 80˚C for 120mins followed by 125˚C for 180mins

Table 4-2. Cure and exposure conditions for hygrothermal exposure in monitoring the changes in T_gs using DSC and changes in cross-link density using FT-IR.

Type of Experimental Work	Condition	Temp. (°C)	Time (days)
Cure	Air	RT	28
Hygrothermal Exposure	Water Immersion	30/40/50/60	1/2/4/7/14/28

To construct a master plot of T_g versus cross-link density for each system of the unexposed epoxies, we employed various cure conditions to obtain specimens with a wide range of conversion values. The specific information for cure conditions for these specimens is shown in Table 4-3.

Table 4-3. Cure conditions for the master plot of T_g vs. conversion for unexposed systems I and II.

Cure Condition	System I		System II	
	T_g (°C)	Epoxide Conversion	T_g (°C)	Epoxide Conversion
RT/0~28days	-45.9~52.5	0.00~0.80	-30.7~53.0	0.23~0.88
80°C/110min	59.7	0.89	56.6	0.90
90°C/80min	65.5	0.91	66.3	0.95
90°C/110min	76.9	0.96	—	—
50°C/60min + 80˚C/120min + 125˚C/180min	82.1	1.00	74.2	1.00

Techniques

Differential scanning calorimetry (DSC; DSC 220, Seiko instruments) was utilized to identify changes in T_g with hygrothermal exposure. Samples were prepared by depositing a small amount of the epoxy formulation directly into the bottom of a DSC aluminum pan before the system was cured in order to maximize the thermal contact

between the sample and the pan and avoid the artifacts often observed during first DSC scans when there is poor thermal contact. After the sample was cured in the bottom of the pan either the pan with the sample in it was immersed in water for hygrothermal exposure, or the pan was immediately used for T_g measurement. Following hygrothermal exposure, the surface of the sample was wiped carefully with a paper tissue to remove any excess surface water. The pan was immediately sealed and placed directly into the DSC chamber for measurement. To reduce the potential for any cure occurring during the measurement, the T_g was determined from the first run of each specimen.

After placing the sample in the DSC, the heat flow signal was allowed to fully equilibrate before beginning the temperature scan. The temperature range for the measurement was -20 to 120~130°C at a heating rate of 10°C/min, and three replicas were fabricated for each exposure condition to obtain the average value. The T_g was chosen from the midpoint of the tangent between the extrapolated baselines before and after the transition.

To measure cross-link density and the amount of absorbed water, we used Fourier transform infrared spectrometry (FTIR; Nicolet Magna 760, Thermo Electron Cooperation) with a CaF2 beamsplitter and an MCT detector. Near-infrared spectra were recorded over the range of 3800-7400 cm^{-1} using 32 scans at a resolution of 4 cm^{-1}. Thin films with 0.5 mm thickness were cast between glass plates using Teflon® spacers. After the selected cure condition as shown in Tables 4-2 and 4-3, the films were either immersed in water for hygrothermal exposure or directly used for the FTIR measurement.

Typical NIR spectra for each system without exposure are shown in Figure 4-1. The reduction in the epoxide absorbance at 4530 cm^{-1} for the higher temperature cure is evident in this figure. For the quantitative analysis of cross-link density changes, the area of the epoxide peak around 4530 cm^{-1} normalized to the phenyl peak around 4622 cm^{-1} was calculated for each system I and II. The epoxy conversion was then calculated by $\alpha = 1 - A(t)/A(0)$, where $A(t)/A(0)$ is the ratio of normalized peak area with respect to the uncured and unexposed system. For quantitative analysis in accordance with the Beer-Lambert law, the absorbance was less than 1.0. The baselines for area calculation of those peaks were chosen as suggested by Dannernberg without any baseline correction.[102, 103]

To estimate the amount of absorbed water for each exposure condition, the normalized area of the characteristic water peak around 5230 cm^{-1} was obtained, which has been assigned to a combination of asymmetric stretching (uas) and in-plane deformation (δ) of water.[142-144] The normalized area of the characteristic water peak provide another method to measure the amount of absorbed water in various polymer-water systems, where the normalized area is proportional to the real amount of absorbed water.[142-145] In this work, the area of this region was also normalized by the phenyl absorbance at 4622 cm^{-1}. Because these are normalized values we can not use them to determine absolute concentrations of water present; however, because the normalized areas are proportional to the amount of water they can be used for relative comparisons. Although this peak includes hydroxyl groups generated in the epoxy network due to the cure reaction, the change in absorbance of the peak by the cure reaction is negligible compared with the amount of absorbed water.[152]

A summary of characteristic NIR absorption band for both systems I and II is shown in Table 4-4.

Table 4-4. Assignment of observed peak for systems I and II in NIR spectra

Peak position (wavenumber, cm^{-1})	NIR Assignment
4530	Combination of C-H stretching and bending of epoxide ring
4622, 4680	Combination of aromatic conjugated C=C stretching ($1626cm^{-1}$) with aromatic CH fundamental stretching ($3050cm^{-1}$)
5230	Characteristic water peak by combination of asymmetric stretching (u_{as}) and in-plane deformation (δ) of water
5986	Overtone of Phenyl CH stretching
6065	First overtone of the terminal CH fundamental stretching

Results

As shown in Figure 4-2, the DSC curves for each system after 7 days of hygrothermal exposure show that the changes of T_gs are difficult to understand due to the fact that both increase and decrease in T_gs were observed during the course of exposure. Samples exposed at 40, 50, and 60°C in system I show significant increases in T_gs compared with unexposed, while T_g decreased for exposed at 30°C. On the other hand, decreases in T_gs for all the exposure conditions were observed for system II after 7 days of exposure, compared to unexposed samples.

From the DSC curves in Figure 4-2, it is also revealed that endothermic aging peaks are superimposed around the glass transition region. This well-known behavior is structural enthalpy relaxation or physical aging, a result of the recovery of enthalpy trapped in the glassy state of the material during aging.[146-151] This phenomena is easily observed for the amorphous polymers being cooled down to below T_g or isothermally cured at a temperature below T_g, typically showing enthalpy relaxation upon reheating.

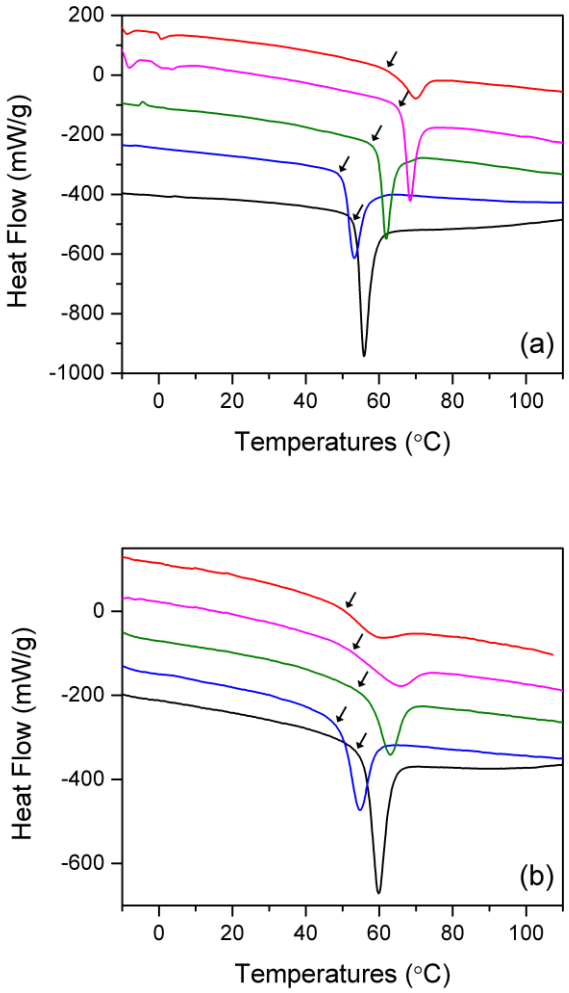

Figure 4-2. Typical DSC curves after water immersion for 7 days at different temperatures compared with no exposure: (a) System I, (b) System II. The arrows indicate T_g for each condition.

In order to monitor the changes in T_gs during the entire course of the exposure, the T_gs of both systems are plotted as a function of exposure time as shown in Figure 4-3. The results clearly indicate complex hygrothermal behaviors in terms that both increase and decrease in T_g values were observed in a complicated manner during the course of exposure although each system exhibits a different behavior in terms of the manner of changes in T_gs for each exposure condition. For system I, the samples exposed at 50 and 60°C show continuous increases in T_g with exposure until the rates

of increase slow down and approach saturation points while, for samples exposed at 30 and 40°C, an initial decrease in T_g was followed by an increase.

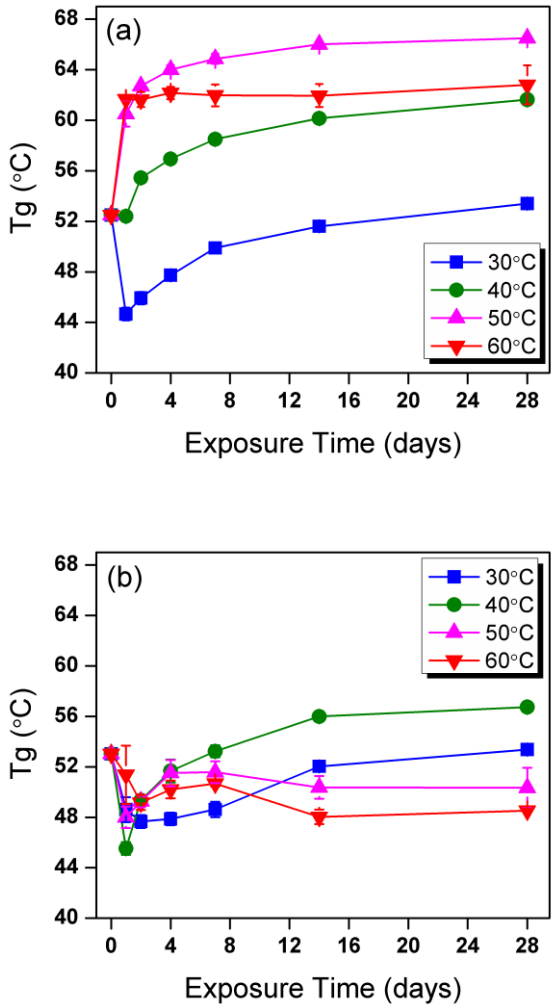

Figure 4-3. Changes in T_g at different exposure conditions after curing 4 weeks at room temperature in air: (a) System I, (b) System II. In this picture, the size of the error bars displaying the standard deviation is too small to be shown at some points.

On the other hand, for system II, the T_g values for all the exposure condition starts from decreases at the beginning stage of exposure, but followed by increases after 1~2 days of exposure. At the later stage of exposure, the samples exposed at 30 and 40°C

keep continue to increase T_g until the rates of increase slow down and approach saturation points. On the contrary, samples exposed at 50 and 60°C exhibit additional decrease of T_g at the later stage and approach saturation points.

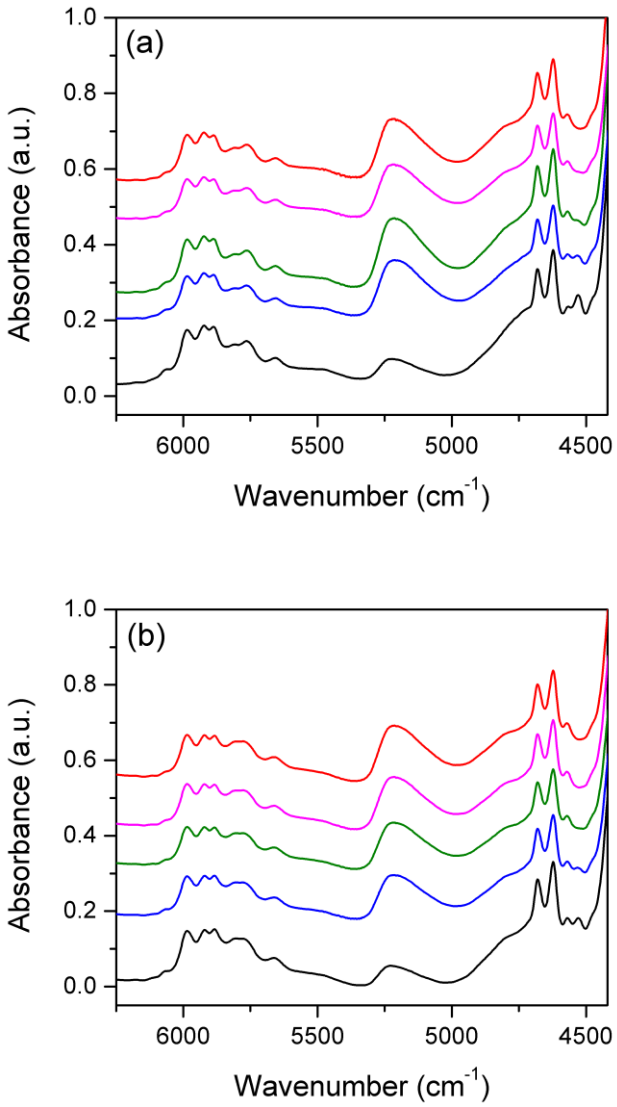

Figure 4-4. Near-infrared spectra for samples immersed in water for 7 days at different temperatures compared with an unexposed/control sample: (From bottom to top) control (exposed in air), exposed at 30°C, exposed at 40°C, exposed at 50°C, and exposed at 60°C): (a) System I, (b) System II. Cure condition was 4 weeks at room temperature in air before the exposure was started.

In order to figure out how post curing reactions affect hygrothermal behaviors, changes in conversion in terms of decreases in epoxide group were also monitored during the same course of the exposure. The cure condition, in this experiment, was also the same to that used for measuring changes in T_g, namely, 4 weeks at room temperature in air before the exposure was started. As shown in Figure 4-4 where the samples exposed to water immersion for 7 days at different temperatures are compared with control samples which had been exposed to air for 7 days, both systems clearly show that decreases in the area of epoxide group around 4530cm^{-1} with increase of exposure temperature, indicating post-curing reaction obviously occurred.

In monitoring the changes in conversion during the entire course of exposure as shown in Figure 4-5, it shows that the epoxide conversion in both systems increased due to post-curing reaction for all the exposure conditions, resulting in significant increases in cross-link density compared with the unexposed sample. This result shows that the elevated temperature of the water caused additional cure, even at a low temperature such as 30°C.

From the comparison of the features of changes in T_gs and changes in conversion with hygrothermal exposure for each system (Figures 4-3 and 4-5), it clearly indicates that the increase in cross-link density by post-curing reaction leads to the increase in T_gs with exposure. At the same time, it shows that property loss by plasticization simultaneously occurs with additional cure, also playing a significant role in determining the properties. It is evident that two phenomena are in competition with each other during the exposure.

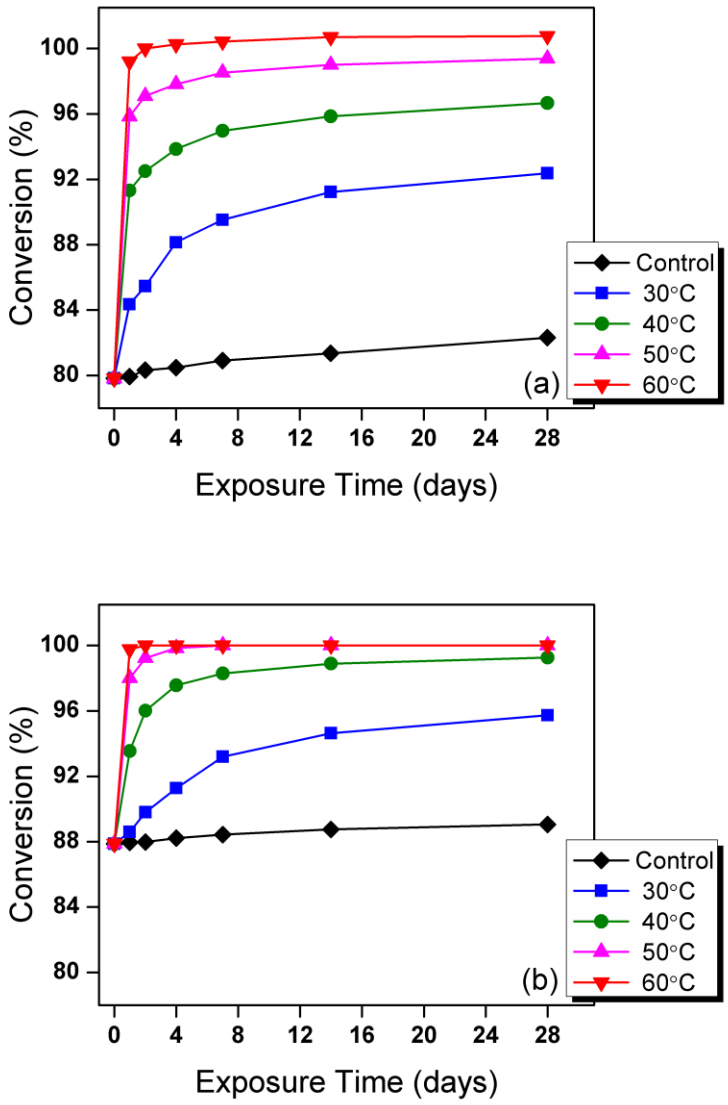

Figure 4-5. Changes in conversion at different exposure conditions after curing 4 weeks at room temperature in air: (a) System I, (b) System II.

For example, in system I, the samples exposed at 30 and 40°C shows an initial decrease in T_g despite continuous increase in cross-link density, which indicates that plasticization effect by water has the predominant effect on T_g at initial stage, compared with additional cure. However, as exposure continues, the additional cure becomes the dominating factor, resulting in an increase in T_g. With regards to exposure at 50°C, it is

observed that the increase in cross-link density is dominant throughout the exposure, resulting in a monotonic increase in T_g. When comparing samples at 50 and 60°C, the T_g for 50°C samples is larger than T_g for 60°C samples after 1 day exposure despite the fact that samples exposed at 60°C always had a higher conversion values. This indicates that at 60°C there is more absorbed water, and therefore greater plasticization.

In a similar manner, system II also shows the combinational effect between two competing factors during the exposure. When observing the samples exposed at 30 and 40°C, they show the initial decreases in T_gs indicating the larger plasticization effect dominant over the effect of additional cure, which was followed by increases in T_gs indicating the changes in dominating factor from plasticization to additional cure. For the samples exposed at 50 and 60°C, it is shown that the dominating factor was changed from plasticization at the initial stage (causing decreases in T_gs at 1~2 days of exposure) to additional cure at the middle stage (causing increases in T_gs at 2~7 days of exposure) and returned back to plasticization later (causing decreases in T_gs at 7~14 days of exposure). In this system, the larger plasticization effect can also be observed at higher temperatures of exposure, in which the samples exposed at 50 and 60°C shows lower T_g values than those exposed at 30 and 40°C at the later stage of exposure despite higher conversion values.

Discussion

From the comparison of the two figures showing changes in T_g and conversion with hygrothermal exposure (Figures 4-3 and 4-5), we can see that the increase in T_g due to additional cure and the decrease in T_g due to plasticization are in competition with each other during exposure. In our previous study, we have successfully proposed

the tool for the evaluation of the relative importance of two effects separately, in which T_g for the unexposed system was plotted as a function of conversion. This “master plot” can then be used to exclude the influence of cross-link density by plotting the results from Figures 4-3 and 4-5 onto this “master plot”, which makes it possible to compare the T_g values directly between exposed and unexposed systems at the same conversion value.

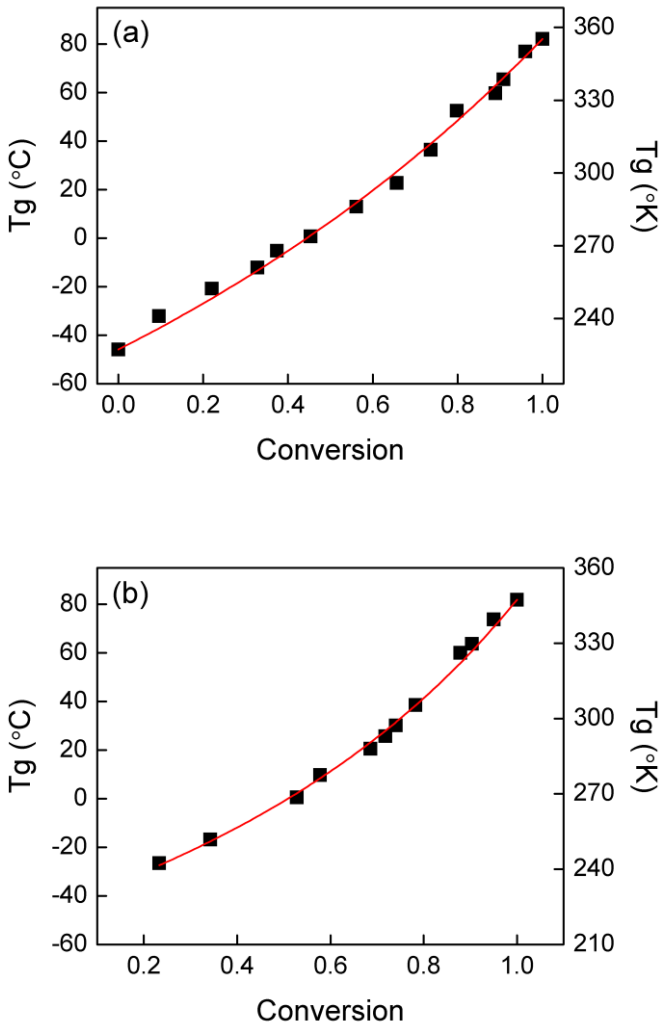

Figure 4-6. T_g versus conversion “master plot” for unexposed systems: (a) System I, (b) System II. Points were experimentally obtained and solid lines are fits to theoretical

For the construction of T_g-conversion master plot, the well-known semi-empirical expression of the relationship between T_g and conversion for cross-linked systems are utilized as shown below[70-72]

$$\ln(T_g) = \frac{(1-\alpha)\ln(T_{g0}) + (\Delta C_{p\infty} / \Delta C_{p0}) T_{g\infty} \alpha \ln(T_{g\infty})}{(1-\alpha) + (\Delta C_{p\infty} / \Delta C_{p0})\alpha} \quad (4.1)$$

where α is conversion, T_{g0} and $T_{g\infty}$ are the T_g values of the monomer and the fully cured network, and ΔC_{p0} and $\Delta C_{p\infty}$ are the heat capacity changes at T_{g0} and $T_{g\infty}$, respectively.

To construct the master plot of T_g as a function of conversion, T_g and conversion values under identical cure conditions were experimentally obtained for unexposed samples of each system. The semi-empirical equation shown above was used for fitting the experimentally obtained data as shown in Figure 4-6. Both systems show good agreements to the experimental data, with coefficients of determination of 0.99 for both cases. The values of $\Delta C_{p\infty}/\Delta C_{p0}$ as a fitting parameter were 0.88 and 0.66 for systems I and II, respectively.

In this construction of “master plot” for system II, the samples with lower values of conversion exhibited multiple T_g values in DSC curves, which might be due to phase separation of mixed specimens between epoxy resin and hardener. Since system II consisted of different blends of amine, it is estimated that the system under low value of conversion still has phase separation after hand mixing which resulted in having multiple Tgs. This behavior, however, disappeared from the point with the conversion value of 0.23 and showed a single value of T_gs thus, for system II, samples with conversion values greater than 0.23 were used to construct the “master plot”. On the contrary, system I does not have the phase separation from the initial mixture between

epoxy resin and hardener, which can be estimated that blends of amines used in this product was well-mixed even at initial condition. T_{g0} for system II was estimated by fitting using the semi-empirical equation shown above and the value was −48.6°C.

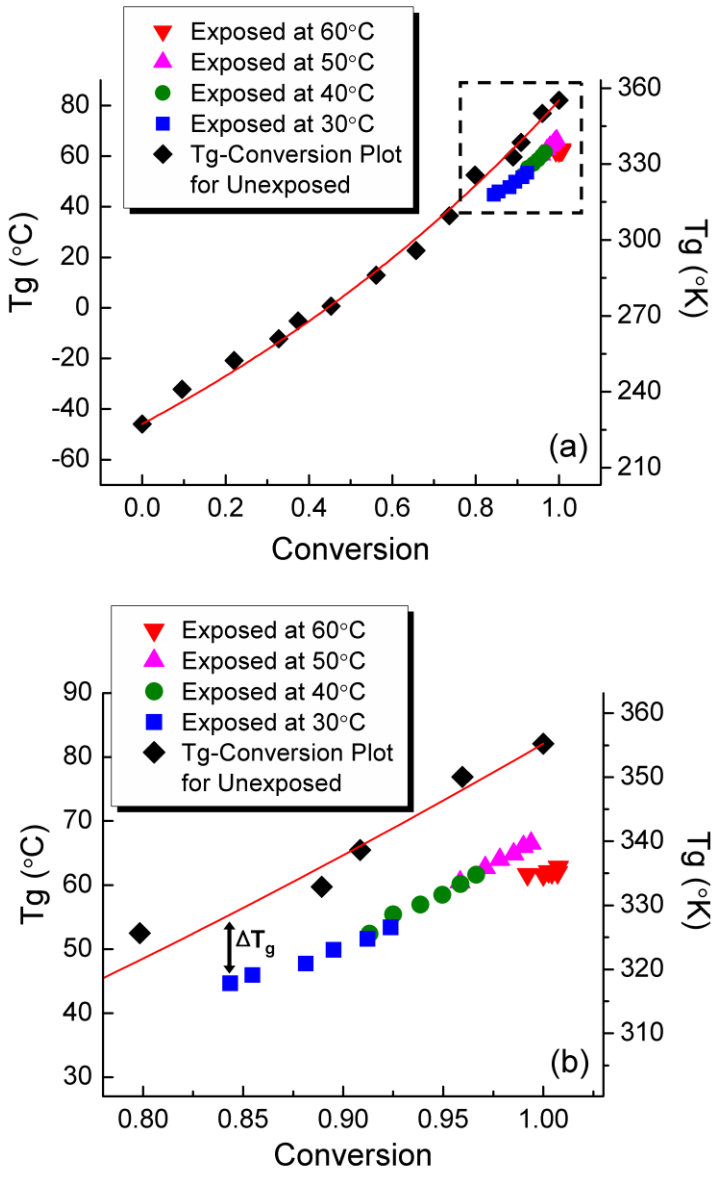

Figure 4-7. Direct comparison of T_g between unexposed and exposed for system I using the master plot of T_g versus conversion. The section marked with dotted lines in (a) is magnified in (b).

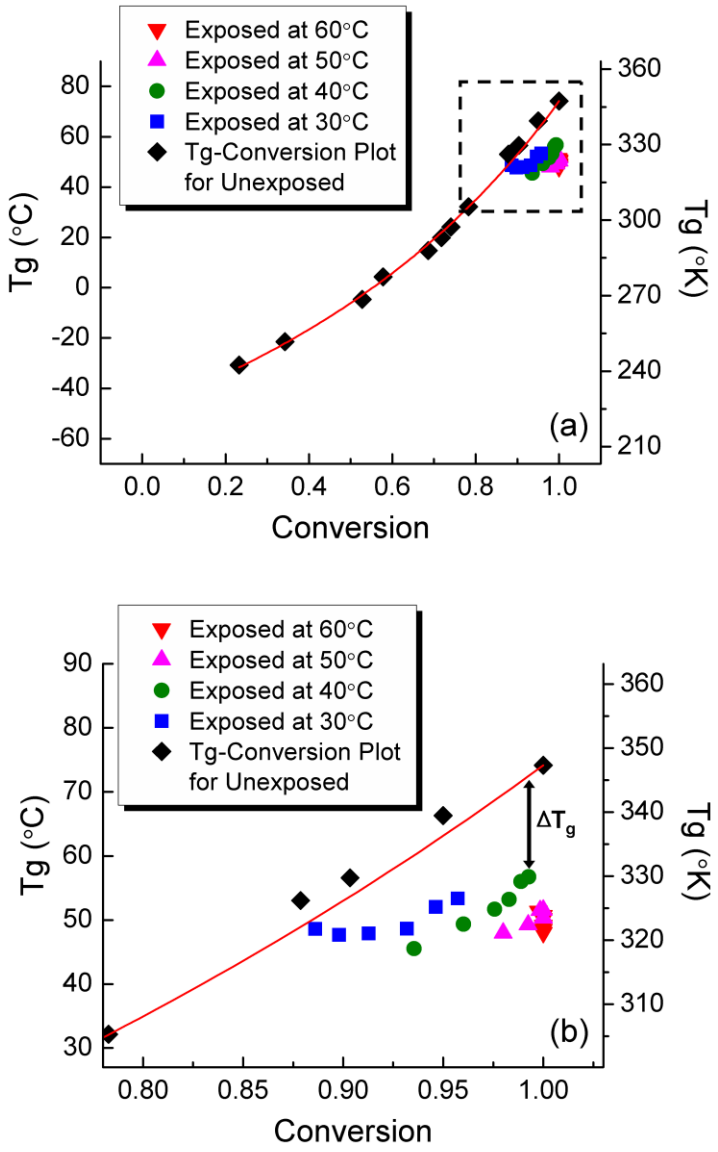

Figure 4-8. Direct comparison of T_g between unexposed and exposed for system II using the master plot of T_g versus conversion. The section marked with dotted lines in (a) is magnified in (b).

Into these constructed master plots for unexposed systems, the values of T_g and conversion for each exposed system I and II, which shown in Figures 4-3 and 4-5, were finally applied as displayed in Figures 4-7 and 4-8. In this application, ΔT_g, the difference in T_g between unexposed and exposed samples at the same conversion value can successfully propose a parameter indicating plasticization effect quantitatively

while excluding the influence of changes in cross-link density with exposure. In this calculation of T_g differences, T_gs for the exposed system were determined directly from DSC measurements, whereas T_g values at the corresponding conversion for the unexposed system were obtained from the values on the fitted curve, as indicated in Figures 4-7 (b) and 4-8 (b).

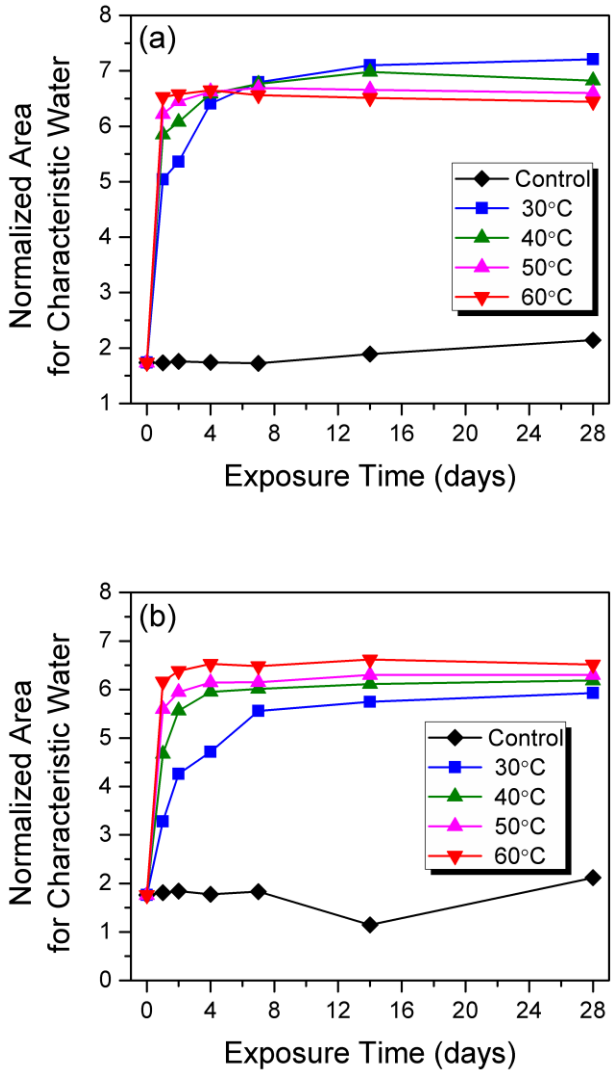

Figure 4-9. Relative amount of water absorption with exposure time estimated by normalized area of the characteristic water peak from NIR: (a) System I, (b) System II.

In order to correlate ΔT_g with the absorbed water amount at each exposure condition, the relative amount of water uptake was determined from the characteristic water peak around 5230 cm^{-1}, which was well-resolved in the NIR spectra of each system. When the relative amount of absorbed water is evaluated by this method, both systems exhibit the same typical trends that the amounts of water absorption increases as exposure continues and that the rate of increase in absorbed water at the initial stage of the exposure is enhanced as exposure temperature increases by an increase in diffusion rate as temperature increases (Figure 4-9).

However, for the features of the amount of water uptakes varied with different temperatures at the later stage of exposure, each system show a different behavior, contrary to each other. After water absorption saturated at some points, system II shows larger water uptakes for exposed at higher temperatures, which is not unusual, while system I shows the opposite behavior, that is larger water uptakes for exposed at lower temperatures. Regarding this abnormal behavior of water absorption in system I, it is probably related to an imperfect cure of the system.[153] Since system I still has larger difference in conversion value at the later stage of exposure between the samples exposed at different temperatures, it is estimated that there is also larger difference in density of the network structure of polymer chains, where the samples exposed at lower temperatures which has lower conversion value have loose network with more free volume, resulted in easier ingress of water.

On the other hand, for system II, although there is also difference in conversion values between the samples exposed at different temperatures at the later stage of exposure, the amount of differences in percent conversion is not so much as that for

system I. In addition, system II had already reached a higher conversion value compared with system I before the exposure started. It is estimated that there was not huge differences in polymer networks between the samples exposed at different conditions of post-curing reactions, resulted in the normal hygrothermal behavior having a larger water uptakes with higher temperature of water exposure.

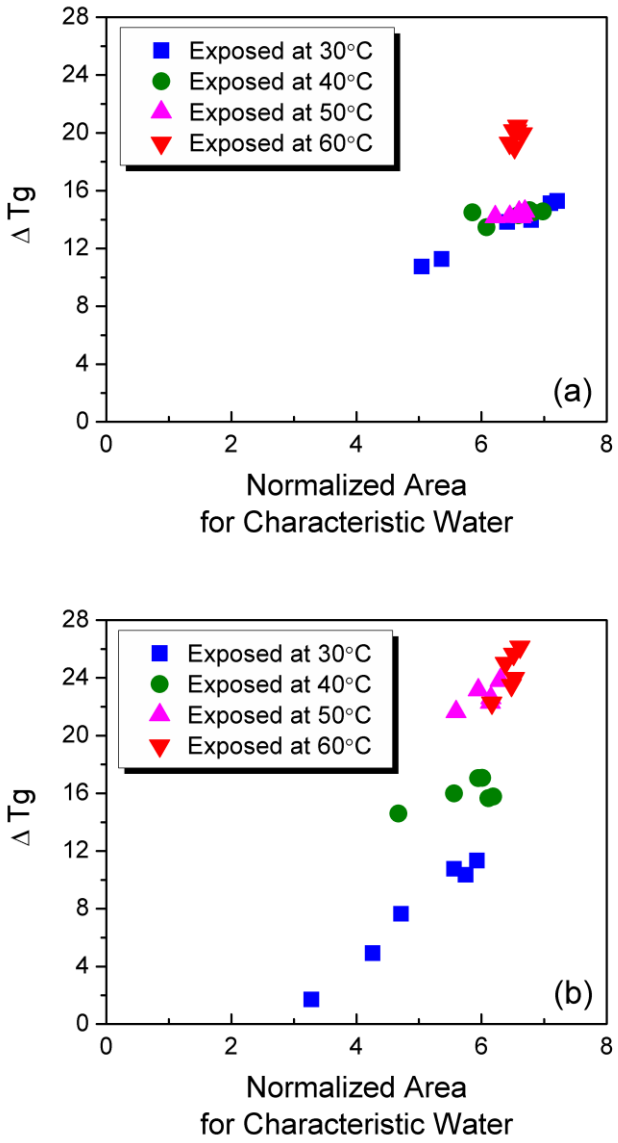

Figure 4-10. T_g differences between unexposed and exposed systems as a function of estimated amount of absorbed water: (a) System I, (b) System II.

Finally, ΔT_g was plotted as a function of the relative absorbed water amount for each exposure system. As shown in Figure 4-10, ΔT_g increases with water amount, showing the expected behavior of increase in plasticization as the amount of absorbed water increases. From the comparison of two systems in this figure, system II shows larger deviation of ΔT_g values with different exposure temperatures, indicating that small chages in water uptakes resulted in larger plasticization effect in this system.

Summary

In this work, complex hygrothermal behaviors of two commercial products, both used as a seal coat and impregnating resin for structural strengthening applications have been investigated, in which property loss by plasticization simultaneously occurs with additional cure during the exposure.

From the comparison of two features describing changes in T_gs and cross-link density with water immersion at different temperatures, it clearly shows that the plasticization effect due to water absorption and the effect of additional cure due to post-curing reaction are in competition with each other during the exposure.

Construction of the plot of T_g versus conversion for the unexposed system successfully provided an excellent method to exclude the factor of cross-link density. By applying the results for the exposed system onto this “master plot”, it was possible to directly compare the T_g values between exposed and unexposed samples while ruling out the factor of cross-link density. Combined with the estimated amounts of water absorption, it provided a tool to evaluate plasticization effect quantitatively, which was due to their own environmental exposure.

The suggested method will contribute to the understanding of the complex behavior having property increase and decrease at the same time for various cross-linked polymer areas employing low-temperature curing under environmental effects.

CHAPTER 5
EFFECT OF WATER ADDITION ON CURE KINETICS OF AN EPOXY-AMINE THERMOSET

Background

Although epoxy systems have numerous advantages over other thermoset resins such as lower cure shrinkage, lower residual stress, chemical resistance, and insulating properties the most distinctive attraction of the epoxy resins can be described as "*a convenient use of a wide range of temperatures by judicious selection of curing agents enabling good control over the degree of cross-linking"*.[3]

In these uses of epoxy materials, additional variables are often included into a given system such as solvent, concentrations, viscosity, and mixing rates, providing another method to control degree of cross-linking or the speed of reaction.[4-9] Also, an additional incorporation of catalysts such as imidazole have extensively been utilized as a convenient way to regulate the condition of manufacturing processes.[10-13] This has been preferred in many industrial areas such as outdoor or electronic applications where high temperature cannot be used easily as a means of accelerating the curing reaction in order to take advantages of easy installation. Addition of hydroxyl containing coupounds such as water or various types of alcohols and phenols has also known to increase the rate of cure reaction.[4, 14, 15] Catalysis effects of hydroxyl groups in those types of added compounds contribute the ring opening of epoxides, although the exact impact of added water has not been suggested quantitatively.

In the previous studies in Chapters 3 and 4, it has also been revealed that water may largely affects the kinetics of the post-curing reaction, in which conversion of an epoxy-amine thermoset has been significantly accelerated with the help of water immersion even at low temperatures such as 30°C.[152]

Understanding of the moisture effect on cure kinetics is very important, especially in the case of the systems employing slow curing at ambient condition for easy installation such as the application of structural adhesives, where absorption of moisture at initial condition of storage or during the course of curing could result in huge different states of cure degree at the final products. Although some previous studies have reported that added water can significantly contribute to accelerate curing reaction in epoxy-amine thermosets, the effect of added water itself with a view to the kinetic aspect has not been quantitatively evaluated.[4, 14]

In this study, we have focused on how the added water influences the polymerization kinetics and reaction chemistry. This suggests the direct comparison of the kinetic values between catalyzed hydroxyl effect by added water and that by auto-catalysis, using a modified mechanistic modeling. Such an effort will contribute to the understanding of the relationship between the materials' properties and the processing environments, which will also be very useful in designing materials with tuned properties.

Experimental Section

Materials

The material used in this work is a two-part epoxy, diglycidyl ether of bisphenol A (DGEBA, EPON 826, epoxy equivalent weight=178~186g/equiv, n=0.08, information provided by manufacturer,) and poly(oxypropylene) diamine (POPDA, Jeffamine D-230, n=2~3, information provided by manufacturer), purchased from Hexion and Huntsman, respectively. Figure 5-1 illustrates the chemical structures of DGEBA and POPDA. The mass ratio of DGEBA to POPDA was 100 to 32.9, to reach stoichiometric equivalence between functional groups based upon manufacturers' information.

The two liquid components with selected amount of deionized water (0, 1, 2 and 3wt%) were mixed vigorously for 3 min to ensure even mixing. The limit of the amount of added water was determined by the solubility of water in the epoxy resin. When the excessive water of 4wt% is added into the epoxy resin, the system no longer shows intimate mixing, in which phase-separated forms of microdroplets of water are easily observed by the naked eye after being cured. Since the intent of this study is to investigate the water or moisture effect by spontaneous absorption of the system itself from the environment, which could occur during the service of the products, the limit of the water content was set to 3wt%.

The mixed material was put into 15~18 replicates of preheated teflon® spacers at different cure temperatures of 50, 55, 60, 65 and 70°C with a convection oven. After curing for the selected time, the specimens were periodically removed from the oven, followed by immediate quenching using liquid nitrogen to minimize the effect of residual heat and were then the spectra were ready to be taken.

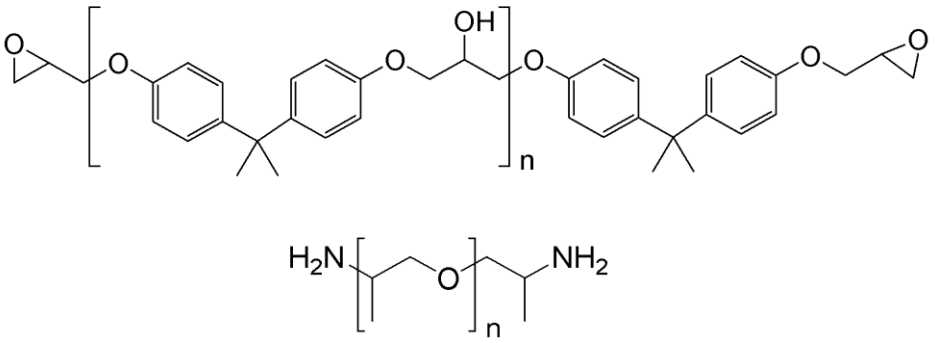

Figure 5-1. Chemical structures of diglycidyl ether of bisphenol A (DGEBA, top) and poly(oxypropylene)diamine (POPDA, bottom).

Techniques

To monitor the cure kinetics of the epoxy-amine system, we used Fourier transform infrared spectrometry (FTIR; Nicolet Magna 760, Thermo Electron Cooperation). The prominent advantages of FTIR to monitor the cure kinetics of epoxy systems have been well-established, in which quantitative amount of functional groups involved in the reaction can be easily observed.[73, 74, 154] In this study, near-infrared spectra were recorded with a CaF_2 beamsplitter and an MCT detector over the range of 3800-7500 cm^{-1} using 32 scans at a resolution of 4 cm^{-1}. For the recording of IR spectra for the initial cure stage of the samples which did not solidify after the selected cure time, KBr IR disposable cards were used. The other samples which solidified after the selected cure time were prepared by casting thin films with approximate 0.5~1 mm thickness using Teflon® spacers.

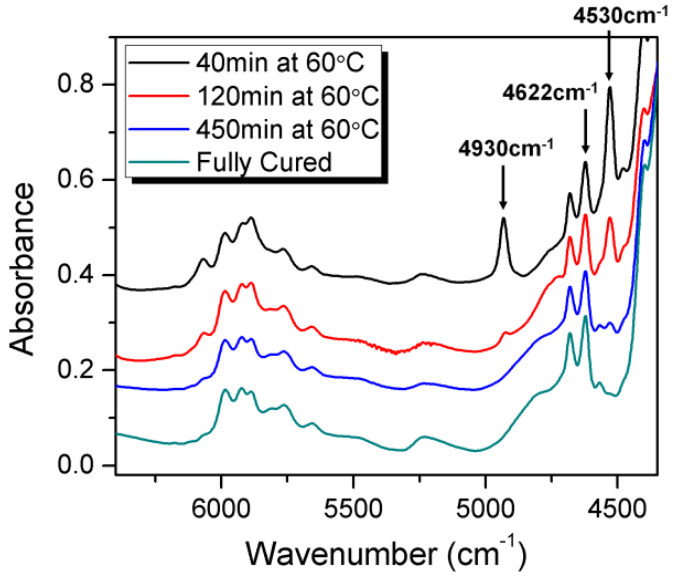

Figure 5-2. Typical FT-IR Spectra for DGEBA-POPDA system(from top to bottom): Cured at 60°C for 40 min, Cured at 60°C for 120 min, Cured at 60°C for 450 min, and Cured at 50°C/1hr followed by 80°C/2hrs and 125°C/3hrs. Spectra were moved parallel to the y-axis for the display.

Typical NIR spectra for the systems are shown in Figure 5-2. To measure the concentrations of primary amines and epoxides, IR spectra have been directly observed. For the quantitative analysis of the epoxide group, the area of the epoxide peak around 4530 cm^{-1} was normalized to the phenyl peak around 4622 cm^{-1}. The epoxy conversion was then calculated by $\alpha = 1 - A(t)/A(0)$, where $A(t)/A(0)$ is the ratio of the normalized peak area with respect to the uncured system. The baselines for area calculation of those peaks were chosen as suggested by Dannernberg without any baseline correction.[102, 103] For the measurement of concentrations of primary amines, the area of the primary amine peak around 4930cm^{-1} was also normalized to the phenyl peak around 4622 cm^{-1}.

Although the reliability of this quantitative analysis of the epoxy cure reaction was confirmed by previous workers,[102, 103, 152, 155] we reconfirmed it for our system. In this experiment, to demonstrate the validity of using Beer-Lambert's law, the normalized peak areas for both the epoxide and primary amine in the spectra were measured with respect to different epoxide concentrations. To monitor the normalized area for the epoxide group, specimens with different epoxide concentrations were cured at high temperatures for enough time to ensure complete reaction between epoxide and amine functional groups. The cure condition was 50°C for 1 hr followed by 80°C for 2 hrs and 125°C for 3 hrs. On the other hand, for the primary amine, IR spectra of specimens with different epoxide concentrations were recorded right after mixing the 2 components. As shown in Figure 5-3, the normalized absorbance either decreases or increases linearly as epoxide concentration decreases, which indicate that our analysis is reliable and

obeys the Beer-Lambert law. For quantitative analysis in accordance with the Beer-Lambert law, the absorbance of all the specimens was less than 1.0.

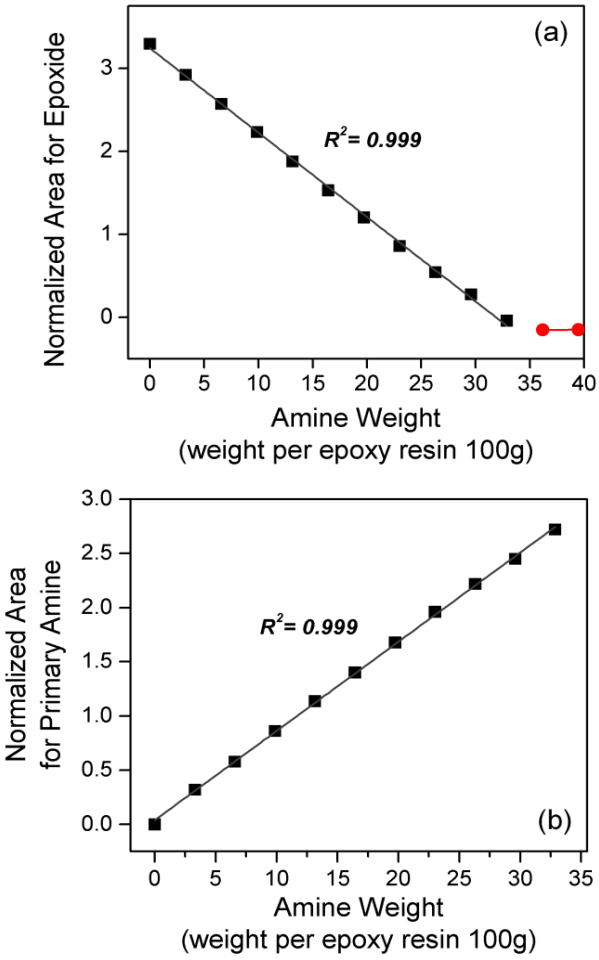

Figure 5-3. Experimental confirmation of the reliability of quantitative analyses from FTIR: (a) Plot of normalized area assigned to epoxide at 4530 cm^{-1} with variation in epoxide/amine ratio. The correlation coefficient value, R^2 is 0.99. (b) Plot of normalized area assigned to primary amine at 4930 cm^{-1} with variation in epoxide/amine ratio. The correlation coefficient value, R^2 is 0.99.

In addition, when Figure 5-3 (a) is carefully observed, it reveals that the determined mixing ratio between part A and part B, which was based upon the manufacture's information, was slightly off-stoichiometric ratio. From the interception of the fitted linear regressions between excess-epoxide condition (square) and excess-

amine condition (circle), it shows that the stoichiometric mass ratio is 100 to 33.4 between DGEBA and POPDA, which slightly deviated from the selected ratio of 100 to 32.9 in this study. For the calculation of concentrations in this study, we follow the information obtained from the IR spectra, which corresponding to the concentration ratio of 4.14 to 2.03 mol/kg between epoxide and primary amine.

Results and Discussion

Reaction Chemistry – Epoxide Conversion

For the epoxy-amine reaction, it is well-known that the main features include (1) reaction of primary amine with an epoxide to form a secondary amine and (2) further reaction of the secondary amine with another epoxide to form a tertiary amine.[73, 74] Although other possible mechanisms can be also included such as homo-polymerization by epoxide-epoxide and etherification by epoxide-hydroxyl reactions, those only occur under certain conditions, such as in the presence of acid/base catalysts or at higher cure temperatures.[75-80] Given the system in our study employs only neutral water and relatively low cure temperatures, they can be safely ignored.

In the meantime, water in the system could influence the reaction chemistry in terms that weaker nucleophiles of water can even react with epoxides in the presence of acid catalysts. Although no acid or base catalyst was included in this study, in order to estimate the possibilities of the reaction between pure epoxide and water, only part A containing pure epoxides were mixed with deionized water and cured at various conditions. As shown in Figure 5-4, the normalized areas for the epoxide around 4530cm^{-1} obtained from IR spectra did not vary with all the cure conditions, which indicates there is no reaction between epoxide and water in this study.

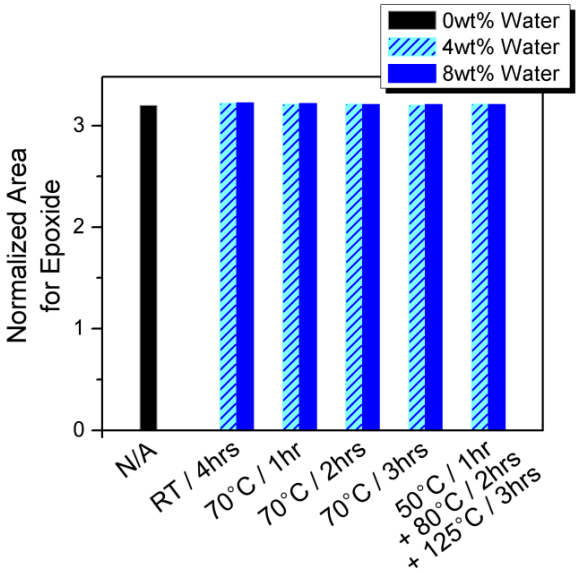

Figure 5-4. Comparison of normalized area for epoxide around 4530cm^{-1} obtained from IR spectra for different water contents and cure conditions.

Finally, to evaluate the effect of added water on cure kinetics, conversion in terms of a decrease of epoxide functional groups has been plotted as a function of cure time with different water contents and different cure temperatures. As shown in Figure 5-5, FT-IR demonstrates that the rate of cure reactions significantly increased with increases in water contents. Furthermore, it reveals that the added water also affects the final conversion values at the later stage of cure, which also slightly increased with added water. Combined with the prior results in Figure 5-4, it can be concluded that water only contributes to the ring opening reaction of epoxides as a catalyst to increase curing rate.

In order to understand the entire chemical reaction and kinetic relations of the system, the changes in concentrations of the epoxide and primary amine were directly calculated from the monitoring of IR absorption bands. In this calculation, the initial concentration of each specie before the curing reaction proceeds allows us convert the changes in the area of IR absorption bands to the concentration profiles, based on our validation of Beer-Lambert's law as shown in Figure 5-3.[74]

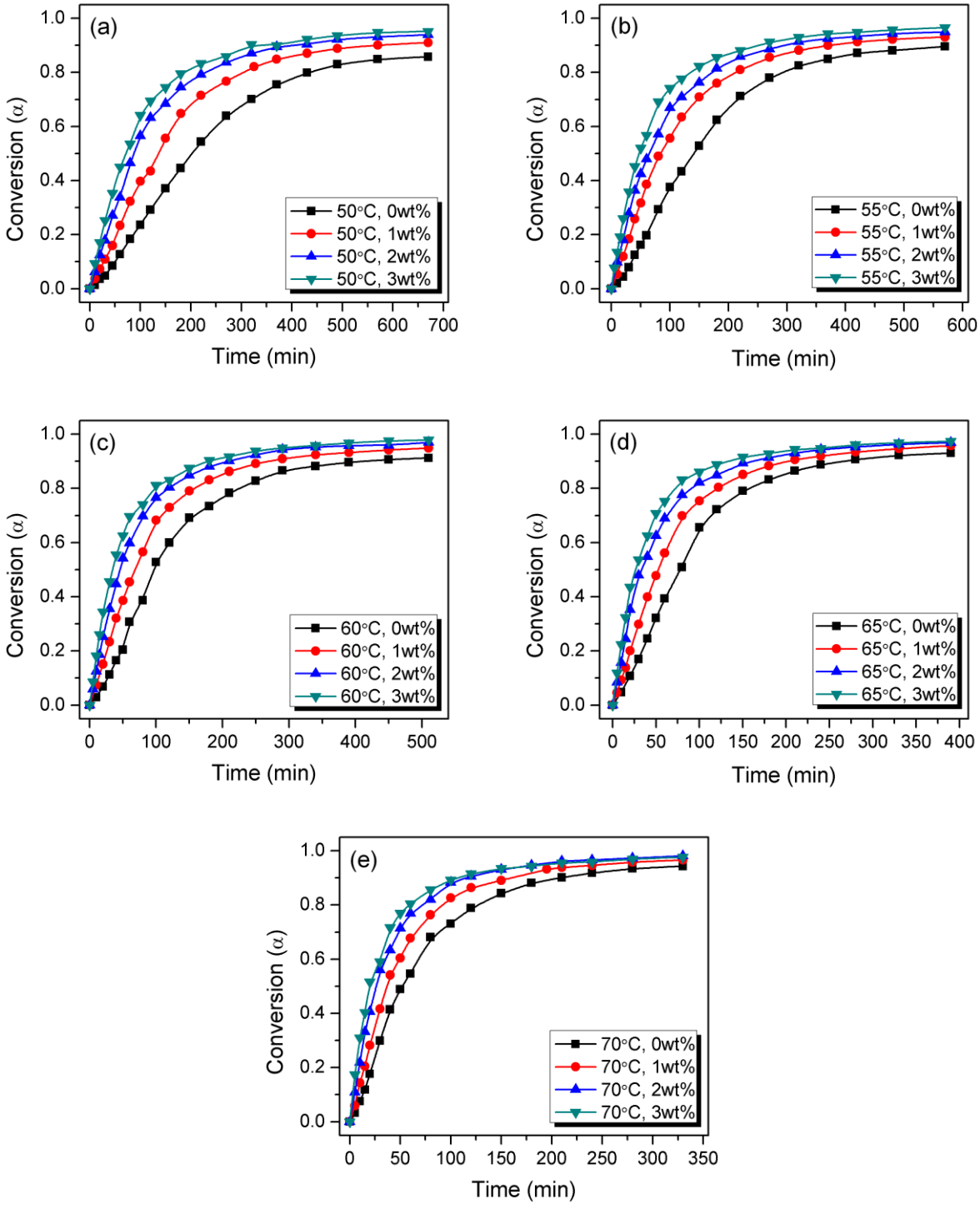

Figure 5-5. Epoxy conversion versus cure time with different contents of added water: (a) Cured at 50°C, (b) Cured at 55°C, (c) Cured at 60°C, (d) Cured at 65°C, (e) Cured at 70°C

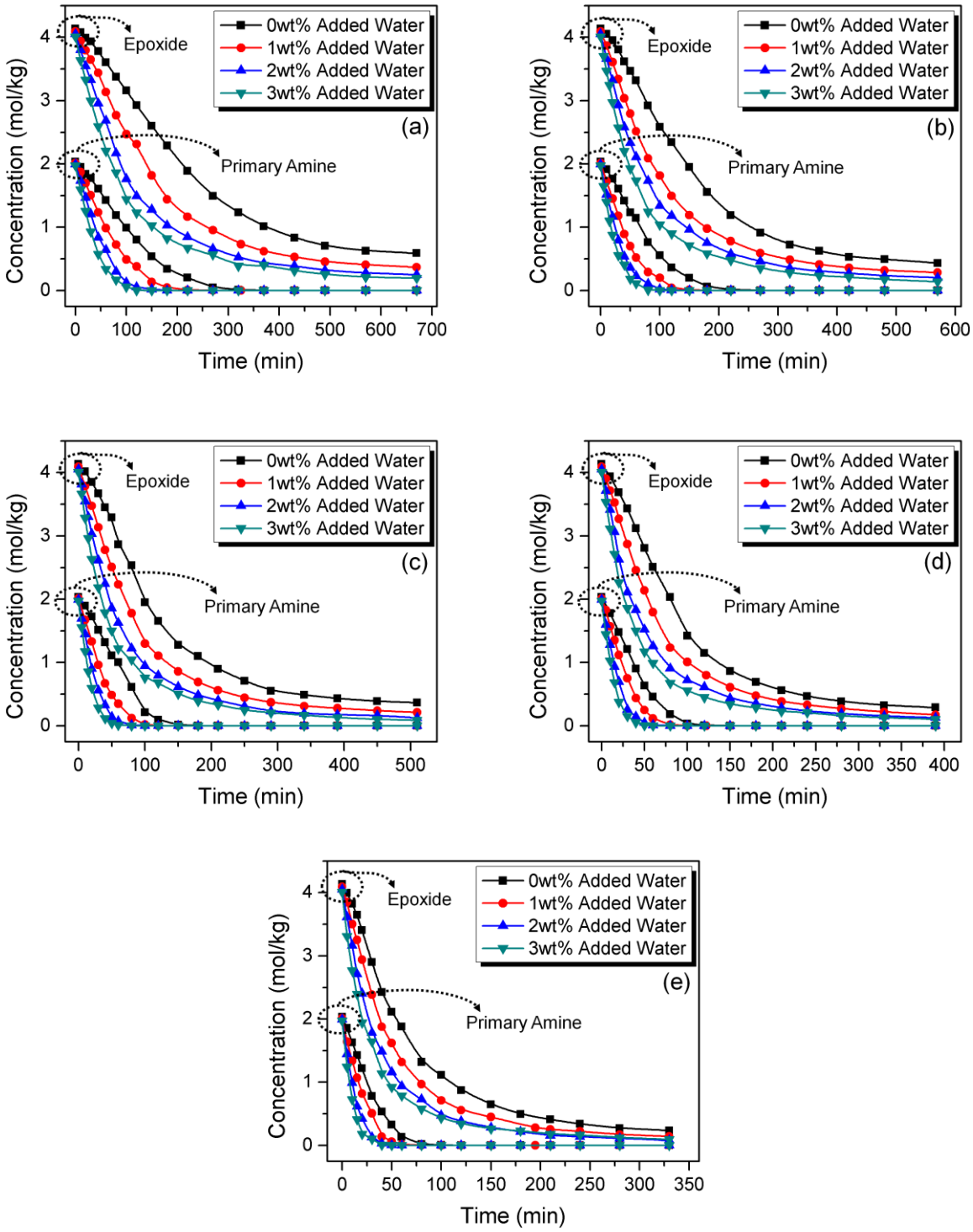

Figure 5-6. Concentration profiles for epoxide and primary amine. The profiles were directly obtained from FT-IR measurement: (a) Cured at 50°C, (b) Cured at 55°C, (c) Cured at 60°C, (d) Cured at 65°C, (e) Cured at 70°C

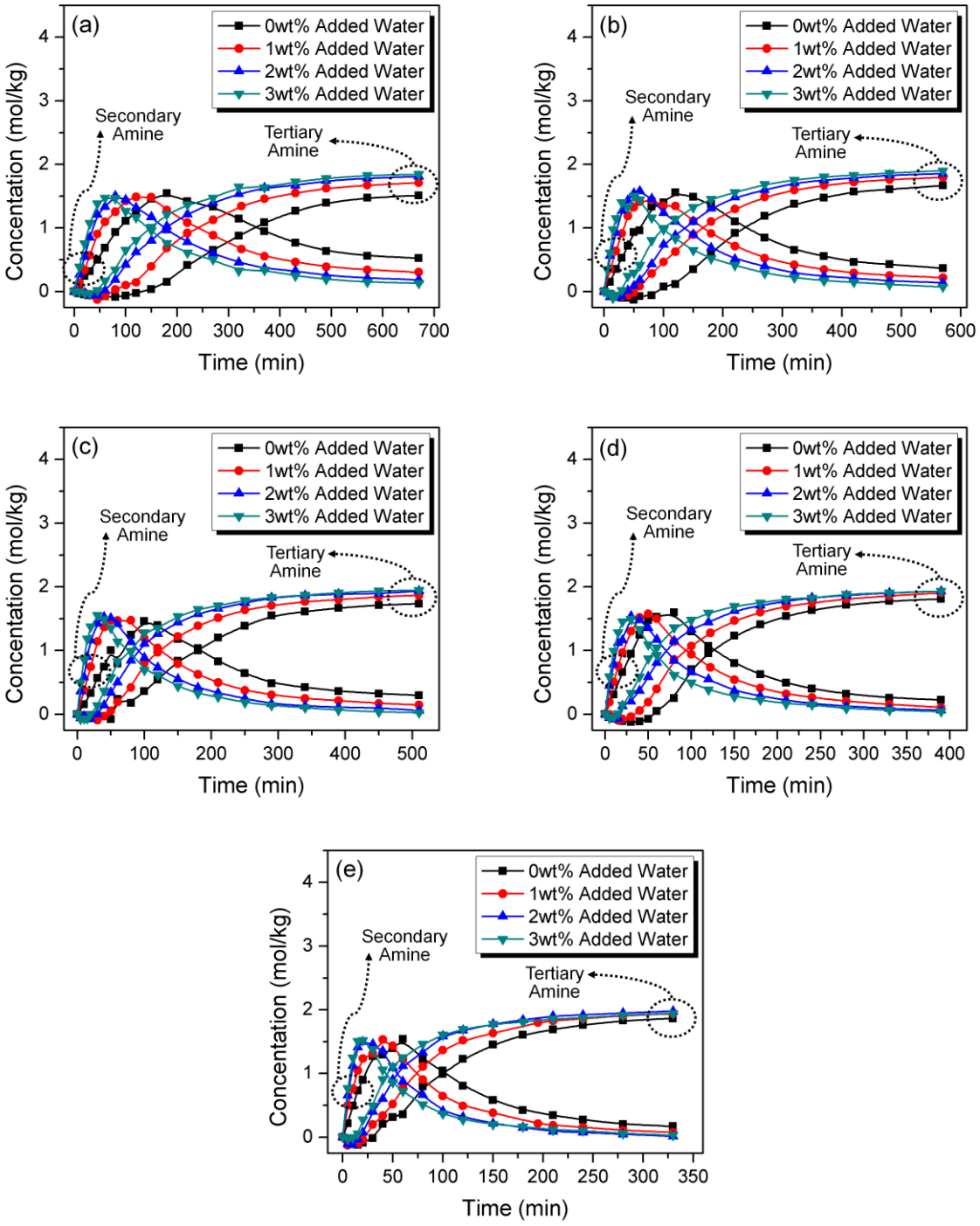

Figure 5-7. Concentration profiles for secondary and tertiary amine. The profiles were obtained using mass balance equations: (a) Cured at 50°C, (b) Cured at 55°C, (c) Cured at 60°C, (d) Cured at 65°C, (e) Cured at 70°C

On the other hand, the mass balance equations also allow us to monitor the changes in other functional groups of interest which are involved in the reaction, such as secondary amines and tertiary amines. In this mass balance equation shown below, it is assumed that the total number of nitrogen atoms is constant during the entire reaction (Equation 5-1), while the number of the generated hydroxyl functional groups counted by the epoxide consumption corresponds to that counted by the generation of secondary and tertiary amines (Equation 5-2). In this hydroxyl balance, etherification reactions are ignored.[6, 74]

$$[A_1] + [A_2] + [A_3] = [A_1]_0 \quad (5\text{-}1)$$

$$[E]_0 - [E] = [A_2] + 2[A_3] = [OH]_{auto} \quad (5\text{-}2)$$

where [E], [A_1], [A_2], [A_3], and [OH] are the concentrations of epoxide, primary amine, secondary amine, tertiary amine and hydroxyl groups present in the system, respectively. $[OH]_{auto}$ refers to the hydroxyl groups generated by autocatalysis during the chemical reaction.

In Figures 5-6 and 5-7, the changes in concentration for the functional groups of interest can be finally monitored during the entire course of the curing reaction. As shown in Figure 5-6, primary amines are consumed faster with the increase of the added water for all the reaction temperatures, indicating faster reactions of primary amines with epoxides to form secondary amines. In the meantime, tertiary amines exhibit the faster production with the increase of the added water (Figure 5-7). It shows that further reaction of secondary amines with epoxides to form tertiary amines also speed up with the added water, which also confirms that the rate of the cure reaction is accelerated by the addition of water. In accordance with the faster consumption and

production of primary amines and tertiary amines, respectively, secondary amines also exhibit the faster rate of cure reaction with the increase of the added water. In this concentration profile of secondary amines, they were produced faster with the increase of water contents, which was followed by faster consumption to form tertiary amines.

Reaction Kinetics

As has been suggested in a number of previous studies, the main cure mechanism for epoxide amine reactions has been generally described by two reaction paths: (1) reactions catalyzed by compounds containing nitrogen-hydrogen bonds (designated as “non-catalytic” by previous workers) and (2) those by oxygen-hydrogen bonds (designated as “catalytic”).[74, 81-85, 156] In this kinetic expression, it is often described that the reaction of an epoxide group with an amine occurs through the formation of termolecular intermediates consisting of an amine, epoxide, and hydroxyl due to the existence of hydrogen bonding, in which the formation of the termolecular intermediate is the rate determining step.[7, 14, 74, 79, 156-158] The involved reactions with the assumption of the formation of termolecular intermediates can be displayed as shown in Figure 2-1.

When the reactions shown in Figure 2-1 are written in a compact form which containing the reaction rate constants, they can be displayed by following equations,

$$[E\cdots A_1]+[A_1] \xrightarrow{k_1} [E\cdots A_1]\cdots[A_1] \quad (5\text{-}3)$$

$$[E\cdots A_1]+[A_2] \xrightarrow{k_2} [E\cdots A_1]\cdots[A_2] \quad (5\text{-}4)$$

$$[E\cdots OH]+[A_1] \xrightarrow{k_1'} [E\cdots OH]\cdots[A_1] \quad (5\text{-}5)$$

$$[E\cdots OH]+[A_2] \xrightarrow{k_2'} [E\cdots OH]\cdots[A_2] \quad (5\text{-}6)$$

where k_1 and k_1' indicates that the non-catalytic and catalytic kinetic parameters for epoxy-primary amine addition while k_2 and k_2' are those for epoxy-secondary amine addition, respectively. Thus, the well-known kinetic expression for the above epoxy-amine reactions can be described as follows.

$$-\frac{d[A_1]}{dt} = k_1[E][A_1]^2 + k_1'[E][A_1][OH] \quad (5\text{-}7)$$

$$\frac{d[A_3]}{dt} = k_2[E][A_1][A_2] + k_2'[E][A_2][OH] \quad (5\text{-}8)$$

In this expression, the first term of each equation represents the non-catalytic reaction while the second term shows the catalytic reaction by hydroxyl functional groups. For the second term, the effect of hydroxyl generated from added water or absorbed moisture from air has not been separated from that generated from polymer chain such as hydroxyl effect by autocatalysis or the effect of hydroxyls already present in the reactant molecules. However, since the intent of this study is to evaluate the effect of hydroxyl from added water itself, the given equations should be further developed which separates those two effects. In the meantime, the non-catalytic reaction term can be neglected when considering that the catalyzed effect of amine group is much smaller than that of hydroxyl.[74]

Thus, for the purpose of evaluating how much the added water affects the cure kinetics in this work, Equations 5-7 and 5-8 can be further developed into following Equations 5-9 and 5-10 with the assumption of negligible effect of the non-catalytic reaction. In these equations, hydroxyl groups are divided into two groups: (1) $[OH]_{chain}$ which yielded from the polymer chain by initially present ($[OH]_{initial\text{-}chain}$) or auto-generated during the reaction ($[OH]_{auto}$) and (2) $[OH]_{water}$ which given by initially

absorbed moisture ($[OH]_{initial\text{-}moisture}$) or intentionally added water ($[OH]_{add}$). Thus, k_{1C}' and k_{2C}' represents the catalytic kinetic parameters with regard to the hydroxyl groups generated from the polymer chain while k_{1W}' and k_{2W}' are with regard to the hydroxyl groups by added in the form of moisture or added water.

$$-\frac{d[A_1]}{dt} = k_{1C}'[E][A_1][OH]_{chain} + k_{1W}'[E][A_1][OH]_{water} \quad (5\text{-}9)$$

$$\frac{d[A_3]}{dt} = k_{2C}'[E][A_2][OH]_{chain} + k_{2W}'[E][A_2][OH]_{water} \quad (5\text{-}10)$$

where total amounts of $[OH]_{chain}$ and $[OH]_{water}$ can be derived as follows.

$$[OH]_{chain} = [OH]_{initial\text{-}chain} + [OH]_{auto} \quad (5\text{-}11)$$

$$[OH]_{water} = [OH]_{initial\text{-}moisture} + [OH]_{add} \quad (5\text{-}12)$$

Also, $[OH]_{initial\text{-}chain}$ which is present due to the polymer chain of DGEBA (n=0.08) can be calculated using the following equation.

$$[OH]_{initial\text{-}chain} = 0.08\frac{[E]_0}{2} \quad (5\text{-}13)$$

Equations 5-9 and 5-10 can be also represented as Equations 5-14 or 5-15 in the form where all the relative kinetic parameters of k_{1C}', k_{1W}', k_{2C}' and k_{2W}' are combined in one equation.

$$-\frac{d[E]}{dt} = k_{1C}'[E][A_1][OH]_{chain} + k_{1W}'[E][A_1][OH]_{water} + k_{2C}'[E][A_2][OH]_{chain} + k_{2W}'[E][A_2][OH]_{water} \quad (5\text{-}14)$$

$$\frac{d[A_2]}{dt} = k_{1C}'[E][A_1][OH]_{chain} + k_{1W}'[E][A_1][OH]_{water} - k_{2C}'[E][A_2][OH]_{chain} - k_{2W}'[E][A_2][OH]_{water} \quad (5\text{-}15)$$

In order to evaluate the kinetic parameters regarding epoxy-primary amine addition, Equation 5-9 was developed into the following reduced form.

$$-\frac{d[A_1]}{dt}\frac{1}{[E]}\frac{1}{[A_1]} = k_{1C}'[OH]_{chain} + k_{1W}'[OH]_{water} \quad (5\text{-}16)$$

When the reduced reaction rate (the left term of (16)) is plotted as a function of $[OH]_{chain}$, then k_{1C}' and $k_{1W}'[OH]_{water}$ can be derived from the slope and intercept of the linear regression of the early stage of cure for each reaction condition, respectively, as shown in Figure 5-8. In order to obtain pure intrinsic kinetic parameters, the later stage of the reaction was removed from the linear regression of the fitting, in which the main reaction is under the control of diffusion effect. The limit of the linear regression was set up to approximately 50~60% conversion in terms of the values of epoxide conversion.[159-161] Using this method, the determined kinetic parameter of k_{1C}' is shown in Table 5-1 and Figure 5-12.

Also, each intercept value from Figure 5-8 representing $k_{1W}'[OH]_{water}$ for all the conditions of different water contents and cure temperatures can be plotted as a function of the amount of added water ($[OH]_{add}$) as shown in Figure 5-9. From this graph, the slope obtained by the linear regression with regard to each reaction temperature indicates the kinetic parameter k_{1W}' while each intercept represents the value of $k_{1W}'[OH]_{moisture,\ initial}$. In this estimation, we assumed that 1 mole of the added water produces 1 mole of hydroxyl group which have the catalyzed effect on the curing reaction. The determined kinetic parameter of k_{1W}' is shown in Figure 5-12 and Table 5-1. The initial amount of absorbed water by moisture ($[OH]_{moisture,\ initial}$) for each condition was also estimated and shown in Table 5-1.

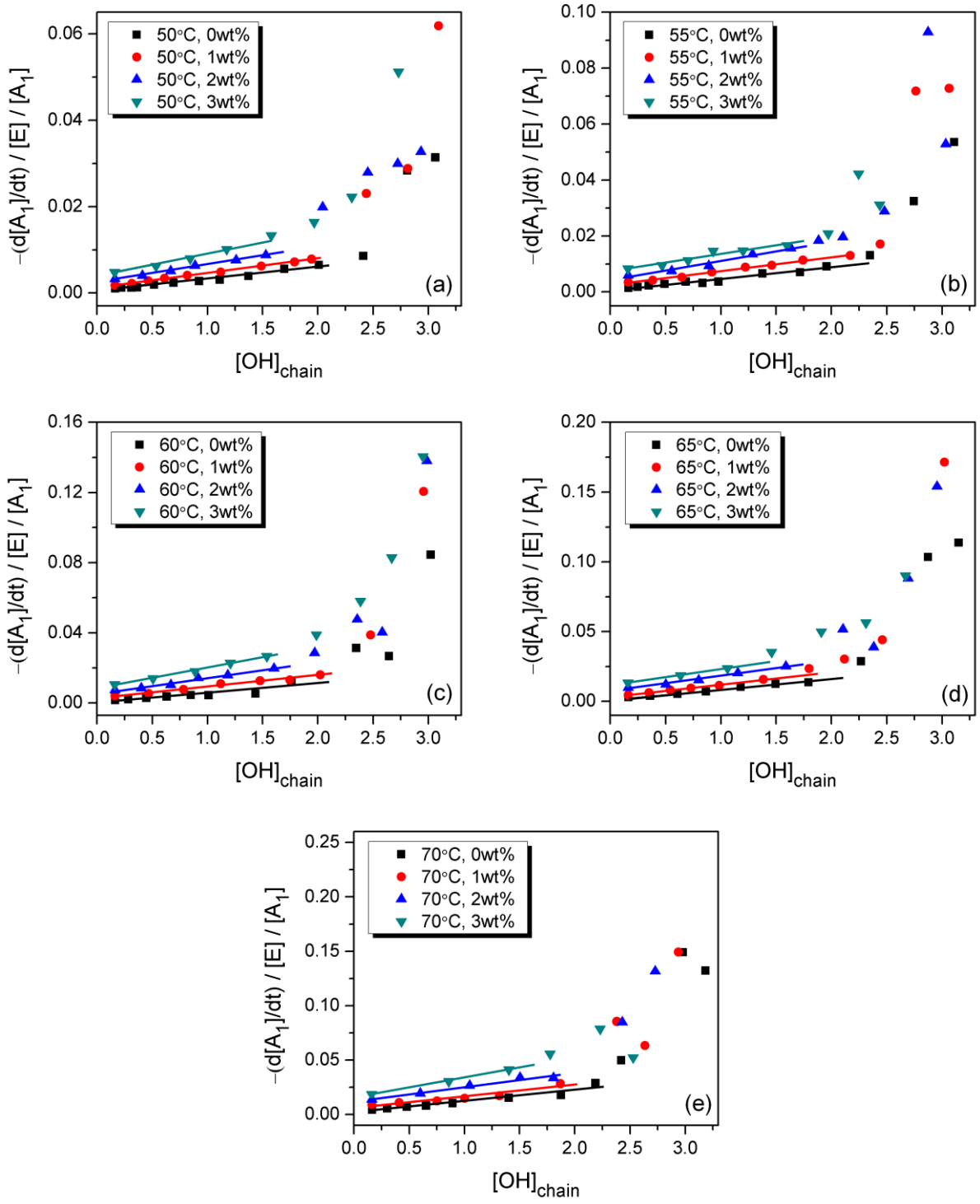

Figure 5-8. Reduced rate of epoxy-primary amine reaction as a function of $[OH]_{chain}$: (a) Cured at 50°C, (b) Cured at 55°C, (c) Cured at 60°C, (d) Cured at 65°C, (e) Cured at 70°C.

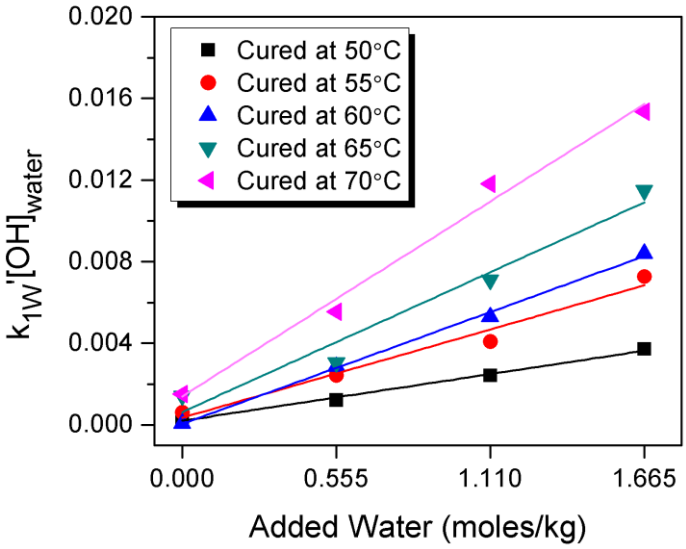

Figure 5-9. Plotting of intercept values (k_1"$[OH]_{water}$) from Figure 5-8 as a function of the contents of added water ($[OH]_{water}$)

With the calculated values of k_{1C}', k_{1W}', and $[OH]_{water}$ by the method suggested above (Figures 5-8 and 5-9), Equation 5-9 presents the predicted values of the reaction rate for the primary amine. These predicted values are compared with the experimental values obtained by differentiation of the concentration changes of primary amines which were directly observed by FT-IR measurement, as shown in Figure 5-6. It is observed that the rate equations derived according to the proposed cure mechanism describe the experimental phenomena during the course of the reaction.

For the evaluation of the kinetic parameters with regard to the epoxy-secondary amine reaction (k_{2C}', k_{2W}'), the concentration profiles for tertiary amines should be obtained by the calculation of the mass balance equation with the values of the concentrations of epoxide and primary amines directly measured by FT-IR.

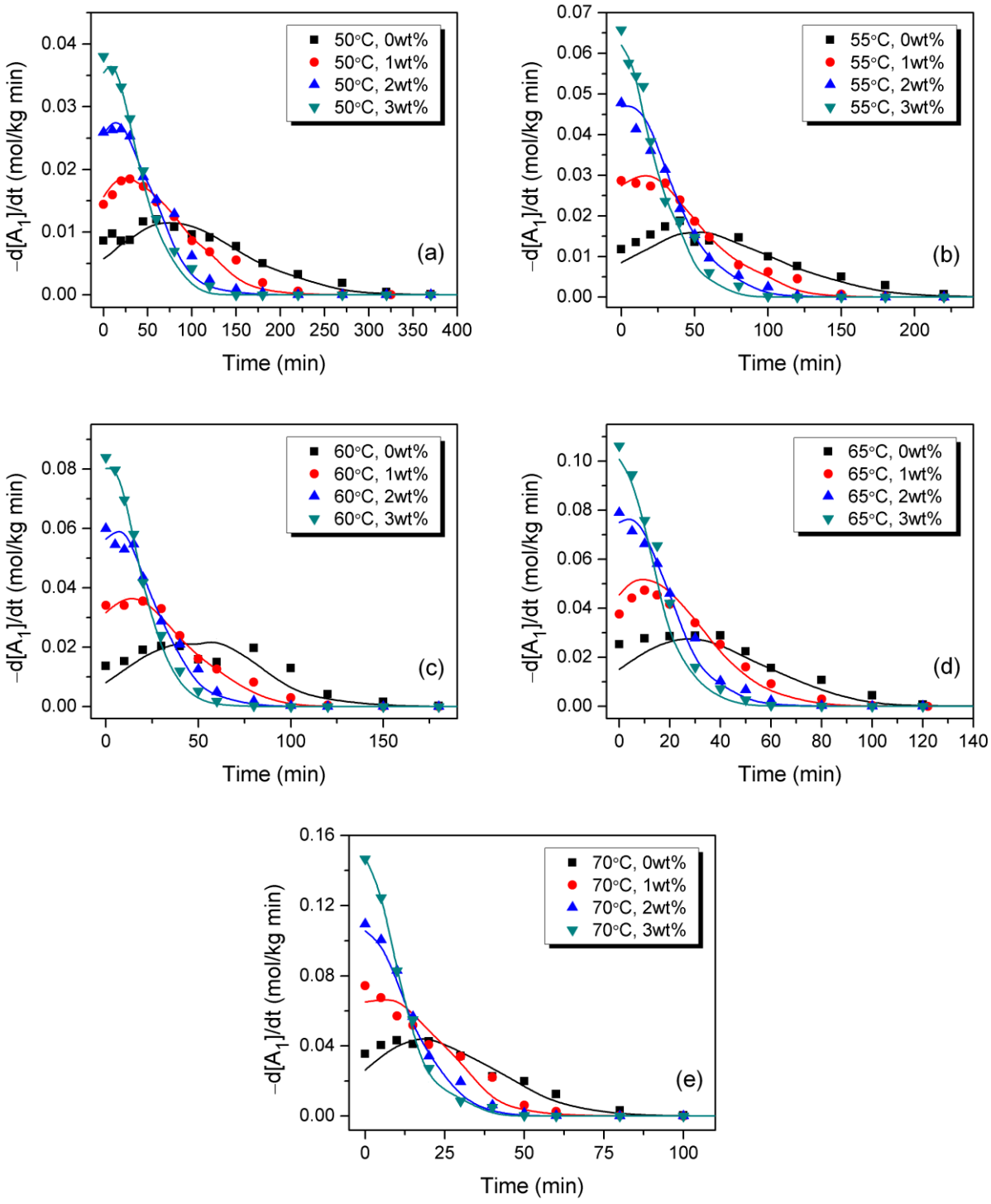

Figure 5-10. Comparison of experimental and predicted values for reaction rate of primary amine (symbols: experimental, lines: predicted): (a) Cured at 50°C, (b) Cured at 55°C, (c) Cured at 60°C, (d) Cured at 65°C, (e) Cured at 70°C

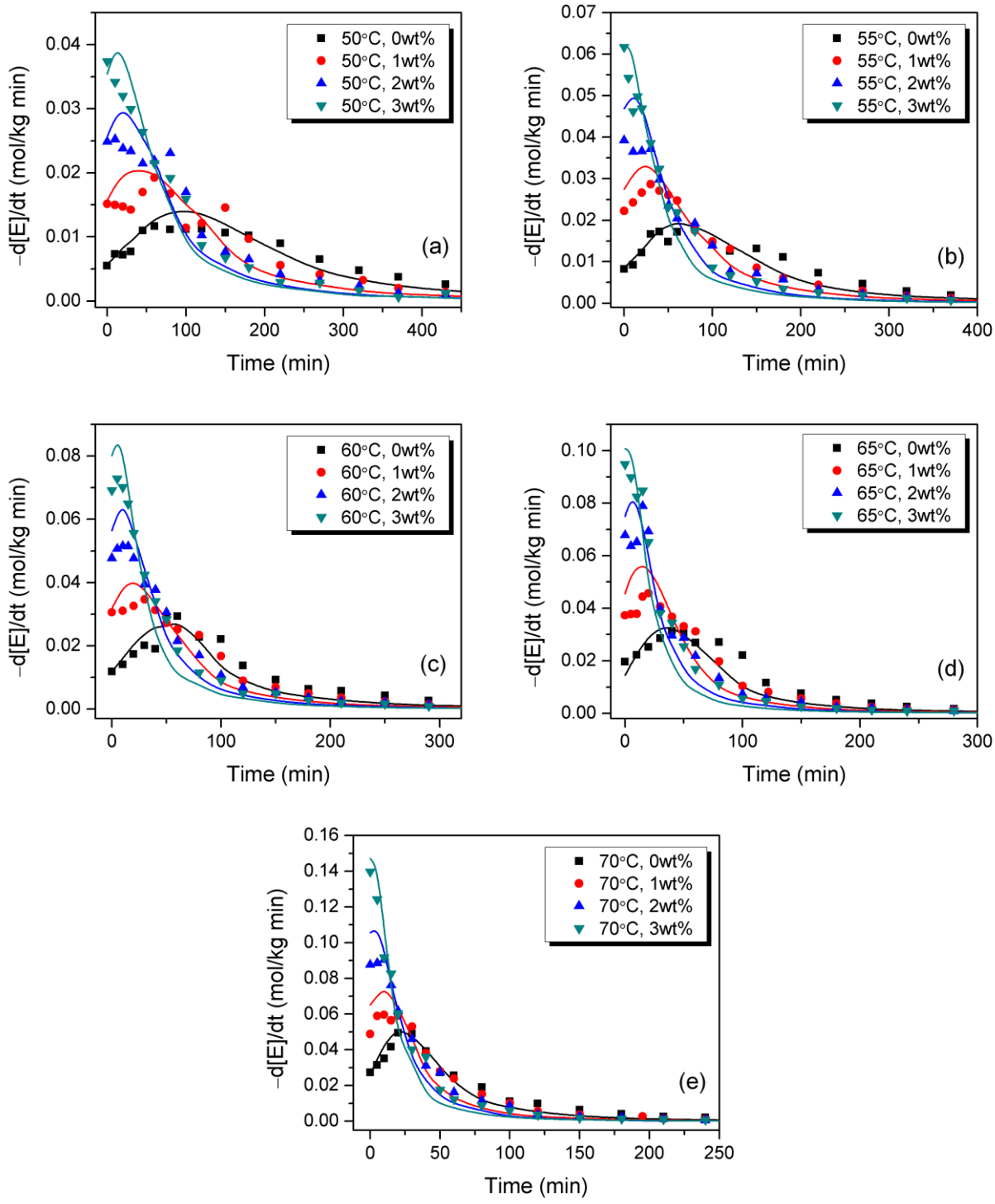

Figure 5-11. Comparison of experimental and predicted values for reaction rate of epoxide (symbols: experimental, lines: predicted): (a) Cured at 50°C, (b) Cured at 55°C, (c) Cured at 60°C, (d) Cured at 65°C, (e) Cured at 70°C

However, it is actually difficult to obtain precise values for the changes in concentration of tertiary amine in that the numerical values of concentrations are much smaller compared with that of the epoxide and primary amine. Given the ex-situ condition to obtain periodical changes in normalized area for epoxide and primary amine while handling the FT-IR spectra, it is inevitable that very small variation of the normalized area of epoxide and primary amine resulted in somewhat large deviation in the calculation of tertiary amine concentrations, which consequently produces much larger statistical errors for the linear regression with the first derivative value as a function of time using Equation 5-10.

For another approach to estimate the kinetic parameters regarding the epoxy-secondary amine reaction, it is suggested that the parameters can be obtained using Equation 5-15, assuming the ratios of k_2/k_1 and k_{2C}'/k_{1C}' (as well as k_{2W}'/k_{1W}' in this study) are independent of the reaction path.[83, 84, 101, 162, 163] In this assumption, the ratio of the reaction constant between epoxide-secondary amine and epoxyde-primary amine addition are assumed to be the same whether the reaction occurs through non-catalytic reaction, catalytic reaction via hydroxyl from polymer chain, or catalytic reaction via hydroxyl from water/moisture ($k_2/k_1 = k_{2C}'/k_{1C}' = k_{2W}'/k_{1W}'$).

Thus, from Equation 5-15, when the concentration of the secondary amine is at the maximum value, it follows that the left hand side is equal to 0. Then, with the assumption of the ratios being independent of the path, the following equation can be derived.[101]

$$\frac{k_{2C}'}{k_{1C}'} = \frac{k_{2W}''}{k_{1W}''} = \left(\frac{[A_1]}{[A_2]}\right)_{\text{at}\left[A_2\right]_{\max}} \tag{5-17}$$

When the values of $[A_1]$ and $[A_2]$ at the maximum point of $[A_2]$ are directly taken from the curves shown in Figures 5-6 and 5-7 for each cure condition, kinetic parameters k_{2C}' and k_{2W}' can be obtained as shown in Figure 5-12 and Table 5-1

Combined with the obtained kinetic parameters of k_{1C}', k_{1W}', k_{2C}', and k_{2W}', the validity of the utilized model for the entire reaction can be compared using Equation 5-14 as shown in Figure 5-11. Again, it is shown that the rate equations derived according to the proposed cure mechanism well describes the experimental changes of concentration in this system.

With the derived values of each kinetic parameter, Arrhenius temperature dependencies can be analyzed for the catalytic reaction rate constants of k_{1C}', k_{1W}', k_{2C}', and k_{2W}', as shown in Figure 5-12. Activation energies and corresponded values of pre-exponetial factors were also calculated from the resulting slopes and intercepts, as shown in Table 5-2. From Figure 5-12, it clearly shows that the rate constants of k_{1C}' and k_{2C}' have slightly higher values than k_{1W}' and k_{2W}', respectively, indicating that the catalyzed effect by hydroxyls from the polymer chain is larger than that by hydroxyls from moisture or water in that the reaction is faster for all the reaction temperatures, where auto-catalyzed nature still has a larger influence to the cure acceleration than the effect of water addition. The comparison of the calculated activation energy which have comparable values of 55.0 and 61.3 kJ/mol for the epoxide-primary amine addition and 46.3 and 52.5 kJ/mol for the epoxide-secondary amine addition also supports the above comparison of rate constants.

Considering the acidity of water is very comparable to that of alcohols (polymer chain) from the fact that pKa values of those are in the range of 14~16,[164] the

comparable values of rate constants between the reaction catalyzed by $[OH]_{chain}$ and $[OH]_{water}$ are reasonable, in which difference in the logarithm value of the reaction constant is less than one order of the magnitude.

Regarding the relative kinetic constant ratio between k_{2C}' and k_{1C}' (also, between k_{2W}" and k_{1W}"), the estimated values ranges from 0.19 to 0.23 as shown in Table 5-1. This value of relative kinetic constant ratio represening the reactive ratio of the primary to secondary amine hydrogens, which is also known as substitution effect suggests an important factor in the formation of network morphology, in which it determines whether extensive branching already occurs in the early stages of curing, or linear polymer chains are predominantly formed.[82, 100, 165] The value of the kinetic constant ratio can be termed negative when the secondary amine is less reactive than the primary amine by sterical hindrance and reduced mobility resulting from the addition of epoxide, while the positive substitution effect is termed when the secondary amine is more reactive.[82, 157, 165, 166]

The low value of the kinetic constants ratio in this study indicates that a lower reactivity of the hydrogen in a secondary amine group with respect to a hydrogen in a primary amine group, result in initial formation of linear polymer chains predominantly.[100, 166, 167] The obtained results of strong negative substitution effect corresponds with the previous report about the epoxy systems containing polyoxypropylene diamine, in which the value of the kinetic constants ratio as low as 0.2.[37] The strong negative substitution effect of epoxy-amine systems is known to be mainly due to the sterical crowding on the nitrogen atoms after the reaction between epoxide and primary amine.[100, 166, 167]

Table 5-1. Summary of kinetic rate constants, kinetic constants ratio and estimated values of amount of initially absorbed moisture for each system

Cure Temp. (°C)	Added Water	Rate Constants ($kg^2/(mol^2 min)$)				Relative Kinetic Constants Ratio	Estimated Amount of $[OH]_{moisture, initial}$
	wt% (mol/kg)	k_{1C}'	k_{2C}'	k_{1W}'	k_{2W}'		
50	0 (0.00)	0.00290	0.00072	0.00206	0.00048	0.25	0.10
	1 (0.56)	0.00335	0.00078			0.23	
	2 (1.11)	0.00414	0.00093			0.22	
	3 (1.67)	0.00522	0.00122			0.23	
55	0 (0.00)	0.00400	0.00095	0.00390	0.00082	0.24	0.09
	1 (0.56)	0.00498	0.00118			0.24	
	2 (1.11)	0.00692	0.00109			0.16	
	3 (1.67)	0.00615	0.00131			0.21	
60	0 (0.00)	0.00552	0.00104	0.00494	0.00096	0.19	0.01
	1 (0.56)	0.00644	0.00141			0.22	
	2 (1.11)	0.00894	0.00184			0.21	
	3 (1.67)	0.01152	0.00189			0.16	
65	0 (0.00)	0.00705	0.00157	0.00617	0.00121	0.22	0.10
	1 (0.56)	0.00896	0.00176			0.20	
	2 (1.11)	0.01111	0.00197			0.18	
	3 (1.67)	0.01142	0.00213			0.19	
70	0 (0.00)	0.01059	0.00201	0.00860	0.00166	0.19	0.16
	1 (0.56)	0.01063	0.00211			0.20	
	2 (1.11)	0.01323	0.00294			0.22	
	3 (1.67)	0.01810	0.00289			0.16	

Table 5-2. Values of activation energies and related pre-exponential factor for each system

	k_0 ($kg^2/(mol^2 min)$)	E_a (kJ/mol)
k_{1C}'	3.03×10^6	55.0
k_{2C}'	2.65×10^4	46.3
k_{1W}'	1.92×10^7	61.3
k_{2W}'	1.62×10^5	52.5

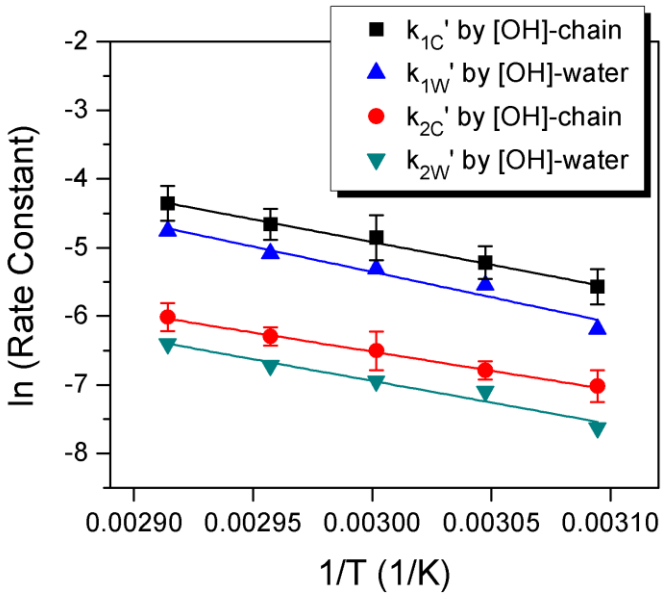

Figure 5-12. Arrhenius relations for the rate constants of k_{1C}', k_{1W}", k_{2C}', and k_{2W}"

Summary

In this study, we examined the effect of water addition on cure kinetics of an epoxy-amine thermoset. The near FT-IR measurement suggested an excellent method to monitor the cure kinetics of the system. Experimental data clearly demonstrated that the cure reaction was significantly accelerated with the addition of a small amount of water. With the modified mechanistic modeling, it successfully compared the kinetic values catalyzed by hydroxyl group generated from polymer chain with those from added water or moisture absorption. From the comparison, it can be concluded that the catalyzed effect by hydroxyl from water is as large as that by hydroxyl from polymer chain. Regarding the huge effect of water which catalyzed cure reaction observed in this system, it can be estimated that the well-known property of hydrophilicity for polyoxypropylene diamine induce intimate mixing between the polymer chains and water, which maximize the influence of hydroxyl from water or moisture.

The obtained results in this study propose that even small amount of water which is absorbed during the course of curing or at the storage condition could largely influence the rate of cure reactions resulting in different states of cure degree at the final products. The water influence could cause more impact especially on the slow curing system. In the field of real application such as outdoor or electronic applications, in order to take advantage of easy installation, many epoxy-amine adhesives and coatings are cured under ambient conditions, thus undergoes slow cure reactions. In such cases, the small changes in humidity during the given cure time could significantly influenced the different rate of cure reaction.

CHAPTER 6
ROLE OF CHEMICAL BONDING ON THE DURABILITY OF EPOXY ADHESION FOR STRUCTURAL STRENGTHENING APPLICATION

Background

Epoxy resin as a seal coat, adhesive and impregnating resin has been widely used for structural strengthening applications such as a rehabilitation of concrete structures using externally bonded carbon fiber-reinforced polymer (CFRP) composites, providing high performances of strength, stiffness, and resistance to creep.[15, 104] One of the most significant advantages of this method is easy installation and considerable cost savings using a wet lay-up or pre-cured laminate. Compared to the conventional repair method of concrete structures by using steel, workers can easily handle the light and flexible FRP materials which involve short labor time and rapid bonding of FRP materials using heat curing epoxy adhesives.[168, 169]

Although epoxy resins provide the high qualities of adhesion for the structural strengthening, the strengthened systems have shown critical degradation of its performance with environmental exposure such as moisture, temperature and various solutions like chloride, alkali, and salt water.[105-112] A number of studies have revealed that degradation of interfacial bonding between cementitious materials and the utilized adhesives with environmental exposure is the main reason for the loss of strength in these systems.[106, 108, 112] Although many studies have reported a loss in performance, few studies have attempted a method to effectively maintain or enhance the durability of the bond strength under the exposure.

As previously stated in Chapter 2, in an attempt to enhance the durability of interfacial bonding properties between an epoxy and cementitious materials with hygrothermal exposure, the mechanism of chemical bonding is taken into account.

Based on the hypothesis that hydrogen bonding plays a large role for the adhesion at the interface between cementitious materials and epoxies, and is responsible for the loss of adhesion under humid environments by displacement of epoxy with water, it is expected that chemical modification of the surface of adherend with coupling agents contributes to the enhancement of bonding properties.

In this work, in order to investigate the effect of the silane treatment of concrete surface on the durability of bonding, slant shear testing method was employed, in which the changes in failure strength for silane-modified samples was compared to those for samples without modification. This work also focused on spectroscopic analysis to identify the chemical modification of concrete. Such an effort will contribute to the understanding of the adhesive bonding properties for structural strengthening applications, which will also be very useful in designing materials with tuned properties.

Experimental Section

Sample Preparation

To prepare the samples in accordance with the slant shear testing method based upon ASTM C882, two equal sections of a cylindrical concrete specimen were fabricated with dimensions of 7.6cm×15.2cm, each section having a diagonally cast bonding area at a 30° angle from vertical. For the fabrication of each specimen a dummy section which fits to a cylindrical mold was prepared (Figure 6-1 (a)). After inserting the dummy section into the mold, the concrete was added into the mold and then cured. The ratios of water/cement and cement/sand were selected as 0.37:1 and 1:1.91, respectively, based upon ASTM C109 and C305. Cement from the same bag was used to produce all of the specimens to ensure consistency in the chemical and mechanical properties of the specimens.

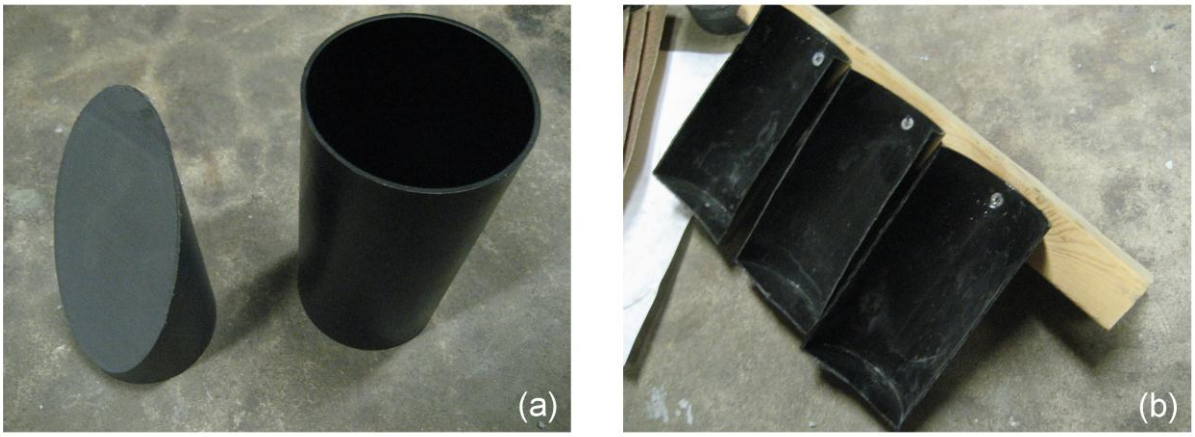

Figure 6-1. Pictures of apparatus to prepare “composite cylinder” samples: (a) dummy section (left) and mold (right), (b) supporting tool to make the bonding surface of “composite cylinder samples” horizontal after epoxy application (photo courtesy of Sungwon Choi)

In this work, different curing schedules of each concrete mixture were employed, which fit the different purposes of each slant shear test: (1) preliminary slant shear testing and (2) primary slant shear testing. The main objective of the preliminary slant shear testing was to find the silane coupling agent that demonstrated the best performance under hygrothermal exposure. In this preliminary test, to simply compare the durability between the samples with silane modification and those without modification, only one exposure condition was chosen: water immersion at 50°C. For the sample preparation of this test, in order to shorten the fabrication time, the concrete mixture was cured for a total of 3 weeks in air (1~2 days in a cylinder mold at RT followed by 19~20 days in air after de-molding).

For the primary slant shear testing, samples were prepared to monitor the changes in durability with the selected silane coupling agent which showed the best performance. In this primary test, the changes in failure load with different exposure

conditions were monitored, after a full cure of concrete specimens. The cure conditions of the concrete specimens for this test included curing in a cylinder mold for 1 week, followed by immersion into a lime solution for 3 weeks after de-molding, followed by curing in air for 1 week.

Two different types of silane coupling agents were utilized in the preliminary slant shear testing to compare their contribution to the enhancement of the durability with hygrothermal exposure: (1) epoxy-functional silane coupling agent (3-glycidoxypropyltrimethoxysilane) and (2) amino-functional silane coupling agent (3-amino-propyltrimethoxysilane). To prepare each silane solution, 1wt% of the selected coupling agent was added to a 90:10 mixture by weight of ethanol:deionized water. After the pH was adjusted to approximately 5 by the addition of a few drops of acetic acid, the solutions were stirred for 60 minutes to allow complete hydrolysis of the coupling agent, and were then ready to be applied. To prepare the “composite cylinders” with treatment of the silane coupling agent, the surfaces were wiped with a piece of clean fabric before the treatment without employing any method of surface roughening such as sand blasting. Subsequently, both surfaces of two equal sections of concrete were painted with the prepared silane solution using a brush for 10 mins. After painting, the samples were put into an oven at 60°C for hydrolysis. Then the surface was ready for bonding, preferably within 1 hour.

A two-part epoxy, diglycidyl ether of bisphenol A (DGEBA, EPON 826; Hexion) and poly(oxypropylene) diamine (POPDA, Jeffamine D-230; Huntsman) was used as an adhesive to bond two sections of concrete mortar in both the preliminary and primary slant shear testing. The mass ratio of DGEBA to POPDA was 100 to 32.9, to reach

stoichiometric equivalence between functional groups based upon the manufacturers' information. The two liquid components were mixed vigorously for 5 mins to ensure even mixing. The mixed material was then degassed for 30 mins under vacuum to remove air bubbles, and ready to be applied. For the application of the epoxy adhesive, the cylinder halves were jacketed at the bonding surface using duct tape. To ensure a uniform separation of 1~2mm between the two cylinder halves, a small piece of plastic was used as a spacer. Finally, the "composite cylinder" samples for slant shear testing were prepared by injecting the epoxy adhesive using a syringe through an opening in the jacketing and allowing it to wick into the space between the two bonding surfaces. Subsequently, the "composite cylinder" was placed so that the bonding surface remained horizontal and the epoxy was allowed to cure (Figure 6-1 (b)). In this work, the epoxy adhesive was cured at RT for 3 weeks before exposure was begun for both the preliminary and primary slant shear testing.

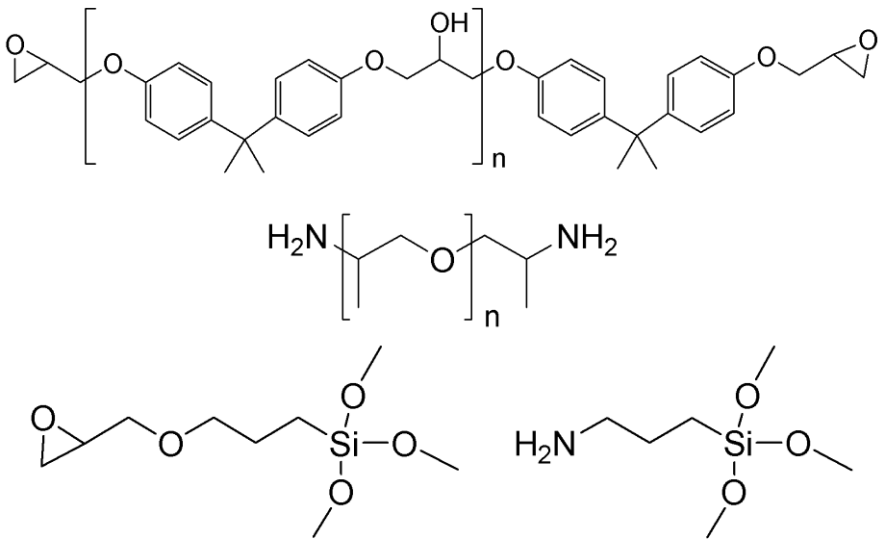

Figure 6-2. Chemical structures of DGEBA, POPDA, epoxy-functional silane (3-glycidoxypropyltrimethoxysilane), and amino-functional silane (3-amino-propyltrimethoxysilane).

Chemical structures of DGEBA, POPDA, epoxy-functional silane (3-glycidoxy-propyltrimethoxysilane), and amino-functional silane (3-amino-propyltrimethoxysilane) are shown in Figure 6-2.

With regard to the fabrication timeline of the “composite cylinders” for the primary testing, the mix number shown in Table 6-2 represents the time sequence as the concrete mixture was prepared. Thus, 6 specimens were fabricated at one time, and the time interval between each mix number was approximately one week. Since this work was conducted over a long period of time, changes in temperature or humidity due to changes in weather varied over the course of the study. The surface condition of the concrete is highly dependent on the humidity and temperature of its environment, which could thus be varied since the concrete cylinders are cured in air for one week before the epoxy adhesive and/or the silane coupling agent are applied. On the contrary, compared to the long-term fabrication time for sample preparation for primary testing, the preliminary testing consumed a very short-term period for fabrication, thus, the changes in weather were not considered to have influenced the results. The detailed impact of this factor on the primary mechanical testing results is discussed in the Results section.

Exposure Environments

Exposure environments used for the preliminary slant shear testing consisted of immersion into tap water at 50°C for 3 weeks. For the primary testing, they consisted of water immersion at temperatures of 30, 40, 50, and 60°C for time periods of 4, 8, and 12 weeks. Details of hygrothermal exposure conditions used for the preliminary and primary slant shear testing are shown in Tables 6-1 and 6-2.

Table 6-1. Cure and exposure conditions for preliminary slant shear testing.

Cure Condition		Exposure Conditions			# of specimens		
Concrete	Epoxy	Types	Time (weeks)	Temp. (°C)	W/O Silane treatment	W/ Amino-Silane	W/ Epoxy-Silane
1~2 days in mold + 3 weeks in air	3 weeks in air	Air (control)	3	RT	3	3	3
		Water immersion	3	50	3	3	3

Table 6-2. Cure and exposure conditions for main slant shear testing.

Mix #	Cure Condition		Exposure Conditions			# of specimens	
	Concrete	Epoxy	Types	Time (weeks)	Temp. (°C)	W/O Silane treatment	W/ Epoxy-Silane
1	1 week in mold + 3 weeks in lime solution + 1 week in air	3 weeks in air	Air (control)	0	RT	3	3
2				12	RT	3	3
3			Water immersion	12	30	3	3
4				12	40	3	3
5				12	50	3	3
6				12	60	3	3
7			Air (control)	8	RT	3	3
8			Water immersion	8	30	3	3
9				8	40	3	3
10				8	50	3	3
11				8	60	3	3
12			Air (control)	4	RT	3	3
13			Water immersion	4	30	3	3
14				4	40	3	3
15				4	50	3	3
16				4	60	3	3

Slant Shear Testing

To investigate the effects of silane coupling agents on the durability of interfacial bonding properties between epoxy and concrete with hygrothermal exposure, a slant shear mechanical testing method was employed based upon ASTM C882. The strength was determined by using the epoxy adhesive to bond the two equal sections of a 7.6cm×15.2cm cylinder, each section of which had a diagonally cast bonding area at a

30° angle from vertical. A schematic of the slant shear testing method is shown in Figure 6-3.

The surfaces of the two concrete sections were pretreated by the silane coupling agent and bonded by the epoxy adhesive as described above, and were then compared to those without any pretreatment by the silane. The loading rate was 0.25±0.05 MPa/sec per ASTM C39 and the test was performed by determining the average compressive failure load of 3 replicas of “composite cylinders”.

To determine the compressive strength of the concrete itself, cylindrical concrete specimens were fabricated with the same dimensions of 7.6cm×15.2cm. The cure conditions were the same as those of the slant shear testing method. The same loading rate of 0.25±0.05 MPa/sec was used for the determination of the compressive strength of the epoxy-bonded cylindrical composite, based upon ASTM C39. Compared with the fabrication time line of the “composite cylinders” used for the primary slant shear testing, the neat cylindrical concrete specimens were fabricated with the 6^{th} and 16^{th} mixes of the “composite cylinders” (Table 6-2).

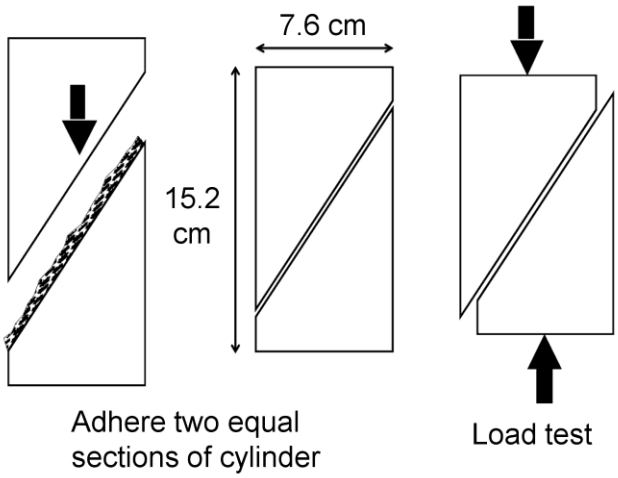

Figure 6-3. Schematic of slant shear testing method.

Analytical Method: FT-IR Spectroscopy

In order to identify the presence of silane coupling agent deposited on concrete, Fourier transform infrared spectroscopy was used (FTIR; Nicolet Magna 760, Thermo Electron Cooperation) in the diffuse reflectance infrared Fourier transform (DRIFT) mode. The DRIFT spectra were recorded over the range of 400-4000 cm^{-1} with a KBr beamsplitter and a DTGS detector using 64 scans at a resolution of 4 cm^{-1}. For the sample preparation, powders of “composite cyinders” were obtained from parts of the sample unexposed to the epoxy or silane coupling agent, after the slant shear testing. The DRIFT spectra of the neat powder was compared with that of the powder treated by the silane coupling agent with the same application procedure as used for “composite cylinders”. No baseline correction or subtraction method was used on the spectra. In this experiment, the DRIFT spectrum for each powder sample mixed with KBr powder in a proportion of 1:100 were obtained to facilitate qualitative measurement.

To compare those spectra with the spectroscopic features of the silane coupling agent itself, the attenuated total reflection (ATR) mode with a KBR beamsplitter and a DTGS detector was utilized. In this experiment, ZnSe was utilized as the internal reflection element with an aperture angle of 63 using 64 scans at a resolution of 4 cm^{-1}.

Results

Since this study focused on interfacial bond degradation between epoxy and concrete with environmental exposure, the strength of the concrete should be high enough to ensure that the concrete itself does not fail, thus forcing adhesive failure during loading. This enables monitoring of the changes in interfacial bond degradation. Table 6-3 shows the compressive failure loads of neat cylindrical concrete, each of which had the same cure conditions as the concrete mixture used for the preliminary

and primary slant shear testing, respectively. From the results, they show higher failure loads compared to the adhesive failure loads of the “composite cylinders” for each test which will be described in the next section.

Table 6-3. Failure loads from neat cylindrical concrete specimen compressive testing

Specimens	Failure Load (kN)					
	Concrete used for preliminary testing		Concrete used for main testing			
			Mix 6		Mix 16	
	Values	Average	Values	Average	Values	Average
#1	155.4	135.5	362.1	352.2	333.0	335.7
#2	107.1		342.7		331.1	
#3	137.8		351.7		343.0	
#4	141.5		–		–	

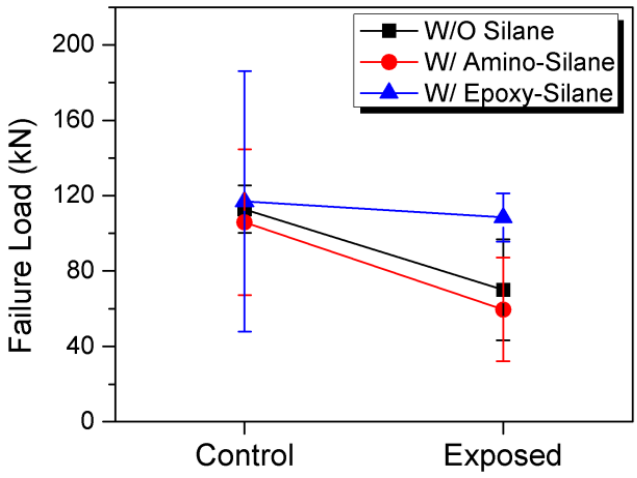

Figure 6-4. Results of preliminary slant shear testing

In order to identify how each coupling agent affects the bond durability, the changes in failure load from the preliminary slant shear testing was observed with a single exposure condition of water immersion at 50°C for 3 weeks, compared to control

specimens exposed in air for the same time period. As shown in Figure 6-4, it is obvious that interfacial bond degradation resulted in significant decrease in the durability of the bond strength with hygrothermal exposure. The control specimens show no difference in failure loads with type of silane when the failure load for the control system of unexposed specimens without any silane application is compared to that of the exposed specimens, over a 40% residual strength decrease was seen after hygrothermal exposure. This difference appears to be significant, as the failure loads for the control (no silane) and exposed (no silane) specimens are different by more than one standard deviation (as shown from the error bars).

Figure 6-4 also clearly shows that the application of epoxy-functional silane coupling agent leads to a significant enhancement of durability with hygrothermal exposure. When the failure loads of the exposed specimens for three groups, which varied with different surface conditions, are compared with each other, it is shown that the average value of the failure load was higher for the exposed specimens modified by the epoxy-functional silane. This difference between the failure loads for the exposed epoxy-functionalized specimens and the exposed unfunctionalized specimens appears to be significant, as the difference is greater than one standard deviation. In the comparison of the average value of failure load, compared to a control group of the exposed specimens without any silane coupling agent, which revealed 61.6% of residual strength with the exposure, the specimens with the epoxy-functional silane showed a significantly higher residual strength (92.8%).

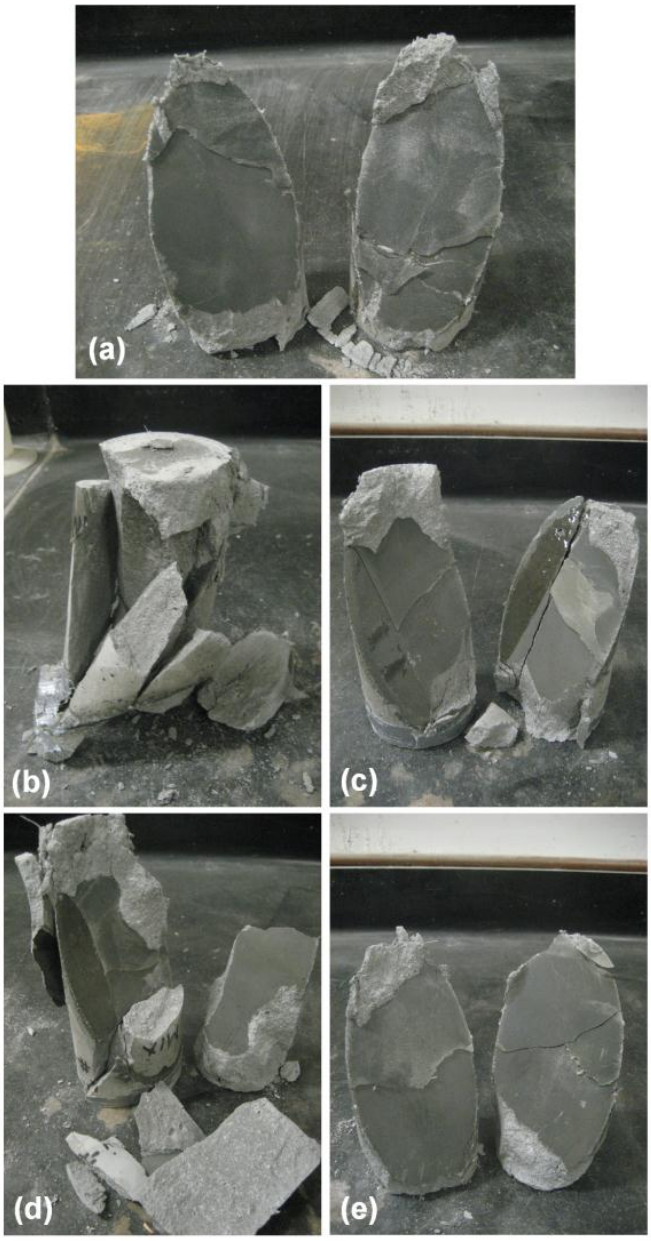

Figure 6-5. Failure surfaces of control specimens for preliminary slant shear testing: (a) without silane treatment, (b) and (c) with amino-functional silane treatment, (d) and (e) with epoxy-functional silane treatment (photo courtesy of Sungwon Choi)

The large deviation within the set of control specimens which employed the amino- and epoxy- functional silane treatment, as shown by the error bars in Figure 6-4, was ascribed to the partial breaking of the concrete itself combined with mostly adhesive

failure due to the lower strength of concrete (Figure 6-5). However, all the exposed samples showed completely adhesive failure, and exhibited relatively low standard deviations, which indicates the interfacial bond degradation with exposure (Figure 6-6) resulting in lower standard deviations due to the more consistent adhesive failure mode.

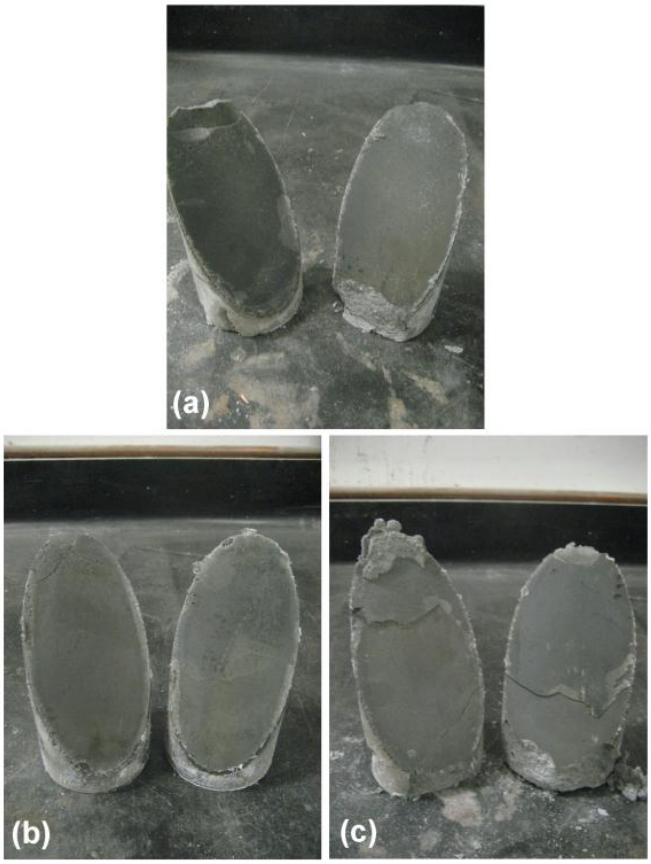

Figure 6-6. Failures of exposed specimens for preliminary slant shear testing: (a) without silane treatment, (b) with amino-functional silane treatment, (c) with epoxy-functional silane treatment (photo courtesy of Sungwon Choi)

On the other hand, the effect of the amino-functional silane on durability was negative, where the average residual strength was 56.3%, which is almost the same as the control. A possible explanation for this behavior can be found in the literature in

which Harun et al. compared the effect of an amino-functional silane coupling agent used as an adhesion promoter for an epoxy coating on steel substrate on a pull-off adhesion test with water immersion.[170] They found that the adhesion strength deteriorated rapidly with water immersion when the amino-functional silane coupling agent was utilized, even compared to no silane treatment. In their analysis from angle-resolved X-ray photoelectron spectroscopy, it was estimated that the coupling agent adsorbs onto the steel substrate with amine groups predominantly oriented towards the substrate while the silanol groups oriented upwards to the organic coating layer. Thus, the amine group was hydrogen bonded to the steel, rather than the coupling agent forming the desired Si-O-Si linkage. This hydrogen bond is considerably less resistant to hydrolysis, resulting in the lower failure strength.

Another possible explanation to describe the negative effect of the amino-functional silane is the possibility of the formation of several silane layers which physically adsorbed on the concrete surfaces during the modification process. Since the multiple silane layers are usually cohesively weak, in such case the failure could easily occur through the silane layers with hydrolysis during water exposure, resulting in even lower failure strength.[35]

In the primary slant shear testing, with the selected epoxy-functional silane coupling agent, changes in failure load from the slant shear testing was monitored with water immersion at different temperatures of 30, 40, 50, and 60°C, compared with control specimens. Exposure in these conditions was conducted over time periods of 4, 8, and 12 weeks, and the changes in failure load with the specimens treated by the silane modification were compared to those without any modification. In this slant shear

testing, all the specimens showed adhesive failure, in which failure occurred between the epoxy and concrete surface at a maximum failure load although some specimens were accompanied with small broken pieces of concrete (Figure 6-7).

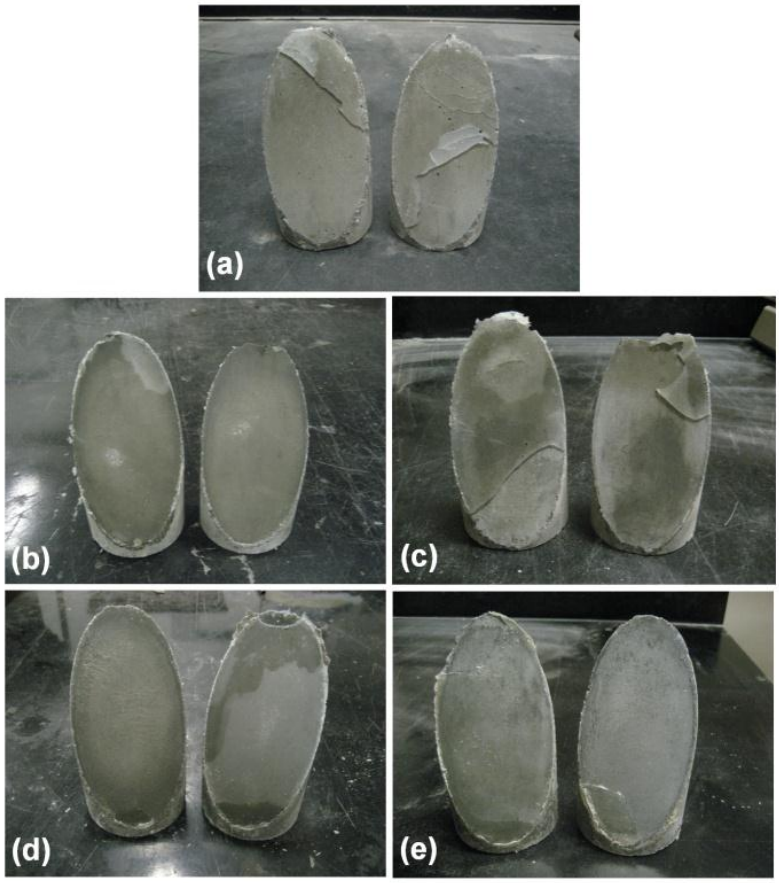

Figure 6-7. Failures for primary slant shear testing: (a) control specimens prior to exposure, (b) exposed at 30°C for 4 weeks, (c) exposed at 40°C for 12 weeks, (d) exposed at 50°C for 8 weeks, (e) exposed at 60°C for 8 weeks (photo courtesy of Sungwon Choi)

Figure 6-8 shows the changes in failure load for the control specimens, which were exposed to air after 3 weeks of epoxy adhesive curing at RT. For samples modified by the silane coupling agent, higher average values of failure loads than those without the modification throughout the entire exposure timeline are evident for the 0-,

4-, and 12-week exposure although the difference at 12 weeks is less than one standard deviation and thus may not be significant.

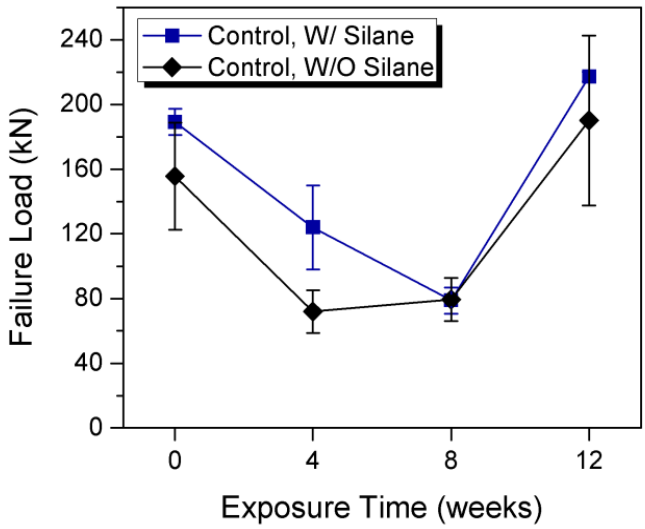

Figure 6-8. Results of primary slant shear testing for control specimens.

With regards to the lower failure load at 4 and 8-week exposure, compared to the initial and the higher failure load at 12-week exposure, some possible explanations can be suggested. Firstly, the concrete specimens for the 8-week exposure showed features of salt leaching out found at the outer surface of the specimen after exposure despite the same experimental conditions with other specimens. We assume that different cure conditions caused by changes in the weather influenced the chemical nature of the concrete surfaces, which induced some abnormal phenomena of salt leaching out of concrete specimens, resulting in the lower strength. Another possible description with respect to the much higher failure load at the 12-week exposure could be related to the properties of the epoxy resins which cured under ambient conditions. Since the tests were also conducted over relatively short exposure time periods, post-curing reaction of

the utilized epoxy adhesive might produce some unusual behavior in which additional cure induces a property increase after the exposure.[152, 171]

On top of that, the larger deviation of the failure load between each exposure time despite the same experimental condition suggests that the changes in the chemical nature of the concrete surface caused by changes in fabrication environments could result in larger difference in interfacial bond properties. As described in the experimental section, each set of the specimens were fabricated at a different time, and included curing in air for 1 week. Since this work was been conducted over a long time period, changes in temperature or humidity varied significantly over the fabrication time. Thus, it is estimated that the fabrication environments strongly influenced the chemical nature of the concrete specimens, which resulted in a large deviation of the failure load. Additional testing would be needed to confirm this result.

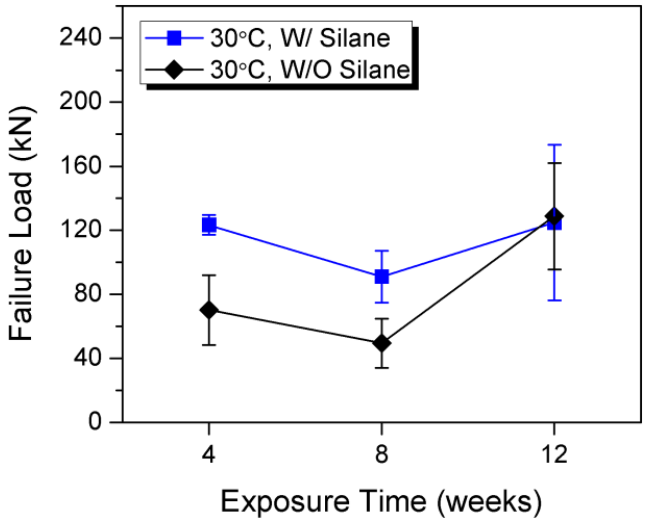

Figure 6-9. Results of primary slant shear testing for water immersion at 30°C.

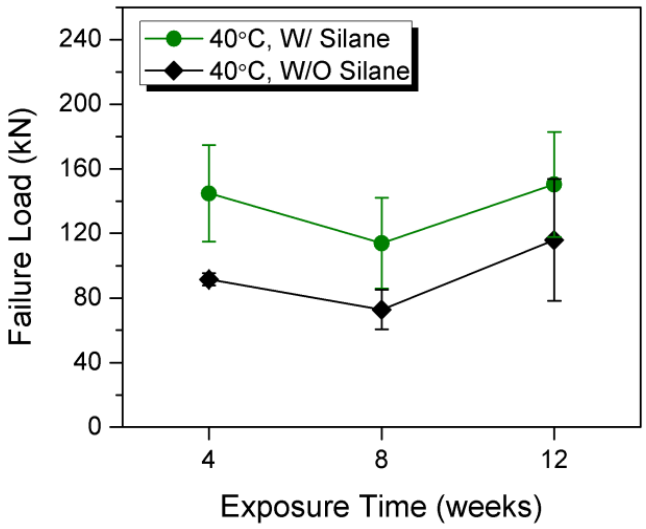

Figure 6-10. Results of primary slant shear testing for water immersion at 40°C.

As shown in Figure 6-9, the specimens with silane modification and water immersion at 30°C exhibit higher failure load compared to those without any modification, with the exception of the 12 week exposure. For the 4- and 8-week exposure the differences between the modified and unmodified specimens is greater than one standard deviation..

Figure 6-10 also shows that the application of the epoxy-functional silane coupling agent leads to a significant enhancement of durability with hygrothermal exposure at 40°C. The average values of the failure loads were higher for all exposure times. As with the data for 40°C exposure, it appears that only the 4 and 8 week exposure times show significant differences (greater than one standard deviation). This might indicate a trend that the silane effect diminishes as exposure time increases. A detailed discussion of this is given in the Discussion section.

For the specimens exposed at 50 and 60°C, the average values of the failure loads clearly shows that the silane modification improves the interfacial bonding properties with the exception of the 12-week exposure at 60°C (Figures 6-11 and 6-12). Although the comparison of the average values for failure loads suggests the epoxy-functional silane clearly contributes to the enhancement of the durability, these differences do not appear to be significant as they are all less than one standard deviation, other than the 4-week exposure at 50°C. Combined with the similar trend that the differences are less than one standard deviation for the samples with longer exposure times of 12 weeks at lower temperatures of 30 and 40°C, it appears that the effectiveness of the silane is reduced under relatively severe exposure conditions.

The increase of the exposure temperature from 30 to 40 to 50°C did not result in larger degradation of failure loads in these short-term exposure time periods, but, for the samples at 60°C, a large degradation due to the higher temperature is evident (Figure 6-12).

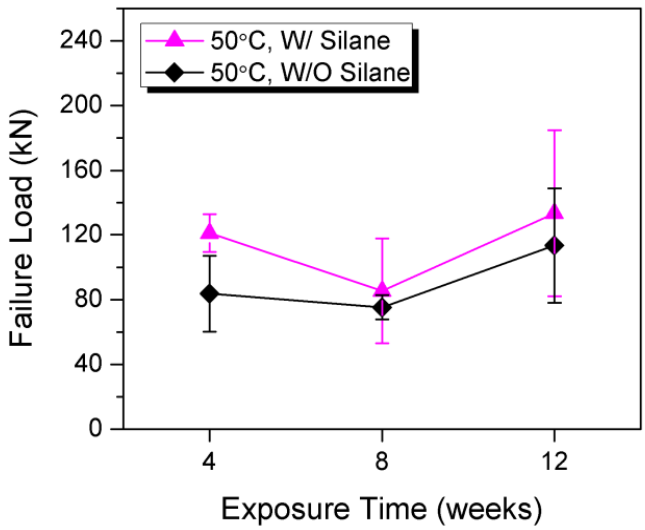

Figure 6-11. Results of primary slant shear testing for water immersion at 50°C.

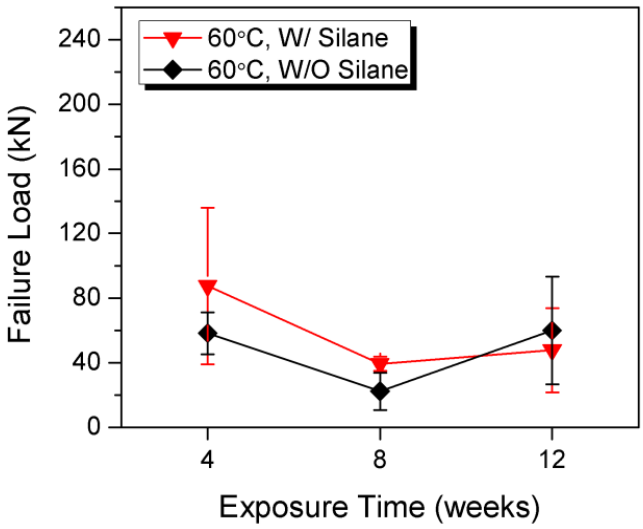

Figure 6-12. Results of primary slant shear testing for water immersion at 60°C.

Discussion

In this study, we observed that the surface modification of concrete surfaces using an epoxy-functional silane coupling agent resulted in a significant increase in the durability of interfacial bonding properties between the epoxy adhesive and concrete. In order to evaluate the possible chemical changes of bonding before and after the silane application, DRIFT spectra were recorded for both the concrete powder sample with the modification using the epoxy-functional silane and without the modification, and were compared with ATR spectra of the silane coupling agent itself. As shown in Figure 6-13, the DRIFT spectra for the concrete powders before the silane treatment shows the typical features of the material composed of cement and sand, in which the primary bands that appear are due to calcium hydroxide –OH around 3643 cm^{-1}, silanol groups around 1620 and 3450 cm^{-1}, $CaCO_3$ around 1350~1550 cm^{-1} and SiO_4 around 1055 cm^{-1}. The detailed assignment of the infrared spectra is summarized in Table 6-4.

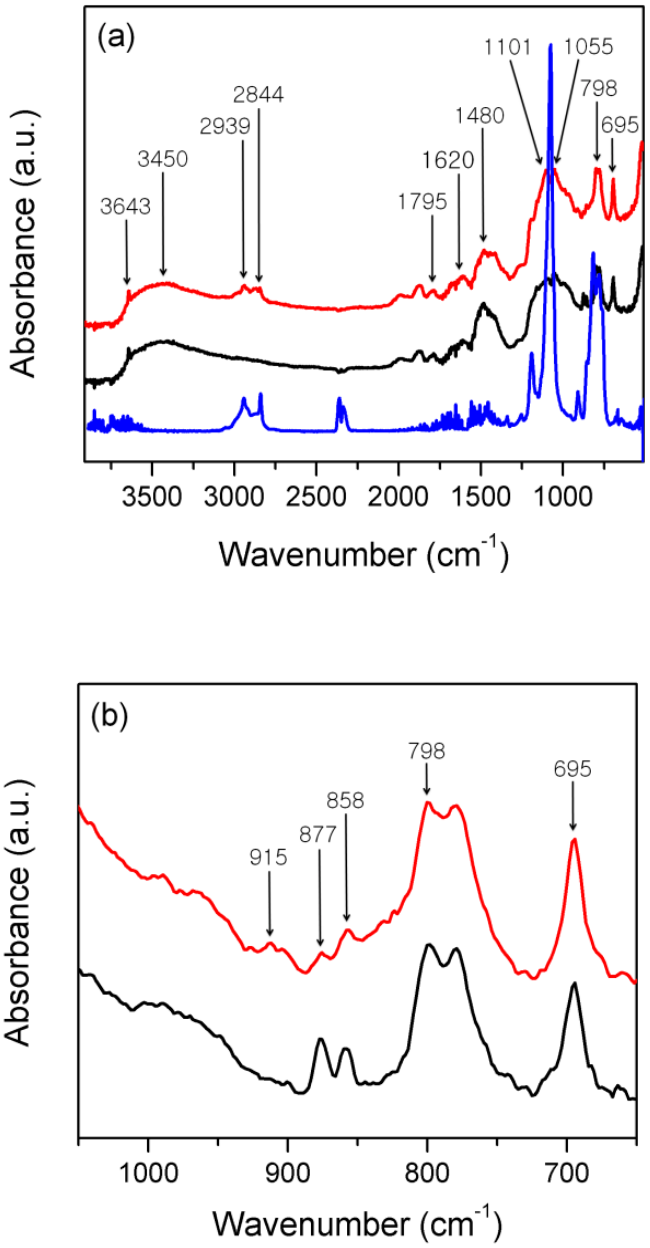

Figure 6-13. Comparison of FT-IR spectra: (a) From top to bottom: FT-IR spectra of concrete powder after the epoxy-functional silane modification (recorded in DRIFT mode) and those before the silane modification (recorded in DRIFT mode), compared to those of the utilized silane coupling agent (recorded in ATR mode), (b) FT-IR spectra for concrete powder from top picture is magnified in the range of 750~1050cm^{-1} (top: after the modification, bottom: before the modification).

Table 6-4. Possible assignment of DRIFT spectra

Peak Position (Wabenumber, cm^{-1})	DRIFT IR Assignment
695	Stretching vibration of Si-O-Si and Si-O from quartz or coupling agent [172, 173]
798	Bending mode of Si-OH from quartz or coupling agent [173-175]
858	Deformation mode of Al-O or Al-OH [176, 177]
877	Asymmetric stretching vibration of CO_3 [177, 178]
915	Combination of C-H stretching/bending of epoxide ring and Si-OH stretching from GPS species [179, 180]
1055	Asymmetric stretching vibration of Si-O [181, 182]
1101	Stretching vibration of S-O [177, 182, 183]
1350~1550	Asymmetric stretching vibration of CO from $CaCO_3$ or CO_2 [176, 182]
1620	Bending mode of OH from H_2O [176, 177]
1795	$CaCO_3$ [177]
2840~2940	Stretching vibration of CH, CH_2 [184, 185]
3450	Symmetric and asymmetric stretching vibration of OH [172, 186, 187]
3643	$Ca(OH)_2$ which formed as silicate phases in the cement dissolve [172, 186, 187]

Compared to the spectrum of the concrete powder without any silane treatment, the sample with silane treatment clearly shows the surface of the concrete powder was chemically modified with the utilized silane coupling agent. When compared to the ATR spectrum of the silane coupling agent, the new absorption peaks around 2840~2940 cm^{-1} are reasonably attributed to the deposition of the silane coupling agent on the concrete surfaces, due to the stretching vibration of C-H in the alkoxy group from the coupling agent. In addition, although the IR bands due to silanol, silicate, and SO_4 contained in concrete mixtures obscures the identification of Si-O bond formation by the

coupling agent around 455, 970, and 1055 cm^{-1}, the increased absorption bands around 915 cm^{-1}, which are due to combination of C-H stretching/bending of epoxide ring and Si-OH stretching from the species of the epoxy-functional silane, clearly indicates that the silane molecules have been successfully grafted onto the surface of concrete powders.

From the previous slant shear testing results, it is evident that the influences of chemical modification can be strongly affected by the fabrication environment due to the changes in humidity or temperature at the curing stage of concrete, which obscure the actual contribution to the enhancement of the durability. In order to exclude the effect of the fabrication environment and estimate the pure contribution of the silane coupling agent to the failure strength, the percent increase of the failure load by virtue of the silane modification was evaluated. In this calculation, the percent increase of the failure load due to the presence of the coupling agent at a given exposure time was calculated with the average values of failure load per specimen group for each mix number, in which the failure load of the “composite cylinders” with the silane modification was divided by that without silane modification. In this calculation, the failure load was used for specimens with and without the coupling agent that had each undergone the same exposure (e.g. immersion in water at 30°C). Since each mix number represents the same fabrication time line, this method excludes the effect of the fabrication environment and evaluates the silane contribution of its own effect.

As shown in Figure 6-14, the silane modification increased the failure load up to 180~190%, of the failure load with no silane treatment. In this figure, until the exposure time reached 8 weeks, the percent value with silane modification were over 100% for all

the exposure conditions, which clearly indicates that the silane coupling agent significantly enhances the durability against water immersion. Furthermore, the increase of failure load was also observed for control samples which were exposed to air.

Interestingly, Figure 6-14 also shows a trend that the silane effect diminishes as exposure time increases. Although the silane layer has a high permeability to water, providing a protective barrier against water absorption, continuous and severe water exposure induces the silane bonds of the substrate to be reactive with water, causing hydrolysis.[188] Thus, it can be estimated that the formation of silane bonds have been broken by hydrolysis with further exposure time, which diminishes the ability of the silane to enhance durability.

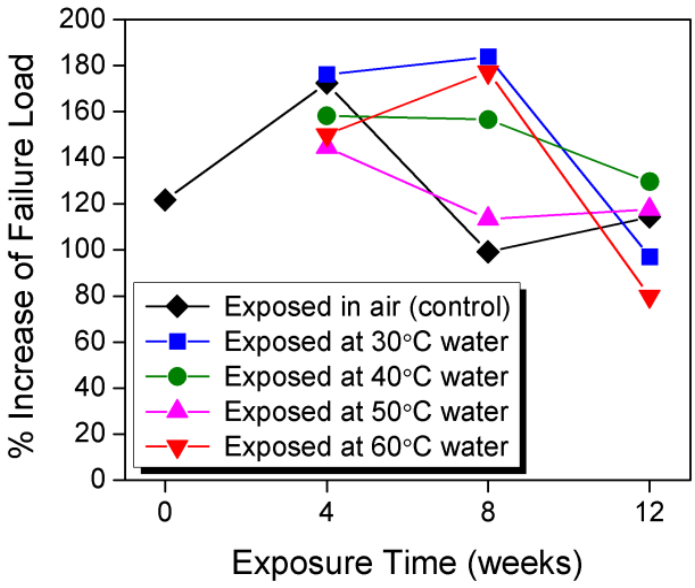

Figure 6-14. Percent increase of failure load for primary testing with the silane modification of concrete bonding surfaces.

Evidence from this study suggests that enhanced bonding at the interface results in improved durability. The improved adhesive properties might also be attributed to the

barrier effect of blocking the diffusion of water due to the presence of the hydrophobic silane. Given that hydrogen bonding is the sole candidate for the description of chemical bonding for the interface between concrete and epoxies when there is no silane treatement, hydrogen bonding is most likely responsible for the degradation under water attack. Thus, it can be concluded that the observed results of the increase in durability with silane treatment confirms the hypothesis that the displacement of epoxy hydroxyl groups from the surface of the concrete by water disrupts the interfacial bonds, resulting in a reduced interfacial bond strength.

Summary

In this study, the effect of a silane coupling agent on the durability of bonding properties between epoxy and concrete was investigated. This investigation intended to examine the hypothesis that hydrogen bonding plays a large role in the degradation of interfacial bonding between epoxy and concrete, in which displacement of epoxy with water induces a disruption of the interfacial hydrogen bond which results in reduced interfacial bond properties. Thus, the durability can be enhanced with the use of a coupling agent by changing the interfacial hydrogen bonds to stronger covalent bonding.

From the slant shear testing, it is clear that the use of the epoxy-functional silane coupling agent leads to significant improvement in durability for all the exposure conditions, which is attributed to the replacement of the weak hydrogen bonds between epoxy and cement by strong covalent bonds. Given that hydrogen bonding is the sole candidate for the description of chemical bonding for the interface between concrete and epoxies when there is no silane treatement, disruption of this hydrogen bond is responsible for the degradation under water attack.

The spectroscopic features from FT-IR confirmed the changes in chemical nature of concrete after the silane modification. With the calculation of the percent contribution to the failure strength for each set of specimens, it is confirmed that the silane application contributes to improve the durability of bonding properties with exposure for all conditions, but the effect diminished as exposure time increased.

CHAPTER 7
GENERAL CONCLUSIONS AND FUTURE WORKS

For the first part of this work, the complex hygrotheraml behavior in epoxy-amine thermosets was investigated, in which glass transition temperatures changed in a complicated manner during hygrothermal exposure in terms that both increase and decrease in T_gs were observed during the course of exposure. FT-NIR spectroscopic studies with a model epoxy-amine system demonstrated that increases in cross-link density due to additional cure during the elevated temperature exposure led to an increase in properties. However, from the feature that the T_g decreased at certain stages of the exposure, it is evident that plasticization by water occurred simultaneously, rendering the hygrothermal behavior to be more complex.

Constructing the plot of T_g versus conversion for the unexposed system provided an excellent method to consider contributions of other factors and exclude the factor of crosslink density. By applying the results for the exposed system onto this “master plot”, it is possible to directly compare the T_g values between exposed and unexposed samples while ruling out the factor of cross-link density. The result indicates that the effect of other factors, such as different types of hydrogen-bonded water and influence of the microstructure, are very small compared to the plasticization effect.

The study about commercial epoxy products which used as a seal coat and impregnating resin for structural strengthening applications confirmed that the same complex hygrothermal behavior occurs, in which the increase in T_g due to additional cure and the decrease in T_g due to plasticization are in competition with each other during exposure despite sufficient cure time at RT before exposure started.

Actually, in order to take advantage of easy installation in outdoor or electronic applications, many adhesives and coatings including epoxy-amine thermosets are cured under ambient conditions, and thus are typically not fully cured. For these systems, changes in the environments such as an increase in temperatures or exposure to water can cause additional cure resulting in an increase in physical property while properties can decrease simultaneously due to plasticization, rendering this hygrothermal behavior to be complex.

Thus, the suggested mechanism of the two competitive factors and the method for the quantitative evaluation of those in separation will contribute to the understanding of the complex behavior having property increase and decrease at the same time for various cross-linked polymer areas employing low-temperature curing under environmental effects, which will also be very useful in designing a material by providing a new method to suggest a materials specification in standards.

At the second part of this work, the effect of hydroxyl from water on cure kinetics was investigated with the hypothesis that water can significantly accelerate the cure kinetics of epoxy-amine systems. From the study of the complex hygrothermal behaviors, it shows that the post-curing reaction of the epoxy-amine thermosets was accelerated by water. Thus, this acceleration renders the effect of additional cure is no longer small, finally introducing complex behavior despite sufficient cure time at RT before exposure started. Thus, the intent of this study was to evaluate the individual water effect on cure kinetics.

Experimental data employing near FT-IR spectroscopic analysis in this study clearly demonstrated that the cure reaction accelerated with the addition of a small

amount of water, in which water acts as a strong catalyst. To evaluate the hydroxyl effect from water separately in this study, a modified mechanistic modeling was utilized. In this modeling, the non-catalytic kinetic term was neglected due to much slower reaction, and the catalytic kinetic term was separated into two different terms: (1) catalytic kinetic term by hydroxyl from auto-catalysis (2) catalytic kinetic term by hydroxyl from added water. With the suggested modeling, it successfully compared the kinetic values generated from catalyzed hydroxyl group by polymer chain with those by added water. The predicted kinetic scheme obtained from the calculated kinetic parameters using the suggested modeling well matched to the experimental values, which confirms that the proposed mechanism well describes the cure reaction of this system. From the comparison, it can be concluded that the catalyzed effect by hydroxyl from polymer chain is larger than that by hydroxyl from moisture or water. Also, this kinetic study confirmed the strong negative substitution effect in DGEBA-Jeffamine system, which is mainly due to the steric crowding on the nitrogen atoms of Jeffamine.

For the last part of this study, role of chemical bonds in the durability of interfacial bonding between epoxy and concrete during hygrothermal exposure was investigated with the application of silane coupling agents. In this attempt of the application of silane coupling agent, it was intended to examine the hypothesis that hydrogen bonding plays a larger role for the degradation of interfacial bonding at the interface between epoxy and concrete, in which displacement of epoxy with water induces the disruption of the interfacial hydrogen bonding, resulting in reduced interfacial bond properties, thus durability can be enhanced with the use of the coupling agent by changing the main type of bonds to stronger covalent bonding.

The slant shear testing results show that the durability of the interfacial bonding was significantly enhanced with the use of a epoxy-functional silane coupling agent, which is attributed to the replacement of the weak hydrogen bonds between epoxy and cement by strong covalent bonds. The results proposed that the bonding systems with epoxy-concrete interface also have the similar mechanism proposed for the description used for the degradation in epoxy-metal adhesion under humid environments, in which a decrease in bond strength have been ascribed to displacement of epoxy with water, which preferentially forms hydrogen bonds with the adherend, the hydrogen bonding at the epoxy-concrete interface is a factor to affect the durability in the bonding of epoxy-cementitous materials. Thus, it can be conclude that the chemical nature of bonding plays an important role at the interface bonding of epoxy resin for the structural strengthening application. The spectroscopic features using FT-IR also confirmed the changes in chemical nature of concrete after the silane modification.

With the calculation of the percent contribution to the failure strength for each set of specimens, it is confirmed that the silane application contributes to improve the durability of bonding properties with exposure for all exposure condition, but over time the improvement diminished.

As in any investigation through this work, there are several issues which remain unanswered. First of all, from the studies of complex hygorthermal behavior of epoxy-amine thermosets (Chapters 3 and 4), although it was revealed that the influences of other factors such as different states of hydrogen bonded water or microstructural effect are very small, the exact impact of these factors remains still unanswered. In order to evaluate the effects of those factors quantitatively, it would be useful if the decrease in

T_g during hygrothermal exposure is correlated with those factors. Near-infrared spectroscopy over a wide range of wavenumbers 6000~7400cm^{-1} which employs a subtraction method between dried and wet samples would be suggested as a method to identify different states of hydrogen bonded water during the exposure. Also, the quantitative analysis of microstructural changes with AFM tapping mode such as changes in relative fractions of hard and soft phases during exposure can suggest an indicator which correlate the hygrothermal behavior with the effect of microstructures in epoxy-amine thermosets.

For a practical issue which need to be addressed from the kinetic study in Chapter 5, in-situ investigation of cure kinetics using IR spectroscopy would be helpful to monitor the cure reactions precisely. When the changes in rate reaction can be obtained in situ IR spectroscopy, sufficient quantities of data with the limited effect of residual heat enable to minimize experimental errors which can largely affect the calculation of concentration of tertiary amines using mass balance equations.

For another issue relating to the work about the enhancement of the durability of bonding properties between epoxies and cementitious materials (Chapter 6), it is suggested that, if surface roughness is also varied with different sample conditions, and different types of silane coupling agents are utilized in which different chemical ends are created with different amount of hydroxyls at the surface, the fractional contribution of each mechanism of the chemical bonding and the mechanical interlocking could be assessed separately.

LIST OF REFERENCES

(1) Chen, J.-S.; Ober, C. K.; Poliks, M. D.; Zhang, Y.; Wiesner, U.; Cohen, C. *Polymer* **2004,** 45, 1939-1950.

(2) Ding, Y.; Liu, M.; Li, S.; Zhang, S.; Zhou, W.-F.; Wang, B. *Macromol. Chem. Phys.* **2001,** 202, 2681-2685.

(3) Ratna, D., *Handbook of Thermoset Resins*. Smithers Rapra Technology: 2009.

(4) Chen, J.; Nakamura, T.; Aoki, K.; Aoki, Y.; Utsunomiya, T. *J. Appl. Polym. Sci.* **2001,** 79, 214-220.

(5) Chiao, L.; Lyon, R. E. *J. Compos. Mater.* **1990,** 24, 739-752.

(6) Raman, V. I.; Palmese, G. R. *Macromolecules* **2005,** 38, 6923-6930.

(7) Shechter, L.; Wynstra, J.; Kurkjy, R. P. *Ind. Eng. Chem.* **1956,** 48, 94-97.

(8) Tung, C.-Y. M.; Dynes, P. J. *J. Appl. Polym. Sci.* **1982,** 27, 569-574.

(9) Varley, R. J. *Polym. Int.* **2004,** 53, 78-84.

(10) Hale, A.; Macosko, C. W.; Bair, H. E. *J. Appl. Polym. Sci.* **1989,** 38, 1253-1269.

(11) Liu, X. D.; Sudo, A.; Endo, T. *J. Polym. Sci., Part A: Polym. Chem.* **2011,** 49, 250-256.

(12) Omrani, A.; Simon, L. C.; Rostami, A. A.; Ghaemy, M. *Int. J. Chem. Kinet.* **2008,** 40, 663-669.

(13) Wartewig, S.; Helmis, G.; Strehmel, V.; Zimmermann, E.; Häusler, K.; Fedtke, M. *Progr. Colloid Polym. Sci.* **1992,** 90, 206-208.

(14) May, C. A., *Epoxy resins: chemistry and technology*. CRC Press: 1988.

(15) Wu, L.; Hoa, S. V.; Ton-That, M.-T. *J. Appl. Polym. Sci.* **2004,** 92, 2261-2268.

(16) Carter, H. G.; Kibler, K. G. *J. Compos. Mater.* **1977,** 11, 265-275.

(17) De'Neve, B.; Shanahan, M. E. R. *Polymer* **1993,** 34, 5099-5105.

(18) Ellis, T. S.; Karasz, F. E. *Polymer* **1984,** 25, 664-669.

(19) Jelinski, L. W.; Dumais, J. J.; Cholli, A. L.; Ellis, T. S.; Karasz, F. E. *Macromolecules* **1985,** 18, 1091-1095.

(20) LaPlante, G.; Lee-Sullivan, P. *J. Appl. Polym. Sci.* **2005,** 95, 1285-1294.

(21) McKague, E. L.; Reynolds, J. D.; Halkias, J. E. *J. Appl. Polym. Sci.* **1978,** 22, 1643-1654.

(22) Moy, P.; Karasz, F. E. *Polym. Eng. Sci.* **1980,** 20, 315-319.

(23) Perrin, F. X.; Nguyen, M. H.; Vernet, J. L. *Eur. Polym. J.* **2009,** 45, 1524-1534.

(24) Theocaris, P. S.; Kontou, E. A.; Papanicolaou, G. C. *Colloid Polym. Sci.* **1983,** 261, 394-403.

(25) Xiao, G. Z.; Delamar, M.; Shanahan, M. E. R. *J. Appl. Polym. Sci.* **1997,** 65, 449-458.

(26) Xiao, G. Z.; Shanahan, M. E. R. *J. Appl. Polym. Sci.* **1998,** 69, 363-369.

(27) Apicella, A.; Nicolais, L. *Adv. Polym. Sci.* **1985,** 72, 69-77.

(28) Lu, M. G.; Shim, M. J.; Kim, S. W. *J. Appl. Polym. Sci.* **2001,** 81, 2253-2259.

(29) Nogueira, P.; Ramirez, C.; Torres, A.; Abad, M. J.; Cano, J.; Lopez, J.; Lopez-Bueno, I.; Barral, L. *J. Appl. Polym. Sci.* **2001,** 80, 71-80.

(30) Nunez, L.; Villanueva, M.; Fraga, F.; Nunez, M. R. *J. Appl. Polym. Sci.* **1999,** 74, 353-358.

(31) Yang, Q.; Xian, G.; Karbhari, V. M. *J. Appl. Polym. Sci.* **2008,** 107, 2607-2617.

(32) Lobanov, Y. E.; Shterenzon, A. L. *Mech. Compos. Mater.* **1971,** 7, 654-656.

(33) Frigione, M.; Aiello, M. A.; Naddeo, C. *Constr. Build. Mater.* **2006,** 20, 957-970.

(34) de Bruyne, N. A. *J. Appl. Chem.* **1956,** 6, 303-310.

(35) Schmidt, R.; Bell, J. *Adv. Polym. Sci.* **1986,** 75, 33-71.

(36) Devasahayam, S. *J. Appl. Polym. Sci.* **2006,** 99, 3318-3327.

(37) Johncock, P. *J. Appl. Polym. Sci.* **1990,** 41, 613-618.

(38) Netravali, A. N.; Fornes, R. E.; Gilbert, R. D.; Memory, J. D. *J. Appl. Polym. Sci.* **1985,** 30, 1573-1578.

(39) Thomson, K. W.; Wong, T.; Broutman, L. J. *Polym. Eng. Sci.* **1984,** 24, 1270-1276.

(40) Wu, L.; Hoa, S. V.; Minh, T.; Ton, T. *J. Appl. Polym. Sci.* **2006,** 99, 580-588.

(41) Papanicolaou, G. C.; Kosmidou, T. V.; Vatalis, A. S.; Delides, C. G. *J. Appl. Polym. Sci.* **2006,** 99, 1328-1339.

(42) Zhou, J.; Lucas, J. P. *Polymer* **1999,** 40, 5505-5512.

(43) Zhou, J.; Lucas, J. P. *Polymer* **1999,** 40, 5513-5522.

(44) Gupta, V. B.; Drzal, L. T.; Rich, M. J. *J. Appl. Polym. Sci.* **1985,** 30, 4467-4493.

(45) Maggana, C.; Pissis, P. *J. Polym. Sci., Part B: Polym. Phys.* **1999,** 37, 1165-1182.

(46) Vanlandingham, M. R.; Eduljee, R. F.; Gillespie, J. W. *J. Appl. Polym. Sci.* **1999,** 71, 787-798.

(47) Chateauminois, A.; Chabert, B.; Soulier, J. P.; Vincent, L. *Polym. Compos.* **1995,** 16, 288-296.

(48) Kelley, F. N.; Bueche, F. *J. Polym. Sci.* **1961,** 50, 549-556.

(49) Browning, C. E. *Polym. Eng. Sci.* **1978,** 18, 16-24.

(50) Wright, W. W. *Composites* **1981,** 12, 201-205.

(51) Bellenger, V.; Verdu, J.; Morel, E. *J. Mater. Sci.* **1989,** 24, 63-68.

(52) Grave, C.; McEwan, I.; Pethrick, R. A. *J. Appl. Polym. Sci.* **1998,** 69, 2369-2376.

(53) Apicella, A.; Nicolais, L.; de Cataldis, C. *Adv. Polym. Sci.* **1985,** 66, 189-207.

(54) Carfagna, C.; Apicella, A.; Nicolais, L. *J. Appl. Polym. Sci.* **1982,** 27, 105-112.

(55) Feng, J. *"Interaction and permeability of water with liquid crystalline thermoset"*. Ph.D. Thesis, University of Florida, Gainesville, FL, 2001.

(56) Adamson, M. J. *J. Mater. Sci.* **1980,** 15, 1736-1745.

(57) Soles, C. L.; Chang, F. T.; Bolan, B. A.; Hristov, H. A.; Gidley, D. W.; Yee, A. F. *Journal of Polymer Science Part B: Polymer Physics* **1998,** 36, 3035-3048.

(58) Soles, C. L.; Chang, F. T.; Gidley, D. W.; Yee, A. F. *J. Polym. Sci., Part B: Polym. Phys.* **2000,** 38, 776-791.

(59) Soles, C. L.; Yee, A. F. *Journal of Polymer Science Part B: Polymer Physics* **2000,** 38, 792-802.

(60) Mikols, W. J.; Seferis, J. C.; Apicella, A.; Nicolais, L. *Polym. Compos.* **1982,** 3, 118-124.

(61) Ngai, K. L.; Rendell, R. W.; Yee, A. F.; Plazek, D. J. *Macromolecules* **1991,** 24, 61-67.

(62) Anderson, S. L.; Grulke, E. A.; DeLassus, P. T.; Smith, P. B.; Kocher, C. W.; Landes, B. G. *Macromolecules* **1995,** 28, 2944-2954.

(63) Chang, Y. P.; Cheah, P. B.; Seow, C. C. *J. Food Sci.* **2000,** 65, 445-451.

(64) Liu, Y.; Roy, A. K.; Jones, A. A.; Inglefield, P. T.; Ogden, P. *Macromolecules* **1990,** 23, 968-977.

(65) Maeda, Y.; Paul, D. R. *Journal of Polymer Science Part B: Polymer Physics* **1987,** 25, 1005-1016.

(66) Roy, A. K.; Inglefield, P. T.; Shibata, J. H.; Jones, A. A. *Macromolecules* **1987,** 20, 1434-1437.

(67) Tiemblo, P.; Martinez, G.; Gómez-Elvira, J. M.; Millán, J. *Polym. Bull. (Berlin)* **1994,** 32, 353-359.

(68) Vrentas, J. S.; Duda, J. L.; Ling, H. C. *Macromolecules* **1988,** 21, 1470-1475.

(69) Venditti, R. A.; Gillham, J. K. *Polym. Mater. Sci. Eng.* **1993,** 69, 434-5.

(70) Couchman, P. R.; Karasz, F. E. *Macromolecules* **1978,** 11, 117-119.

(71) Pascault, J. P.; Williams, R. J. J. *J. Polym. Sci., Part B: Polym. Phys.* **1990,** 28, 85-95.

(72) Wise, C. W.; Cook, W. D.; Goodwin, A. A. *Polymer* **1997,** 38, 3251-3261.

(73) Mijovic, J.; Andjelic, S. *Macromolecules* **1995,** 28, 2787-2796.

(74) Xu, L.; Fu, J. H.; Schlup, J. R. *Ind. Eng. Chem. Res.* **1996,** 35, 963-972.

(75) Byrne, C. A.; Hagnauer, G. L.; Schneider, N. S.; Lenz, R. W. *Polym. Compos.* **1980,** 1, 71-76.

(76) Cuadrado, T. R.; Macgregor, J. F.; Hamielec, A. E. *J. Appl. Polym. Sci.* **1990,** 40, 867-890.

(77) Regnier, N.; Fayos, M.; Moreau, P.; Lafontaine, E.; Mortaigne, B. *Polym. Adv. Technol.* **1999,** 10, 637-646.

(78) Riccardi, C. C.; Williams, R. J. J. *J. Appl. Polym. Sci.* **1986,** 32, 3445-3456.

(79) Xu, L.; Fu, J. H.; Schlup, J. R. *J. Am. Chem. Soc.* **1994,** 116, 2821-2826.

(80) Xu, L.; Schlup, J. R. *J. Appl. Polym. Sci.* **1998,** 67, 895-901.

(81) Dusek, K.; Ilavsky, M.; Lunak, S. *J. Polym. Sci., Polym. Sypm.* **1975,** 53, 29-44.

(82) Girard-Reydet, E.; Riccardi, C. C.; Sautereau, H.; Pascault, J. P. *Macromolecules* **1995,** 28, 7599-7607.

(83) Horie, K.; Hiura, H.; Sawada, M.; Mita, I.; Kambe, H. *J. Polym. Sci., Part A: Polym. Chem.* **1970,** 8, 1357-1372.

(84) Riccardi, C. C.; Adabbo, H. E.; Williams, R. J. J. *J. Appl. Polym. Sci.* **1984,** 29, 2481-2492.

(85) Sung, C. S. P.; Pyun, E.; Sun, H. L. *Macromolecules* **1986,** 19, 2922-2932.

(86) Perrin, F.-X.; Nguyen, T. M. H.; Vernet, J.-L. *Macromol. Chem. Phys.* **2007,** 208, 55-67.

(87) Mijovic, J.; Fishbain, A.; Wijaya, J. *Macromolecules* **1992,** 25, 979-985.

(88) Parker, R. E.; Isaacs, N. S. *Chem. Rev. (Washington, DC, U. S.)* **1959,** 59, 737-99.

(89) Zvetkov, V. L. *Macromol. Chem. Phys.* **2002,** 203, 467-476.

(90) Zvetkov, V. L.; Krastev, R. K.; Samichkov, V. I. *Thermochim. Acta* **2008,** 478, 17-27.

(91) Skordos, A. A.; Partridge, I. K. *Polym. Eng. Sci.* **2001,** 41, 793-805.

(92) Um, M.-K.; Daniel, I. M.; Hwang, B.-S. *Compos. Sci. Technol.* **2002,** 62, 29-40.

(93) Dusi, M. R.; Lee, W. I.; Ciriscioli, P. R.; Springer, G. S. *J. Compos. Mater.* **1987,** 21, 243-261.

(94) Kenny, J. M. *J. Appl. Polym. Sci.* **1994,** 51, 761-764.

(95) Michaud, D. J.; Beris, A. N.; Dhurjati, P. S. *J. Compos. Mater.* **1998,** 32, 1273-1296.

(96) Williams, R. J. J.; Benavente, M. A.; Ruseckaite, R. A.; Churio, M. S.; Hack, H. G. *Polym. Eng. Sci.* **1990,** 30, 1140-1145.

(97) Karkanas, P. I.; Partridge, I. K. *J. Appl. Polym. Sci.* **2000,** 77, 1419-1431.

(98) Karkanas, P. I.; Partridge, I. K.; Attwood, D. *Polym. Int.* **1996,** 41, 183-191.

(99) Mijovic, J.; Fishbain, A.; Wijaya, J. *Macromolecules* **1992,** 25, 986-989.

(100) Mijovic, J.; Wijaya, J. *Macromolecules* **1994,** 27, 7589-7600.

(101) Paz-Abuin, S.; Lopez-Quintela, A.; Pellin, M. P.; Varela, M.; Prendes, P. *J. Polym. Sci., Part A: Polym. Chem.* **1998,** 36, 1001-1016.

(102) Chike, K. E.; Myrick, M. L.; Lyon, R. E.; Angel, S. M. *Appl. Spectrosc.* **1993,** 47, 1631-1635.

(103) Dannenberg, H. *SPE Trans.* **1963,** 3, 78-88.

(104) Qiao, P.; Xu, Y. *J. Compos. Constr.* **2004,** 8, 352-359.

(105) Aiello, M. A.; Frigione, M.; Acierno, D. *J. Mater. Civ. Eng.* **2002,** 14, 185-189.

(106) Au, C.; Buyukozturk, O. *J. Compos. Constr.* **2006,** 10, 35-47.

(107) Chajes, M. J.; Thomson, T. A.; Farschman, C. A. *Constr. Build. Mater.* **1995,** 9, 141-148.

(108) El-Hawary, M.; Al-Khaiat, H.; Fereig, S. *Cem. Concr. Res.* **2000,** 30, 259-266.

(109) Karbhari, V. M.; Engineer, M. *J. Reinf. Plast. Compos.* **1996,** 15, 1194-1216.

(110) Karbhari, V. M.; Engineer, M.; Eckel Ii, D. A. *J. Mater. Sci.* **1997,** 32, 147-156.

(111) Toutanji, H. A.; Gomez, W. *Cem. Concr. Compos.* **1997,** 19, 351-358.

(112) Wan, B.; Petrou, M. F.; Harries, K. A. *J. Reinf. Plast. Compos.* **2006,** 25, 875-890.

(113) Tu, L.; Kruger, D. *ACI Struct. J.* **1996,** *93*, 26-35.

(114) El-Hawary, M.; Al-Khaiat, H.; Fereig, S. *Cem. Concr. Compos.* **1998,** 20, 41-52.

(115) Sen, R.; Shahawy, M.; Mullins, G.; Spain, J. *ACI Struct. J.* **1999,** *96*, 906-914.

(116) Fowkes, F. M. *Ind. Eng. Chem.* **1964,** 56, 40-52.

(117) Fowkes, F. M. *J. Adhes. Sci. Technol.* **1990,** 4, 669-691.

(118) Krump, H.; Hudec, I.; Luyt, A. S. *Int. J. Adhes. Adhes.* **2005,** 25, 269-273.

(119) Mei, L.; He, X.; Li, Y.; Peng, Q.; Wang, R.; Xu, J. *Surf. Interface Anal.* **2010**, n/a. doi: 10.1002/sia.3560.

(120) Owens, D. K.; Wendt, R. C. *J. Appl. Polym. Sci.* **1969,** 13, 1741-1747.

(121) Bakis, C. E.; Uppuluri, V. S.; Nanni, A.; Boothby, T. E. *Compos. Sci. Technol.* **1998,** 58, 1307-1319.

(122) Lin, Y.; Friedrich, K.; Weimer, C.; Mai, Y.-W. *Adv. Compos. Mater.* **1998,** 7, 47-61.

(123) Momayez, A.; Ehsani, M. R.; Ramezanianpour, A. A.; Rajaie, H. *Cem. Concr. Res.* **2005,** 35, 748-757.

(124) Merlin, F.; Guitouni, H.; Mouhoubi, H.; Mariot, S.; Vall, F.; Van Damme, H. *J. Colloid Interface Sci.* **2005,** 281, 1-10.

(125) Perruchot, C.; Chehimi, M. M.; Vaulay, M.-J. h.; Benzarti, K. *Cem. Concr. Res.* **2006,** 36, 305-319.

(126) Viallis-Terrisse, H. e.; Nonat, A.; Petit, J.-C. *J. Colloid Interface Sci.* **2001,** 244, 58-65.

(127) Ramrus, D. A.; Berg, J. C. *J. Adhes. Sci. Technol.* **2006,** 20, 1615-1623.

(128) Ji, W.-G.; Hu, J.-M.; Liu, L.; Zhang, J.-Q.; Cao, C.-N. *Surf. Coat. Technol.* **2007,** 201, 4789-4795.

(129) Witucki, G. L. *J. Coating Tech.* **1993,** 65, 57-60.

(130) Kinloch, A.; Korenberg, C.; Tan, K.; Watts, J. *J. Mater. Sci.* **2007,** 42, 6353-6370.

(131) Rattana, A.; Abel, M.-L.; Watts, J. F. *J. Adhes.* **2005,** 81, 963-988.

(132) Ji, W.-G.; Hu, J.-M.; Zhang, J.-Q.; Cao, C.-N. *Corros. Sci.* **2006,** 48, 3731-3739.

(133) Lassila, L. V. J.; Nohrstr, T.; Vallittu, P. K. *Biomaterials* **2002,** 23, 2221-2229.

(134) Oksanen, C. A.; Zografi, G. *Pharm. Res.* **1993,** 10, 791-799.

(135) Sung, Y. K.; Gregonis, D. E.; Russell, G. A.; Andrade, J. D. *Polymer* **1978,** 19, 1362-1363.

(136) Tan, Y. Y.; Challa, G. *Polymer* **1976,** 17, 739-740.

(137) Birkinshaw, C.; Buggy, M.; Daly, S. *Polym. Commun.* **1987,** 28, 286-8.

(138) Hodge, R. M.; Bastow, T. J.; Edward, G. H.; Simon, G. P.; Hill, A. J. *Macromolecules* **1996,** 29, 8137-8143.

(139) Jin, X.; Ellis, T. S.; Karasz, F. E. *J. Polym. Sci., Polym. Phys. Ed.* **1984,** 22, 1701-1717.

(140) Lagaron, J. M.; Powell, A. K.; Bonner, G. *Polym. Test.* **2001,** 20, 569-577.

(141) Pissis, P.; Apekis, L.; Christodoulides, C.; Niaounakis, M.; Kyritsis, A.; Nedbal, J. *J. Polym. Sci., Part B: Polym. Phys.* **1996,** 34, 1529-1539.

(142) Musto, P.; Mascia, L.; Ragosta, G.; Scarinzi, G.; Villano, P. *Polymer* **2000,** 41, 565-574.

(143) Musto, P.; Ragosta, G.; Mascia, L. *Chem. Mater.* **2000,** 12, 1331-1341.

(144) Musto, P.; Ragosta, G.; Scarinzi, G.; Mascia, L. *J. Polym. Sci., Part B: Polym. Phys.* **2002,** 40, 922-938.

(145) Fukuda, M.; Kawai, H.; Yagi, N.; Kimura, O.; Ohta, T. *Polymer* **1990,** 31, 295-302.

(146) Bockenheimer, C.; Fata, D.; Possart, W. *J. Appl. Polym. Sci.* **2004,** 91, 369-377.

(147) Fraga, F.; Castro-Diaz, C.; Rodriguez-Nunez, E.; MartInez-Ageitos, J. M. *Polymer* **2003,** 44, 5779-5784.

(148) Fraga, F.; Payo, P.; Rodriguez-Nunez, E.; Martinez-Ageitos, J. M.; Castro-Díaz, C. *J. Appl. Polym. Sci.* **2007,** 103, 3931-3935.

(149) Janssson, J.; Gedde, U.; Ribas, S. *Progr. Colloid Polym. Sci.* **1992,** 87, 78-82.

(150) Montserrat, S.; Cortés, P.; Calventus, Y.; Hutchinson, J. *J. Therm. Anal. Calorim.* **1997,** 49, 79-85.

(151) Shi, X.; Fernando, B.; Croll, S. *J. Coat. Technol. Res.* **2008,** 5, 299-309.

(152) Choi, S.; Douglas, E. P. *ACS Appl. Mater. Interfaces* **2010,** 2, 934-941.

(153) Abdelkader, A. F.; White, J. R. *J. Appl. Polym. Sci.* **2005,** 98, 2544-2549.

(154) Rigail-Cede, A.; Sung, C. S. P. *Polymer* **2005,** 46, 9378-9384.

(155) Fu, J. H.; Schlup, J. R. *J. Appl. Polym. Sci.* **1993,** 49, 219-227.

(156) Bella, R.; Fenouillot, F. i.; Cassagnau, P.; Falk, L. *Polymer* **2007,** 48, 6902-6912.

(157) Rozenberg, B. A. *Adv. Polym. Sci.* **1986,** 75, 113-165.

(158) Smith, I. T. *Polymer* **1961,** 2, 95-108.

(159) Deng, Y.; Martin, G. C. *Macromolecules* **1994,** 27, 5147-5153.

(160) Fraga, F.; Soto, V.; Rodriguez-Nunez, E.; Martinez-Ageitos, J.; Rodriguez, V. *J. Therm. Anal. Calorim.* **2007,** 87, 97-100.

(161) Fraga, F.; Vazquez, E. C.; Rodriguez-Nunez, E.; Martinez-Ageitos, J. M. *Polym. Adv. Technol.* **2008,** 19, 1623-1628.

(162) Paz-Abuin, S.; Pellin, M. P.; Paz-Pazos, M.; Lopez-Quintela, A. *Polymer* **1997,** 38, 3795-3804.

(163) Barton, J. M. *Polymer* **1980,** 21, 603-606.

(164) Ballinger, P.; Long, F. A. *J. Am. Chem. Soc.* **1960,** 82, 795-798.

(165) Dusek, K. *Adv. Polym. Sci.* **1986,** 78, 1-59.

(166) Matejka, L. *Macromolecules* **2000,** 33, 3611-3619.

(167) Strachota, A.; Whelan, P.; Kr, J.; Brus, J.; Urbanov, M.; Slouf, M.; Matejka, L. *Polymer* **2007,** 48, 3041-3058.

(168) Hag-Elsafi, O.; Alampalli, S.; Kunin, J. *Compos. Struct.* **2001,** 52, 453-466.

(169) Khalifa, A.; Gold, W. J.; Nanni, A.; M.I, A. A. *J. Compos. Constr.* **1998,** 2, 195-202.

(170) Harun, M. K.; Lyon, S. B.; Marsh, J. *Prog. Org. Coat.* **2003,** 46, 21-27.

(171) Karbhari, V. M.; Chin, J. W.; Hunston, D.; Benmokrane, B.; Juska, T.; Morgan, R.; Lesko, J. J.; Sorathia, U.; Reynaud, D. *J. Compos. Constr.* **2003,** 7, 238-247.

(172) Chollet, M.; Horgnies, M. *Surf. Interface Anal.* **2011,** 43, 714-725.

(173) Sood, R. K.; Krishnamoorthy, S.; Khandelwal, B. L. *Int. J. Cem. Compos. Lightweight Concr.* **1984,** 6, 93-98.

(174) Martinez-Ramirez, S.; Zamarad, A.; Thompson, G. E.; Moore, B. *Build. Environ.* **2002,** 37, 933-937.

(175) Zhang, L.; Glasser, F. P. *Cem. Concr. Res.* **2005,** 35, 2252-2260.

(176) Trezza, M. A.; Lavat, A. E. *Cem. Concr. Res.* **2001,** 31, 869-872.

(177) Ylmen, R.; Jaglid, U.; Steenari, B.-M.; Panas, I. *Cem. Concr. Res.* **2009,** 39, 433-439.

(178) Kjellsen, K. O.; Justnes, H. *Cem. Concr. Compos.* **2004,** 26, 947-956.

(179) Chu, L.; Daniels, M. W.; Francis, L. F. *Chem. Mater.* **1997,** 9, 2577-2582.

(180) Wood, D. L.; Rabinovich, E. M. *Appl. Spectrosc.* **1989,** 43, 263-267.

(181) Lee, T.-C.; Wang, W.-J.; Shih, P.-Y.; Lin, K.-L. *Cem. Concr. Res.* **2009,** 39, 651-658.

(182) Mollah, M. Y. A.; Yu, W.; Schennach, R.; Cocke, D. L. *Cem. Concr. Res.* **2000,** 30, 267-273.

(183) Hughes, T. L.; Methven, C. M.; Jones, T. G. J.; Pelham, S. E.; Fletcher, P.; Hall, C. *Advn. Cem. Bas. Mat.* **1995,** 2, 91-104.

(184) Iijima, M.; Sato, N.; Wuled Lenggoro, I.; Kamiya, H. *Colloid Surf. A-Physicochem. Eng. Asp.* **2009,** 352, 88-93.

(185) Shanmugharaj, A. M.; Sabharwal, S.; Majali, A. B.; Tikku, V. K.; Bhowmick, A. K. *J. Mater. Sci.* **2002,** 37, 2781-2793.

(186) Delgado, A. H.; Paroli, R. M.; Beaudoin, J. J. *Appl. Spectrosc.* **1996,** 50, 970-976.

(187) Yilmaz, B. e.; Olgun, A. *Cem. Concr. Compos.* **2008,** 30, 194-201.

(188) Wypych, G., *Handbook of Materal Weathering*. 3rd ed.; ChemTee publishing: 2003.

BIOGRAPHICAL SKETCH

Sungwon Choi was born in Seoul, Republic of Korea in 1977. He was admitted to Korea University in 1998, and received his Bachelor of Engineering degree in materials science and engineering in 2004. He worked at Korea Institute of Science and Technology in 2004, where he participated in the research about the organic-inorganic hybrid thin films for the application of organic thin film transistors. He was admitted to the Department of Materials Science and Engineering at the University of Florida and started Ph. D program in 2006. Finally, he received his Ph.D. from the University of Florida in the spring of 2011.